AD NUMBER

AD834960

LIMITATION CHANGES

TO:

Approved for public release; distribution is unlimited.

FROM:

Distribution authorized to U.S. Gov't. agencies only; Administrative/Operational Use; JUN 1986. Other requests shall be referred to Army Missile Command, Attn: AMSMI-RB, Redstone Arsenal, AL 35809.

AUTHORITY

USAMC ltr dtd 18 Sep 1973

AD

RSIC-798

RADAR CLUTTER IN AN AIR DEFENSE SYSTEM

PART I: CLUTTER PHYSICS

by

Donald E. Barrick

Contract No. DAAHO1-67-C-1921
Battelle Memorial Institute
505 King Avenue
Columbus, Ohio 43201

January 1968

DISTRIBUTION LIMITED
SEE NOTICES PAGE

REDSTONE SCIENTIFIC INFORMATION CENTER
REDSTONE ARSENAL, ALABAMA

JOINTLY SUPPORTED BY

U.S. ARMY MISSILE COMMAND

GEORGE C. MARSHALL SPACE FLIGHT CENTER

STATEMENT #1 UNLIMITED

Each transmittal of this document outside the agencies of the U.S. Government must have prior approval of C.G. Army Missile Comd. Attn: AMSMI-RB Redstone Arsenal, Ala 35809

121

26 January 1968 RSIC-798

RADAR CLUTTER IN AN AIR DEFENSE SYSTEM

PART I: CLUTTER PHYSICS

by

Donald E. Barrick

Contract No. DAAH01-67-C-1921
Battelle Memorial Institute
505 King Avenue
Columbus, Ohio 43201

DISTRIBUTION LIMITED
SEE NOTICES PAGE

Research Branch
Redstone Scientific Information Center
Research and Development Directorate
U. S. Army Missile Command
Redstone Arsenal, Alabama 35809

ABSTRACT

This report provides an analysis and physical interpretation of the various mechanisms giving rise to radar clutter. Both volume-distributed clutter (rain, chaff, etc.) and surface-distributed clutter (terrain, sea, etc.) are considered. The statistics of the clutter radar cross sections are related to the statistics and properties of the particles or surfaces producing the echoes. The spectral densities of clutter signals are derived in terms of the physical parameters of the clutter sources. Measured results are provided, and examples are calculated which indicate the magnitude of the clutter problem for a mid-frequency (S-band) radar system.

FOREWORD

This document is one of two summary reports examining the problem of radar clutter in an air defense system. The study was performed at the request of the Advanced Sensors (Electromagnetics) Laboratory, U. S. Army Missile Command, Redstone Arsenal, Alabama.

Part I, which is unclassified, is devoted to an analysis and interpretation of the mechanisms giving rise to radar clutter. Two appendices relating to this problem are included, and each is self-contained, including references. RSIC-799, Part II, classified Confidential, is an examination and evaluation of clutter rejection techniques suitable for the application. Timely items from both the classified and unclassified literature are included.

The following sources were searched:

Battelle Library
RSIC holdings
DDC and NASA tape searches
Personal contacts

The helpful suggestions of W. E. Rife and G. J. Falkenbach are gratefully acknowledged.

CONTENTS

CONTENTS (Concluded)

ILLUSTRATIONS

ILLUSTRATIONS (Concluded)

Section I. INTRODUCTION

Radar clutter denotes the received signals from unwanted targets. The unwanted targets of interest in this report include volume- and surface-distributed scattering sources. Raindrops, snowflakes, and chaff particles are the commonly encountered types of volume clutter, while the terrain and sea represent the surface clutter of concern in radar system engineering. Clutter physics is defined as the study of the relationship between the nature of the clutter scatterers and the characteristics of the radar echoes they produce. Without an elementary understanding of the physical parameters of the clutter scatterers and their effect on the clutter echoes, the radar engineer is at a loss to assess the operating capability of his system under various environmental conditions. Furthermore, clutter physics provides a sort of necessary background to the successful study and implementation of clutter rejection techniques.

The report first establishes the relationship for received power at the radar for three classes of targets: isolated "point targets" (such as an aircraft), volume-distributed clutter sources, and surface-distributed clutter sources. The latter quantities are statistical in nature, since the exact configuration of clutter scatterers is neither known nor of concern to the engineer. Hence it is convenient to represent the average clutter power at the receiver in terms of the average radar cross section of the sources within a radar resolution cell; the size of this average radar cross section can then be compared with that of a typical target to obtain a direct estimate of the strength of the clutter and target signals at the receiver. For volume-distributed clutter, the average scattering cross section per resolution cell is defined in terms of a radar cross section per unit volume times the volume of the resolution cell. The average radar cross section for surface-distributed clutter is likewise defined in terms of a radar cross section per unit area times the area of the surface contained within the resolution cell. Hence, it is these average radar cross sections per unit volume (for volume clutter) and per unit area (for surface clutter) and their relationship to the scatterers themselves which is of concern in this report.

The report relates the radar cross section per unit volume to the number of volume scatterers and the characteristics of each individual scatterer. This is done for both raindrops and half-wave chaff dipoles. Both the average radar cross section per unit area and its variance are studied; the variance provides an estimate of the degree of fluctuation about the mean received power level one can expect for volume clutter echoes. Theoretical predictions are compared with measured values.

A region of space filled with volume scatters will attenuate a radar wave propagating through it. While this attenuation is not of itself the same as clutter, it is usually associated with this subject because the same particles are responsible for both the clutter echoes and the attenuation, and both phenomena degrade the performance of a radar system. Both theoretical and experimental results for radar wave attenuation through rain are given and discussed.

The radar cross section per unit area of surface-distributed clutter is analyzed. The average value of this quantity for various types of surfaces is given and interpreted physically; curves of this radar cross section are shown as a function of the surface roughness parameters. The variance of the radar cross section per unit area is derived. Both small scale and large scale surface roughness components are analyzed and their role in the scattering process for natural surfaces is explained. Measured radar cross sections per unit area for terrain and sea surfaces are presented and compared with theoretical predictions.

Finally, the spectra of echoes scattered from clutter sources are studied. In general, clutter source and/or radar motion produce two effects: a spreading of the incident signal spectrum and a Doppler frequency shift in its position. The mechanisms responsible for these clutter spectrum changes are examined. It is shown how several of these spectrum-degrading effects acting simultaneously combine to produce a total received clutter spectrum. Measured data are given where available.

Several theoretical results and physical interpretations given here have been derived by this author and have not as yet appeared in the literature. Unfortunately, the scope of this reported effort is not consistent with the presentation of the detailed derivations. Two analyses are included, however, as appendices. Appendix A provides a theoretical treatment of scattering from volume-distributed particles; it covers both the clutter radar cross section and its statistics as well as the attenuation of waves propagating through the medium. Appendix B interprets the radar cross section of a very rough surface expressed in terms of the average number of specular points times their average Gaussian curvatures; the derivation of these quantities is presented. These appendices were written earlier in the year for publication in the open literature. They are included here because of their direct application to the area of clutter physics. They are as such self-contained articles, having their own references and figures.

Section II. RADAR RECEPTION OF TARGET AND CLUTTER SIGNALS

Clutter is defined to be radar reflections from unwanted targets. These unwanted targets, or clutter sources, are usually distributed randomly over the area to be searched by the radar;* this "range-distributed" clutter is the only type to be considered here. In most cases the radar signal reflected from a single clutter source is small compared to the signal from an aircraft target. However, the total signal from many such clutter sources seen by the radar simultaneously may be larger than that of the aircraft. In this case the target will not be visible above the clutter return if one merely observes signal intensity at the receiver. It will be the purpose of this section to examine quantitatively the intensity of the clutter and target signals at the receiver and their relationships to the scattering characteristics. Later sections will be concerned with the reflecting and spectral characteristics of the clutter.

A further breakdown of clutter into two categories is necessary to understand its echo characteristics. Volume-distributed clutter refers to clutter sources which are randomly spaced in three dimensions. Examples of such volume-distributed clutter sources include such natural phenomena as raindrops, snowflakes, flocks of birds, and swarming insects, as well as artificial or man-made obstacles such as chaff particles. These sources, though having random positions, are said to be uniformly distributed over space meaning that each volume increment in a local region of space is as likely to have the same number of sources as each other volume increment in the same local region. Surface-distributed clutter refers to clutter sources which are randomly spaced over two dimensions. Examples include trees scattered over the ground, specularly oriented reflection regions of sea surface waves, buildings in a city, and heads of grain in a wheat field.

Clutter physics is a term used to describe the study of the origin of clutter echoes and the relationships between clutter echo characteristics and the clutter source characteristics. When the class of targets to be considered is aircraft, as it is in this report, one can immediately set down some of the properties of the clutter sources which will hopefully give their echoes different characteristics than target echoes. One of these properties is the distributed nature of the two types of clutter sources, as discussed in the above paragraphs. The echo from each clutter source, as mentioned above, is in this case smaller than that of the target. Also, the target is always in motion with respect to the

---

*Some types of isolated, unwanted targets are occasionally termed clutter. For example, a water tower located a mile away from an air search radar may produce a large unwanted echo. Such an isolated target is not considered clutter here, and techniques used to mask such single objects usually differ from those used for range-distributed clutter.

clutter sources. For air defense radar systems, velocity differential is usually the most important characteristic as far as rejecting the clutter echoes; this relative motion produces a Doppler frequency difference between clutter echoes and target echoes. Target body shape is different from that of clutter sources; hence one can expect that the polarization properties of their scattered radar waves will differ. Furthermore, difference in size between clutter sources and target should mean that the frequency dependence of clutter echo strengths will differ; the average echo intensity of an aircraft is nearly constant over most of the useful radar spectrum as a function of frequency, while that of clutter will be shown to increase with frequency.

The relationship for the power received by a radar antenna from a target complex at a range R_T is derived in many standard radar textbooks.[1-4] They are repeated and interpreted here for three classes of targets. For simplicity, only backscattering is considered here.

1. Aircraft Target at Range R_T

If the radar beam is pointed directly at the target, the power received is

$$P_R = \left(\frac{P_T G_T}{4\pi R_T^2}\right) \cdot \left(\sigma_T\right) \left[\frac{G_R \lambda^2}{(4\pi)^2 R^2}\right] . \qquad (1)$$

In this equation, P_T is the transmitted power, G_T is the maximum gain of the transmitting antenna, σ_T is the target radar cross section, G_R is the maximum gain of the receiving antenna ($G_R = G_T$ if the same antenna is used for transmit and receive), and λ is the radar wavelength. The quantity in the first set of brackets gives the transmitted power density at the target. The radar cross section in the second set of brackets is the area of a fictitious body which scatters the same amount of power back toward the radar as the aircraft, but also scatters this same amount in all other directions. The quantity in the third set of brackets then accounts for the propagation of this backscattered energy back to the radar and its reception. One sees from this equation the familiar dependence of received power on the inverse fourth power of radar range.

2. Volume - Distributed Clutter Sources at Range R_T

At this point it is convenient to define the radar geometry (Figure 1). Since only backscattering is considered, the depth of the range resolution cell* is $\frac{c\tau}{2}$, where τ is the time duration of the radar pulse and c is the velocity of light. The quantities $\Delta\theta$ and $\Delta\varphi$ are the half-power beamwidths of the main antenna beam in elevation and azimuth respectively. (While the radar geometry shown in Figure 1 may not be appropriate to all situations, it is probably the most common one typical of air and surface search radars. Furthermore, it

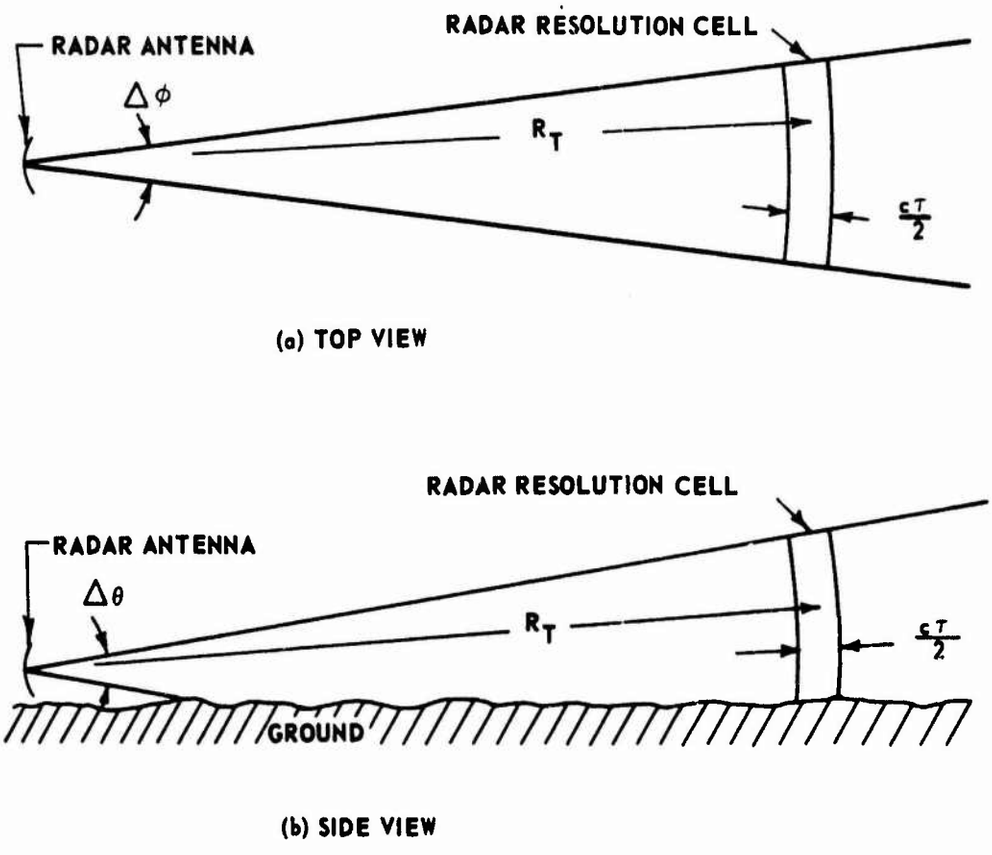

FIGURE 1. RADAR ANTENNA AND PROPAGATION GEOMETRY FOR GROUND-BASED SYSTEM

* The range resolution cell is the depth in range within which reflecting targets can produce echoes which all are received simultaneously. For backscattering it is exactly equal to one-half of the spatial pulse length $c\tau$.

illustrates well the effect of both volume- and surface-distributed clutter. If the clutter problem is understood for this geometry, other radar geometries can be easily handled.)

Assume now that the resolution cell at range R_T is filled with volume-distributed clutter sources such as rain. Then the average power received is

$$\overline{P}_R = \left(\frac{P_T G_T}{4\pi R_T^2}\right) \cdot \left(\sigma^c V\right) \left(\frac{G_R \lambda^2}{(4\pi)^2 R_T^2}\right) . \qquad (2)$$

All the quantities in this equation have the same interpretation as in Eq. (1) except the quantity in the second set of brackets. This quantity $\sigma^c V$ is the average total backscattering cross section of all the clutter source particles within the resolution cell. Since this quantity is shown later to be merely the sum of the scattering cross sections of each particle, it is directly proportional to the number of such particles. Assuming the particles are randomly but uniformly distributed, their total number is proportional to their average density times the volume of space inside the resolution cell. Hence it is convenient to define the total average cross section $\sigma^c V$ as the average backscattering cross section per unit volume (with dimensions of inverse length) times the volume of space containing the particles observed simultaneously by the radar, i.e., the volume of the radar resolution cell.

It will be the task of a later section to study the quantity σ^c, the average volume-distributed clutter cross section per unit volume. That quantity is usually a constant, independent of range. However, it is important to give the volume V of the resolution cell to see how the clutter power depends upon the radar parameters and range. For the radar geometry of Figure 1, the volume V is approximately

$$V = \left(\pi R_T^2 \frac{\Delta\theta}{4} \frac{\Delta\varphi}{2}\right)\left(\frac{c\tau}{2}\right) = \frac{\pi R_T^2 c\tau \Delta\theta \Delta\varphi}{16} , \qquad (3)$$

where the first expression in brackets is the area of the half-ellipse across the beam face with semi-major and semi-minor axes $\frac{R_T \Delta\theta}{2}$ and $\frac{R_T \Delta\varphi}{2}$. The second set of brackets contains the depth of the cell. Thus one can see that as the resolution cell grows in size proportional to R_T^2, the apparent total radar cross section of this clutter $\sigma^c V$, grows with the square of the range. This is

in contrast with the radar cross section of an aircraft target, as seen in Eq. (1), which is independent of range. Hence one can expect the rain clutter echo, while possibly not a problem at smaller ranges, can definitely become a problem at larger ranges where it will eventually exceed the echo strength from a target.

3. Surface - Distributed Clutter at Range R_T

Referring again to Figure 1(b), assume that the ground at the bottom of the resolution cell produces a surface-distributed clutter echo. Then the average received signal power arising from the surface-distributed clutter sources contained within this resolution cell is given by

$$\overline{P}_R = \left(\frac{P_T G_T}{4\pi R_T^2}\right)\left(\sigma^o A\right)\left[\frac{G_R \lambda^2}{(4\pi)^2 R_T^2}\right] . \qquad (4)$$

All quantities are the same as defined previously for Eq. (1) except the expression inside the second set of brackets. This quantity $\sigma^o A$ is the total average radar backscattering cross section for the surface-distributed clutter contained in this resolution cell. Since it was assumed that the clutter-producing sources are randomly but uniformly distributed over the ground surface, this total radar cross section is proportional to the surface area A contained inside the resolution cell. For this reason, the quantity is usually written as the product of σ^o, the average backscattering cross section per unit surface area of the ground (a constant dependent only on the ground-scattering properties) and A, the surface area within which the ground clutter is seen at a given time at the receiver.

The quantity A, being proportional to the surface area inside the resolution cell, is a function only of the radar parameters and geometry. For the geometry shown in Figure 1, it is given by

$$A = \left(R_T \Delta\varphi\right)\left(\frac{c\tau}{2}\right) = \frac{R_T c \tau \Delta\varphi}{2} . \qquad (5)$$

The first expression in brackets is the arc length in azimuth across the main beam, and the second set of brackets contains the depth of the resolution cell. As can be seen, the total radar cross section of the surface clutter increases linearly with radar range R_T since the area A contributing to surface clutter increases with range. While this increase is not as rapid as that with volume-distributed clutter, nonetheless it does exist while the radar cross section of the aircraft is a constant with range.

One fact stands out clearly from consideration of distributed clutter up to this point: Reduction of the size of the resolution cell (with the corresponding reduction in resolution cell volume V and subtended surface area A) will reduce the power received due to clutter but will not affect the power received from an aircraft target. The resolution cell size should not be smaller than the aircraft dimensions, however, for then the target signal from the resolution cell begins to decrease. While reduction of the resolution cell size definitely helps reduce received clutter power, there are disadvantages which can offset the advantages gained for certain situations. One way of reducing the resolution cell size is to reduce antenna beamwidth. For a given frequency, this means increasing the antenna size and weight. This increased antenna size and weight, while reducing clutter and increasing antenna gains G_T and G_R (and hence maximum radar range), are of themselves disadvantages which necessitate greater mechanical complexity and cost. Furthermore, decreased antenna beamwidth in a search radar means a longer time to scan a given volume of space; this scan time is usually a limiting factor to reducing beamwidths, even in phased array radars.

The remaining recourse in reducing resolution cell size is to reduce the depth $\frac{c\tau}{2}$. This is done by reducing the effective pulse width τ. While present circuitry permits reduction of τ to the minimum (i.e., where $\frac{c\tau}{2}$ is the length of the airplane), most radar transmitters are limited in peak power; reduction in pulse width τ thus results in a corresponding decrease in the total energy in the signal. A well designed receiver has a signal-to-noise ratio which increases not with peak signal power but with the energy in the signal. Hence reduction of τ to reduce range resolution cell size results in a decrease in signal-to-noise ratio. However, modern pulse compression techniques permit one to reduce the effective resolution cell size without sacrificing signal-to-noise ratio. This is discussed in Part II under matched filtering as a means of effectively reducing clutter by reducing the effective cell size.

A further point should be noted concerning surface clutter. In certain cases nearby ground or sea clutter can be reduced in ground-based search radars by using horizontal polarization. At lower radar frequencies (L-band and lower), the ground is a good reflector, especially near grazing incidence; the ground-reflected wave for horizontal polarization, however, is shifted 180 deg in phase upon reflection. Hence an antenna mounted several feet above the surface and pointed near the horizontal will produce a composite pattern which is a result of of the interaction of the direct rays with the ground-reflected rays. For horizontal polarization, this composite pattern has a null in the horizontal direction.*

*In practice, the null never completely goes to zero because of (1) less than perfect reflection at the ground surface, and (2) the antenna boresight is

Hence, surface clutter sources which lie along the horizontal are not seen by by the radar. This effect is treated by Watters and Nathanson,[5] who show that the first pattern maximum up from the horizontal occurs at elevation angle $\alpha = \sin^{-1}\left(\frac{\lambda}{4h}\right)$, where λ is wavelength and h is the height of the radar antenna above the surface. For example, an L-band $\left(f_o = 1000 \text{ MHz}\right)$ radar antenna mounted about 18 ft off the ground has a null along the horizontal and its first maximum at 0.7 deg from the horizontal. While the technique is useful for reducing ground clutter, the resulting elevation pattern consisting of many maxima and minima (at about 0.7 deg apart for the above example) has "blind" angles through which an approaching aircraft must fly and at which it will be seen poorly, if at all. Furtheremore, an enemy aircraft hugging the horizon will be rejected to much the same extent as the surface clutter. For the above example, an aircraft flying at 500 ft altitude will not be visible until it is at a range of about 10 to 15 mi. Nonetheless, the clutter reduction advantages outweigh the disadvantages in many situations.*

As a practical example of the effects of clutter on a typical ground-based S-band $\left(f_o = 3000 \text{ MHz}\right)$ search radar, the radar cross section of various types of clutter in a resolution cell as a function of radar range were calculated[5] and shown in Figure 2. The antenna polarization is horizontal, the beamwidth is 2 by 2 deg, and the pulse width is 1 μsec. Clearly, an aircraft target at a given range should have a radar cross section considerably above that of the clutter. The left ordinate is calibrated in terms of required target cross section to give 13 dB of signal-to-clutter ratio; this 13 dB figure is usually considered desirable for reliable detection. Receiver thermal noise is also shown along with light rain, moderate rain, chaff, sea clutter, and open land. As can be seen, land clutter is the most serious at short ranges for this situation.

---

usually never directed exactly along the horizontal. The pattern minimum along the horizontal, however, may be quite deep, lying as much as 20 to 30 dB below the pattern maxima.

*"Clutter fences" have much the same effect as the technique described here. They are merely metal fences built around the radar site used to shield the antenna from strong nearby ground clutter.

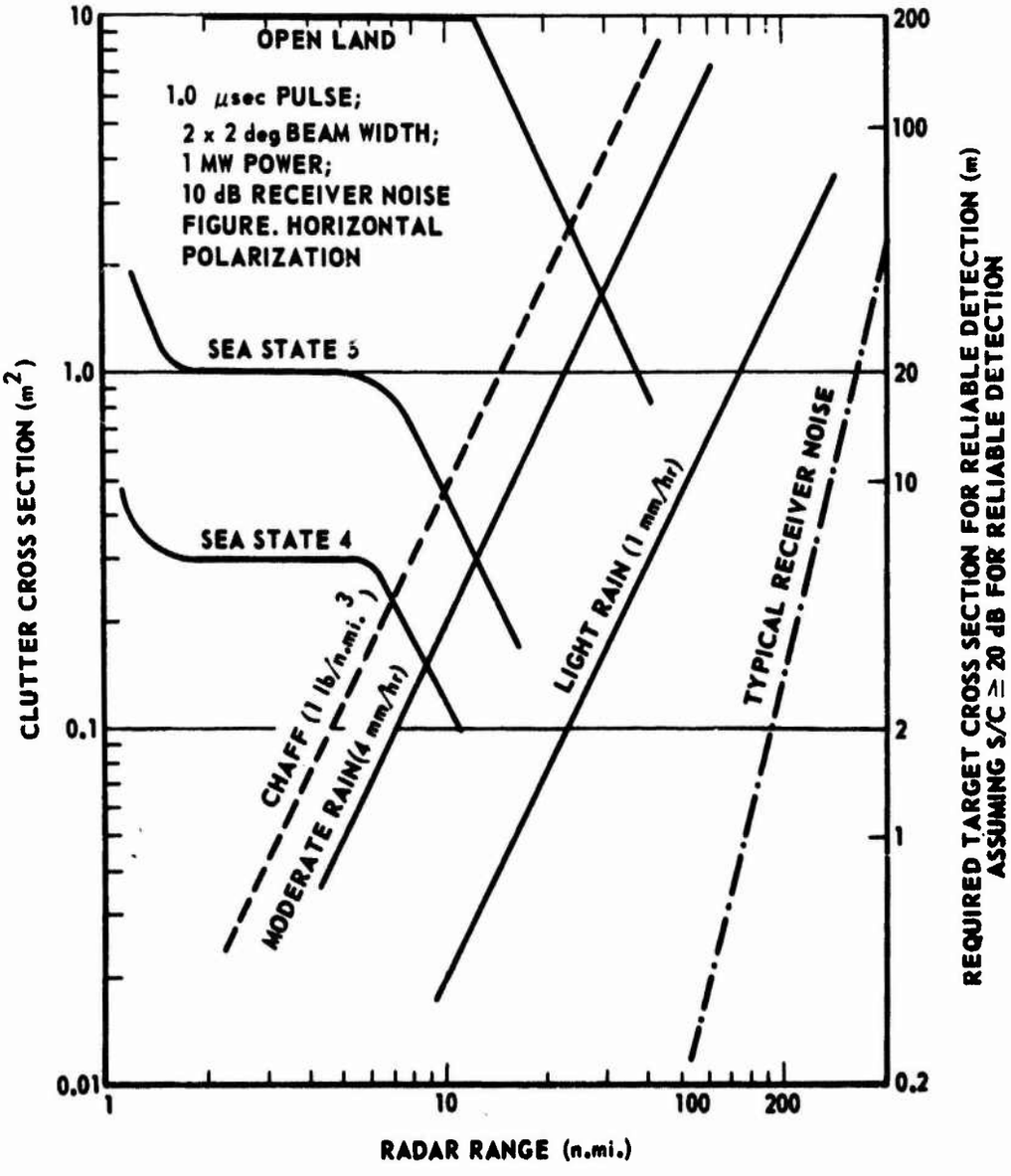

FIGURE 2. RADAR CROSS SECTION FOR VARIOUS TYPES OF CLUTTER WITH A TYPICAL GROUND-BASED, S-BAND SYSTEM EMPLOYING HORIZONTAL POLARIZATION

Section III. RADAR CROSS SECTION OF VOLUME - DISTRIBUTED CLUTTER

1. Radar Cross Section of Single Raindrop

It is necessary to know the scattering cross section of a single average raindrop of radius a in order to compute the effect of many such particles reflecting together. For all practical purposes, the raindrop may be assumed spherical with a radius a significantly less than wavelength; this is usually valid even up through K_a-band ($\lambda = 8$ mm), since raindrop radius rarely exceeds 1 to 2 mm. Hence the backscattering cross section of a single raindrop is that of a dielectric sphere with refractive index m and radius a in the Rayleigh (low frequency) region. This is (Appendix A):

$$\sigma_R = 4\pi a^2 \left| \frac{m^2 - 1}{m^2 + 2} \right|^2 \left(k_o a \right)^2 , \qquad (6)$$

where $k_o = \frac{2\pi}{\lambda}$. It should be noted that the refractive index m of fresh rain water is a complicated function of frequency throughout the microwave region; usually only empirical relationships are available for this frequency dependence. The most significant variation of σ_R with frequency, however, is contained in the factor k_o^4, which shows that the radar power backscattered by a single raindrop increases with the fourth power of frequency. This rapid increase in rain clutter signal with increasing frequency is probably the most serious limitation on the use of high frequencies for long range radars.

2. Radar Cross Section of Single Half-Wave Chaff Dipole

An effective chaff cloud usually consists of thin, conducting half-wave dipoles, where the enemy's operating wavelength is known ahead of time. A combination of theoretical analyses and experimental measurements have shown (Appendix A) that the cross section for such a dipole optimally oriented (i.e., oriented along the direction of the E-field vector of the radar wave) is

$$\sigma_D = 0.75\lambda^2 . \qquad (7)$$

In the more common situation, however, the dipoles are randomly oriented with respect to the E-field. In this case, the best that can be used is a radar cross section averaged over all equally likely orientations. This is

$$\sigma_D = 0.17\lambda^2 . \qquad (8)$$

In general the radar cross section of a chaff dipole cut to be one-half wavelength is considerably greater than that of a raindrop. This dipole represents the particle shape offering maximum radar cross section per unit weight of material.

3. Radar Cross Section of Single Snowflake

The problem of finding a simple scattering model for a snowflake is considerably more complicated than that for a raindrop. The snowflake is neither spherical nor solid. Its structure, consisting mainly of ice particles and air, varies widely with weather conditions. While ice itself has a dielectric constant only about one-fifth that of water, the radar cross section of some snowflakes is substantially greater than that of raindrops. This is undoubtedly because the radar cross section in the low-frequency and resonance regions is much more dependent on the overall size than on the dielectric constant or packing density of the ice; large snowflakes are considerably larger than raindrops, and hence the large radar cross section. Because of the wide variety of snowflake formations, it seems fruitless to give a mathematical model which can be expected to be at all accurate.

4. Average Radar Cross Section per Unit Volume

Paragraphs 1 and 2 above have given expressions for the radar scattering cross sections of individual volume-distributed clutter sources, namely, that of a raindrop and that of a chaff dipole. The average incoherent radar cross section of the entire complex of many such single clutter sources existing together in a given volume is derived in Appendix A. The approximations under which the theory is valid are stated there. In particular, it is shown that the average radar cross section of the complex is merely the average number of particles times the radar cross section per particle. This is valid when distance between particles is a random variable and thus any phase shift between 0 and 2π due to these path length distances is equally likely. This assumption is usually valid for rain showers and nearly always valid for chaff clouds. Under this assumption, one merely adds the scattered power, or radar cross section, from each individual particle, and hence the term "incoherent" scattering cross section.

Define N as the total number of clutter sources in a particle cloud of volume V. Then the average number of particles per unit volume is $\rho = \frac{N}{V}$. In this case, the average cross section per unit volume is

$$\sigma^c = \frac{N}{V} \langle \sigma \rangle = \rho \langle \sigma \rangle \ , \qquad (9)$$

where $<\sigma>$ is the average value of the radar cross section of an individual particle. For rain, $<\sigma>$ is the same as σ_R given in Eq. (6), where an average raindrop radius is used. For randomly oriented half-wave chaff dipoles, $<\sigma>$ is the same as σ_D given in Eq. (8).

As an example, consider a moderate rainstorm with particle density $\rho \simeq 100/m^3$; the typical drop radius from Figure A-2 of Appendix A is $a \simeq 1$ mm. At X-band ($\lambda = 3.21$ cm), the value computed from the Eq. (6) and (9) for σ^c (in m^2/m^3) is about -58 dB. This compares favorably with experimentally observed values to be given later.

As mentioned previously, only the incoherent scattering cross sections are considered here, even though coherent scattering is treated in Appendix A. However, it can be shown that the coherent backscattering cross section of typical sized rainstorms and chaff clouds is so small throughout the microwave region that only the incoherent backscattered power need be considered.

5. Variance of Radar Cross Section per Unit Volume

The average radar cross section per unit volume is given in the preceding sections. If one were to measure the average received power from volume clutter, the average reading would be a true measure of this quantity σ^c. If the radar output power indicator were sufficiently fast, one would see a fluctuation about the average value. It is desirable to have an estimate of this fluctuation in order to know how much any given reading is likely to deviate from the average.

It can be shown that the variance (defined as the average of the cross section per unit volume squared minus the square of the average cross section per unit volume) has a definite relationship to this fluctuation. In fact, the Chebyshev inequality, which applies to any general probability distribution, states that the difference between the instantaneous fluctuating cross section and its average value exceeds five times the standard deviation (the standard deviation is defined as the square root of the variance) less than $\frac{1}{25}$ (or 4 percent) of the time. Hence, a knowledge of the variance of the radar cross section per unit volume gives a good idea of how wildly the instantaneous value is likely to fluctuate about its average.

The variance for ρ particles per unit volume is given in Appendix A, and it is found to be exactly the square of σ^c, the average cross section per unit volume, i.e.,

$$\text{Var } (\sigma/\text{vol}) = \left(\sigma^c\right)^2 = [\rho<\sigma>]^2 \quad . \tag{10}$$

Hence, one can expect to see instantaneous fluctuations in volume-distributed clutter power which are as great as the average power itself. It is a common misconception that the more clutter particles one observes simultaneously, the less the instantaneous cross section deviates from its average value; such is not true. It may be true that a radar system time constant in certain situations is so large that instantaneous fluctuations about the average are smoothed, but this is only due to the inability of the radar to follow the instantaneous swings in clutter power.

6. Probability Density of Radar Cross Section per Unit Volume

It is relatively easy to derive the probability density function of the radar cross section per unit volume. From this probability density function, all higher moments can be derived. The probability density is derived in Appendix A. It is shown there that the total received voltage from N signals arising from N clutter sources becomes a Gaussian variable as N becomes sufficiently large. This follows the well known "Central Limit Theorem" of statistics. (Usually the approximation is valid for $N > 10$.) Then the probability density function $p(\sigma)$ for the radar cross section per unit volume σ is exponential, i.e.,

$$p(\sigma) = \frac{1}{\sigma^c} e^{-\frac{\sigma}{\sigma^c}} \quad , \tag{11}$$

for $0 \leq \sigma \leq \infty$, where σ^c is the average radar cross section per unit volume as defined in Eq. (9).

7. Measured Values for Average Radar Cross Section per Unit Volume for Rain Clutter

In preceding sections an attempt was made to physically interpret σ^c and the variance of this quantity in terms of the individual scattering particles and their density. This was done to gain an understanding as to what causes the clutter and what physical parameters affect its value. In this

section, measured values for σ^c are given in Table I for various frequencies and at various rain rates.[5] Also given is the probability, or relative amount of the time, that such a rain rate occurs in Washington, D. C., so that one can get an idea of how often a radar may have to deal with such rain clutter.

TABLE I. MEASURED AVERAGE RADAR CROSS SECTION PER UNIT VOLUME σ^c FOR RAIN (m^{-1})

Rainfall Type	Rainfall Rate (mm/hr)	Probability of Occurrence at Washington, D. C. (%)	σ^c in dB m^{-1}					
			L-Band 1.25 GHz	S-Band 3.0 GHz	C-Band 5.6 GHz	X-Band 9.3 GHz	K_u-Band 24 GHz	K_a-Band 35 GHz
Drizzle	0.25	6		-102	-91	-82	-64	-57
Light Rain	1.0	3	-107	- 92	-82	-72	-54	-47
Moderate Rain	4.0	0.7	- 97	- 83	-72	-62	-46	-49
Heavy Rain	16.0	0.1		- 73	-62	-53	-42	-32

Section IV. ATTENUATION OF RADAR WAVES DUE TO RAIN

1. Theoretical Interpretation

While the attenuation of radar waves passing through volume-distributed particles such as raindrops is not exactly a clutter problem, it is a propagation problem confronting the radar designer which is a result of the presence of clutter sources. A coherent radar wave propagating through a region containing many scattering particles experiences two effects: its phase is shifted by the presence of the particles, and it is attenuated in amplitude by the particles. The first effect is usually of no concern to the radar engineer while the latter effect is of great concern. Appendix A treats this problem by two techniques. One employs a multiple scattering theory and is quite precise in its formulation, while the other, simpler analysis is based upon energy considerations.

The attenuation of radar waves is due to two phenomena: Energy is removed from the incident wave by absorption by the particles and converted to heat if the particle material is lossy, and energy is removed from the incident wave by the particles and incoherently scattered in other directions. For small particles compared to wavelength, only the first mechanism is important, while the second mechanism dominates when the particles are large compared to wavelength. Raindrops are essentially small in size compared to wavelength up through X-band and possibly even up to K_a-band. Under these conditions, the following approximation for the power attenuation coefficient α (derived in Appendix A) is valid:

$$\alpha = (4.343)\ 4\pi\rho a^3 k_o\ I_m\left(\frac{m^2 - 1}{m^2 + 2}\right)\ (\mathrm{dB/m}) \quad , \tag{12}$$

where ρ is the particle density (number per m^3), a is the average particle radius, $k_o = \frac{2\pi}{\lambda}$, m is the complex refractive index of the particle material, and Im [x] means the imaginary part of x. As can be seen, the attenuation in the low frequency limit is zero unless the refractive index m is complex (representing a lossy material). The quantity α given above is the one-way attenuation of radar waves and must be multiplied by two to give the round-trip attenuation for backscattering.

An example is given in Appendix A. At $\lambda = 3.21$ cm ($f_o = 9.35$ GHz or X-band), the measured refractive index of rainwater is $m = 7.14 + i2.89$ at 0°C. Assuming an average drop radius a of 1 mm and a density ρ of $100/m^3$

(typical of a moderate rain shower), one arrives at an attenuation of 0.0652 dB/n. mi. (one-way) or 0.1304 dB/n. mi. (round-trip). This compares to a fair degree with measured results to be given below.

2. Measured Rainfall Attenuation of Radar Waves

The first extensive set of measurements of rain attenuation was made by Medhurst.[6] A mean value of his observations is plotted in Figure 3 as a function of frequency. The ordinate gives the two-way attenuation per rainfall rate (dB/n. mi per mm/hr rainfall rate). To use the curve, one multiplies the ordinate value by the rainfall rate to get the round-trip attenuation in dB/n. mi. Rainfall rates typical of different types of showers can be found in Table I. Nathanson[5] used later measurements to modify the Medhurst's curve; his result is shown as the dashed curve. His curve is believed to be more accurate for rainfall rates less than 4 mm/hr. The curves are accurate to no closer than 3 dB (a factor of 2).

It can be seen from the curves that attenuation in heavy rain can become a serious problem at frequencies of X-band and higher over ranges of tens of nautical miles. It was also shown previously that the received rain clutter intensity increases sharply above these frequencies. Hence, these two factors tend to limit the frequencies used for long-range search radars to C-band or lower.

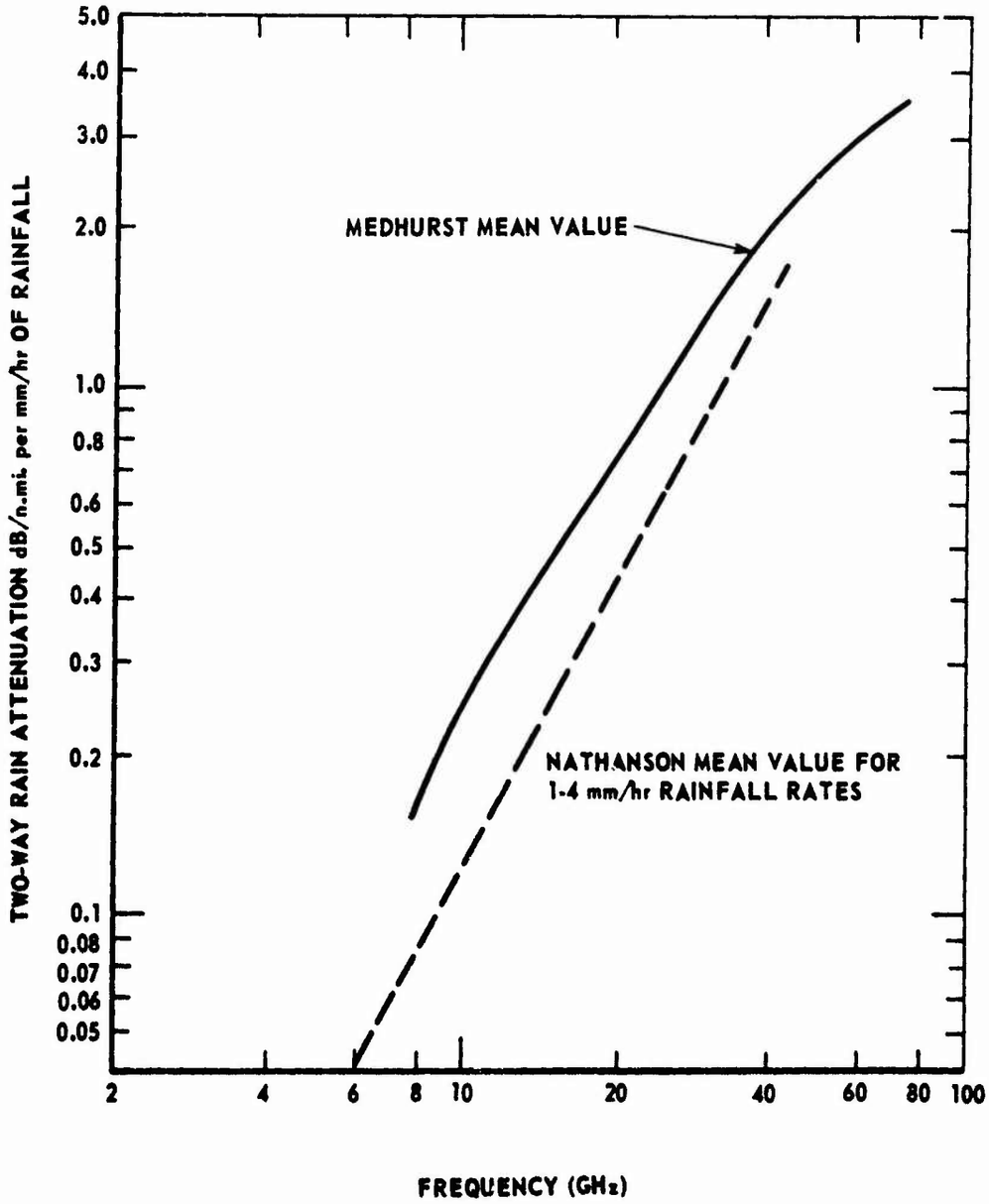

FIGURE 3. MEASURED VALUES OF RAIN ATTENUATION VERSUS FREQUENCY FOR A MICROWAVE RADAR

Section V. RADAR CROSS SECTION OF SURFACE-DISTRIBUTED CLUTTER

1. Slightly Rough Surface: Average Radar Cross Section per Unit Area

One of the most general analyses of rough surface scattering treats the surface height itself as a random variable. A recent report by Barrick and Peake[7] presents the analysis. The term "slightly rough" refers to a surface whose height deviation about a mean surface is small compared to a wavelength. Hence it applies to any rough surface in the low frequency limit. In practice, the slightly rough surface model accounts for HF and possible VHF scatter from the sea surface and some local terrain surfaces (whose roughness does not exceed a few feet).

The analysis and mathematical details are given by Barrick and Peake,[7] only the results and their interpretation will be presented here. Only backscattering is considered in this report for the sake of brevity and simplicity. The mean surface is planar and the angle of incidence θ_i is measured from the mean normal, or vertical, to the surface. The backscattered power is termed incoherent because the phase angle of the scattered field varies randomly between 0 and 2π rad from one surface to another in an ensemble. This is in contrast to the reflected fields, which are coherent; these reflected fields exist at and near the specular direction and are proportional to the Fresnel reflection coefficients. For backscattering, one expects a strong coherent reflection (compared to the incoherent scatter) around normal incidence. However, in most situations involving surface clutter, the radar antenna rarely views the surface from directly overhead, and hence one need consider only the incoherent backscattering cross section.

For backscatter, the incoherent average radar cross section per unit surface area, σ^o,[7] is given by

$$\sigma^o = 4\pi k_o^4 \cos^4 \theta_i \, |\alpha|^2 W_1\left(-2k_o \sin \theta_i, \, 0\right) \quad , \tag{13}$$

where α is a function of the surface materials and polarization states; it will be given below for the vertical and horizontal states. The quantity $W_1(p, q)$ provides the interpretation of the scattering process; it is the spectral density of the surface roughness height and is defined in terms of the surface height correlation function, $\langle \zeta(x, y)\, \zeta(x + \Delta x, y + \Delta y) \rangle = h^2 R_1(\Delta x, \Delta y)$ as follows:

$$W_1(p, q) = \frac{h^2}{\pi^2} \int_{-\infty}^{\infty} \int_{-\infty}^{\infty} R_1(\Delta x, \Delta y)\, e^{-i\Delta x p \, - \, i\Delta y q} \, d(\Delta x)\, d(\Delta y) \quad , \tag{14}$$

where $\zeta(x, y)$ is the random variable representing the rough surface height above the x, y plane. The x-direction is taken here to be along the plane of incidence while the y-direction is perpendicular to it; the x, y plane is the mean plane of the rough surface. The quantity h^2 is the mean square surface height and $R_1(\Delta x, \Delta y)$ is the surface height correlation coefficient for two surface points separated by Δx, Δy. Hence, Eq. (13) shows that the only roughness spectral frequencies which produce backscatter are those with radian wave numbers $p = -2k_o \sin\theta_i$ and $q = 0$. Near grazing incidence, for example, where $\sin\theta_i \to 1$, it is roughness frequencies near $2k_o$ rad/m which are responsible for backscatter.

The quantities α_{vv} and α_{hh}, proportional to scattering matrix elements,[7] are

$$\alpha_{hh} = -\frac{\left(\mu_r - 1\right)\left[\left(\mu_r - 1\right)\sin^2\theta_i + \epsilon_r\mu_r\right] - \mu_r^2\left(\epsilon_r - 1\right)}{\left(\mu_r\cos\theta_i + \sqrt{\epsilon_r\mu_r - \sin^2\theta_i}\right)^2},$$

$$\alpha_{vv} = \frac{\left(\epsilon_r - 1\right)\left[\left(\epsilon_r - 1\right)\sin^2\theta_i + \epsilon_r\mu_r\right] - \epsilon_r^2\left(\mu_r - 1\right)}{\left(\epsilon_r\cos\theta_i + \sqrt{\epsilon_r\mu_r - \sin^2\theta_i}\right)^2}, \qquad (15)$$

for a surface made up of a homogeneous material having relative permeability and permittivity μ_r and ϵ_r. For a highly reflecting or conducting surface $\left(\epsilon_r \to \infty\right)$, these become

$$\alpha_{hh} = 1, \quad \alpha_{vv} = \frac{1 + \sin^2\theta_i}{\cos^2\theta_i}. \qquad (16)$$

From the above equations, it can be seen that backscattered power near grazing incidence is always greater for the vertical polarization states than for the horizontal states. This has been confirmed experimentally also, as will be seen later.

Equation (13) for σ^o was obtained by a perturbation technique and is correct to the first order in $\left(k_o h\right)^2$. As such it represents a true low frequency solution and exhibits the familiar fourth power of frequency dependency shown by power scattered from small volume-clutter particles. If the roughness height is not small so that $k_o h$ is not small compared to unity, then higher order

terms omitted in the solution here become important. Neglecting higher order terms, no depolarization for backscattering takes place (i.e., α_{vh} and α_{hv} are zero); if higher order terms are large enough to be included, then depolarization does occur in the form of non-zero α_{vh} and α_{hv}; such higher order terms are complicated and have been derived by Valenzuela.[8]

As an example, consider a Gaussian surface height correlation coefficient, $R_1(\Delta x, \Delta y) \approx -\exp[(\Delta x^2 + \Delta y^2)/\ell^2]$, where ℓ is termed the correlation length. Then the roughness spectrum to be used in Eq. (13) becomes

$$W\left(-2k_o \cos\theta_i,\ 0\right) = \frac{h^2\ell^2}{\pi} \exp\left(-k_o^2 \ell^2 \sin^2\theta_i\right) . \qquad (17)$$

Curves plotted from this function for the vertical and horizontal polarization states versus incidence angle are shown in Figure 4 for $k_o \ell = 1.0$. The curves are normalized to $\frac{\sigma^o}{k_o^2 h^2}$, in dB. The parameter which changes between curves is the dielectric constant of the surface material, which varies from infinity to $1\frac{1}{12}$. Other curves of this type for different parameter values are given by this author.[9]

2. Very Rough Surface: Average Radar Cross Section per Unit Area

Like the slightly rough surface, the roughness height here is also treated as a random variable. However, the other frequency limit defines a "very rough" surface, i.e., the roughness height is large in terms of wavelength, or $\left(k_o h\right)^2 >> 1$. In this limit, any of the optics techniques are available to predict the average backscattering cross section, and they all give the same solution if the analysis is performed correctly. A review of these various optics approaches is given by Barrick and Peake.[7] One of these approaches, developed by this author, is presented here as Appendix B. This approach is termed the specular point theory.

The specular point theory (Appendix B) has as its basis the simple interpretation that the backscattered power is proportional to the number of surface points with surface slopes such that they can specularly reflect into the backscattering direction. These surface elements in this case must have normals which point in the incidence (and scattering direction). In addition, the backscattered power is proportional to the average radii of curvature at

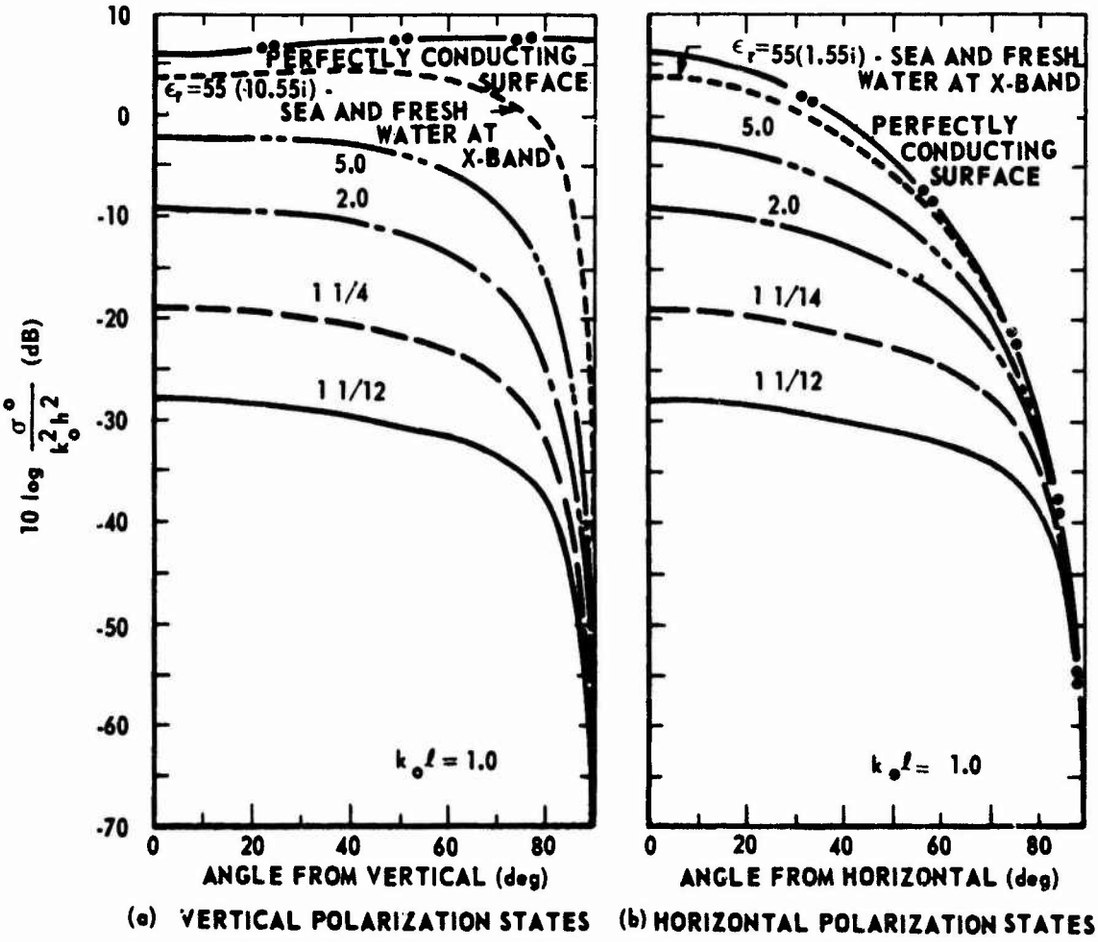

FIGURE 4. AVERAGE INCOHERENT RADAR CROSS SECTION PER UNIT SURFACE AREA σ^o FOR SLIGHTLY ROUGH SURFACE MODEL VERSUS INCIDENCE ANGLE EMPLOYING A GAUSSIAN SURFACE HEIGHT CORRELATION COEFFICIENT

these specular points. While this theory agrees with simple geometrical optics predictions, it can also be derived rigorously starting from a physical optics integral.[10]

As derived in Appendix B, the average backscattering cross section per unit area σ^o for a two-dimensionally rough surface with incidence angle θ_i (measured the vertical, or z-axis) and with the incidence plane taken to be the x, z plane (same geometry as for the slightly rough surface) is

$$\sigma^o = \pi \sec^4 \theta_i \, |R(0)|^2 \, P\left(\tan \theta_i, 0\right) \quad , \tag{18}$$

where R(0) is the Fresnel reflection coefficient for the surface at normal incidence, i.e., it is $\frac{\sqrt{\epsilon_r} - \sqrt{\mu_r}}{\sqrt{\epsilon_r} + \sqrt{\mu_r}}$ for a homogeneous surface or unity for a perfectly conducting or reflecting surface. The quantity $P\left(\zeta_x, \zeta_y\right)$ is the probability density function for the surface slopes ζ_x and ζ_y, in the x- and y-directions. Hence the average radar cross section is directly proportional to the probability that the surface will have its x-slope oriented specularly, i.e., with $\zeta_x = \tan \theta_i$.

As examples, consider Gaussian and exponential surface slope probability functions, i.e.,

$$P_G\left(\zeta_x, \zeta_y\right) = \frac{1}{\pi s^2} \exp\left[-\left(\zeta_x^2 + \zeta_y^2\right)/s^2\right]$$

$$P_E\left(\zeta_x, \zeta_y\right) = \frac{1}{\pi s^2} \exp\left[-\sqrt{6\left(\zeta_x^2 + \zeta_y^2\right)/s^2}\right] \quad , \tag{19}$$

where $s^2 = \langle \zeta_x^2 \rangle + \langle \zeta_y^2 \rangle$ is the total mean square slope of the surface at any point. Here the surface roughness is assumed isotropic so that $\langle \zeta_x^2 \rangle = \langle \zeta_y^2 \rangle$, i.e., the slope statistics along the x-direction are the same as along the y-direction.* Then the average radar cross sections for these two surface slope models are obtained from Eq. (18) and (19).

$$\sigma^o = \frac{\sec^4 \theta_i}{s^2} \, |R(0)|^2 \exp\left(\tan^2 \theta_i / s^2\right) \tag{20}$$

---

* This is a simplification which may not be entirely realistic for the sea surface, which often has waves moving in preferred directions. Nonisotropic surfaces can be handled easily with the above equations by permitting the surface slopes ζ_x and ζ_y to be correlated with each other.

for the Gaussian slope model, and

$$\sigma^o = \frac{3 \sec^4 \theta_i}{s^2} |R(0)|^2 \exp\left(\sqrt{6} \tan \theta_i / s\right) \qquad (21)$$

for the exponential slope model. Curves of these radar cross sections normalized as $\frac{\sigma^o}{|R(0)|^2}$, are shown in Figure 5 as a function of incidence angle θ_i. The parameter which varies between curves is the rms surface slope s. Very smooth surfaces, i.e., s small, scatter most of the energy near the specular direction, i.e., $\theta_i = 0$, since the probability is low that the specular point surface slope could be very large. In general, the curves show that the backscattered power falls off much more rapidly near grazing than for the slightly rough surface, even when the rms slope s is fairly large.

Another point to be noted is that no polarization dependence or depolarization is obtained for backscatter for the very rough surface. This is because backscattering according to these theories comes only from surface facets which are normal to the direction of incidence, as from small mirrors, and hence the same polarization is reflected as transmitted.

3. Composite Surfaces: Average Radar Cross Section per Unit Area

In nature, very few surfaces are strictly very rough. Usually a surface which has a roughness scale considerably larger than wavelength also has smaller roughness scale superimposed over it, and a portion of this small roughness falls in the "slightly rough" category discussed previously. As an example, consider regions with gently sloping hills and valleys on the earth's surface; these comprise the "very rough" scale at, say, S-band frequencies. On top of this are found rocks, pebbles, grass, and other slight roughness scale features. Or, for example, the sea surface is made up of the large "swell" waves, which are the very rough scale at S-band, while the tiny ripples or "capillary" waves produce the slight roughness.

In general, surfaces which have a very rough scale can be said to possess three different roughness scales: a very rough scale, an intermediate scale (i.e., wavelength and surface height are of the same order of magnitude), and a slightly rough scale. The first and the last scales can be handled theoretically, and the results have already been presented here. The intermediate scale cannot be treated analytically, unfortunately, because neither

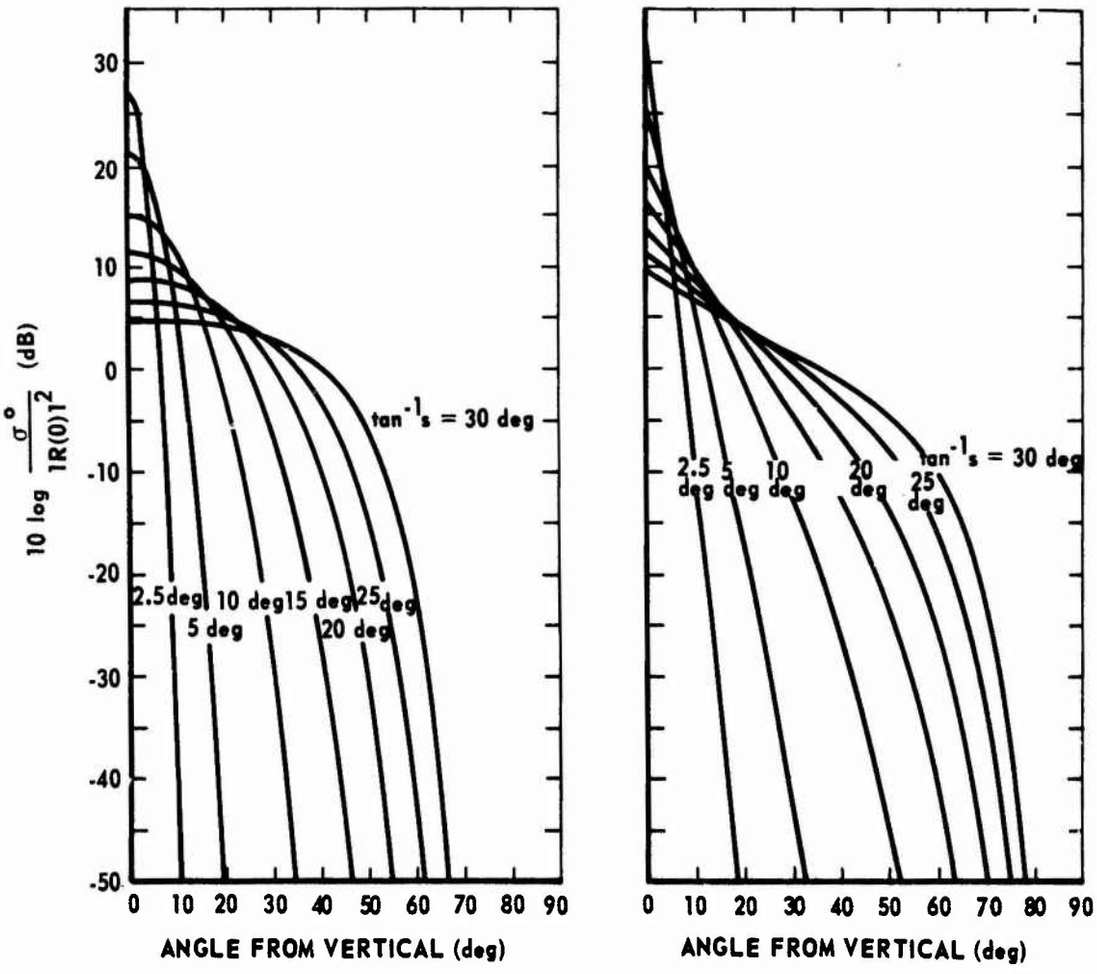

FIGURE 5. AVERAGE RADAR CROSS SECTION PER UNIT SURFACE AREA σ^{o} FOR VERY ROUGH SURFACE MODEL VERSUS INCIDENCE ANGLE EMPLOYING TWO SURFACE SLOPE PROBABILITY DISTRIBUTIONS

the high frequency optics techniques nor the low frequency perturbation techniques are strictly valid for this region. The best one can hope to do is qualitatively interpolate between the low frequency, slightly rough solutions and the high frequency, very rough solutions.

The mathematical treatment of composite surfaces having slightly rough, very rough, and possibly intermediate roughness scales, is conceptually quite simple.[7,9] Since only incoherent backscattered power is considered, one merely

adds the average backscattered power (or σ^o) for the slightly rough surface scale to that for the very rough surface scale. This is possible because the scatter is incoherent for each roughness scale and hence one can add the powers.

An example of the average radar cross section per unit area σ^o is computed and shown in Figure 6 for four different values of surface dielectric constant. Both the vertical and horizontal polarization states are shown. The very rough surface scale is assumed to have a Gaussian slope distribution with mean square slope s such that $\tan^{-1} s = 10$ deg. Two sets of slightly rough scale parameters are assumed, and they are given in the figure; in one case the slight roughness has a larger rms slope, i.e., $\tan^{-1} s = 23.6$ deg, while in the other the rms slope is approximately the same as that of the very rough scale, i.e., $\tan^{-1} s = 11.3$ deg. In nature, the smaller roughness scales are usually more precipitous than the larger scales; consider, for example, the gently sloping hills and valleys along with the more steeply sloping rocks and pebbles.[9]

From the curves of Figure 6, one sees that the backscattering near normal incidence is produced by the very rough scale; at these incidence angles, this component dominates that from the slight roughness. Radar engineers commonly refer to this as the "specular" component of backscatter. This name fits the explanation, for the optics techniques discussed earlier show that those areas of the large roughness which are specularly oriented produce backscatter. On the other hand, near grazing the backscattered power due to the slight roughness dominates. Radar engineers have termed the component in this region the diffuse component and have been at a loss to explain the mechanism producing it. Empirically, this component for certain surfaces has appeared to fit a $\cos \theta_i$ law, while at other times a $\cos^{3/2} \theta_i$ or $\cos^2 \theta_i$ appear to be better fits. It is this author's conviction that this diffuse component is produced by the slight roughness scales present, and the theory presented in paragraph 1 above is adequate to explain it, especially close to grazing.

Other physical mechanisms, of course, have a hand in the scattering process besides the slightly and very rough surface scales. Intermediate-scale roughness is usually present, and this component will produce an effect around the inflection point of the curves, i.e., around $\theta_i = 30$ deg (Figure 6). In general the intermediate scale will produce an increase in this region of 3 to 4 dB over that shown in the figure, but this can be only qualitatively established. Multiple scattering is another phenomenon which, as yet, has not yielded to analytical solution; this effect is expected to be especially serious for surfaces with extremely precipitous slopes. Consider, for example, an airborne radar looking at downtown Manhattan; nearly all of the backscatter comes after multiple reflections between buildings and ground.

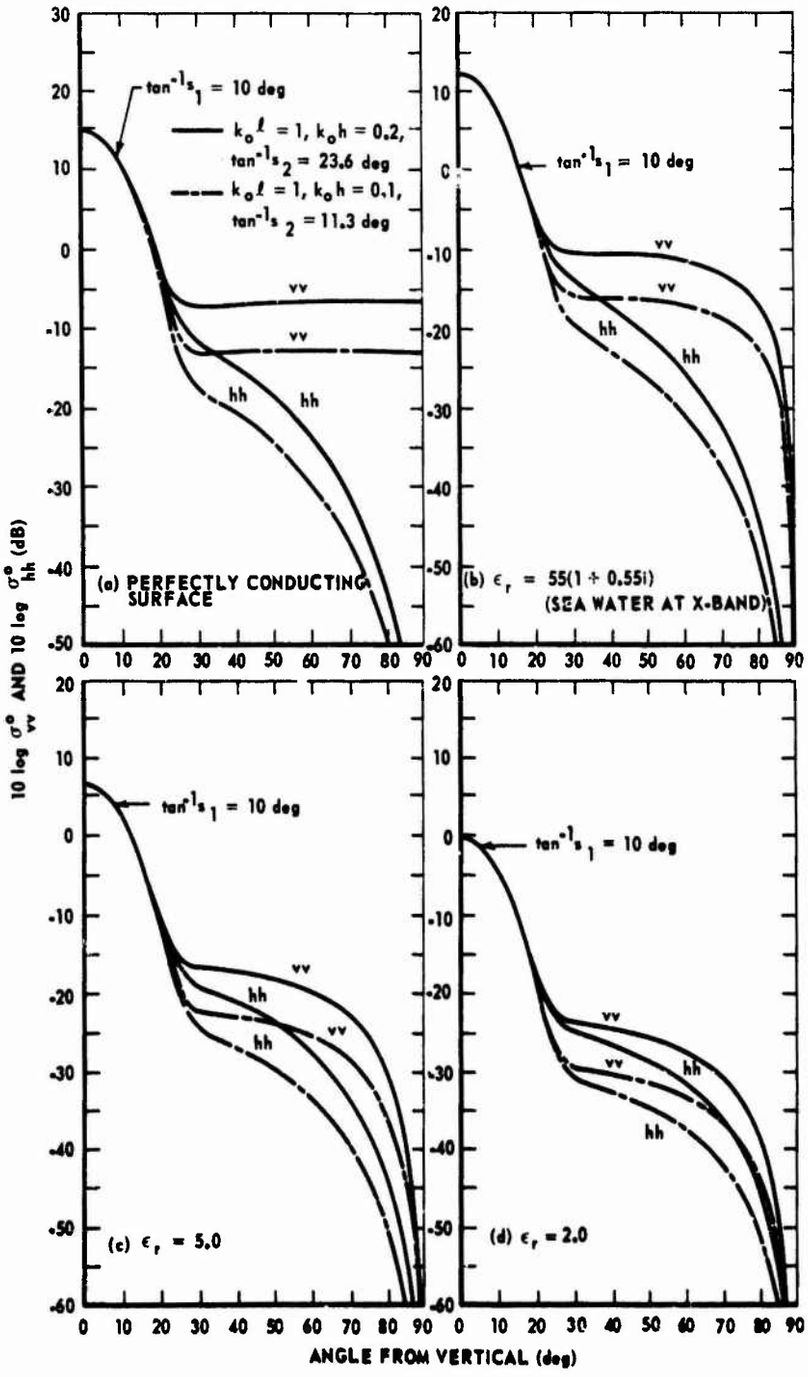

FIGURE 6. AVERAGE RADAR CROSS SECTION PER UNIT SURFACE AREA σ^o FOR COMPOSITE ROUGHNESS MODEL VERSUS INCIDENCE ANGLE FOR VERTICAL AND HORIZONTAL POLARIZATION STATES

Despite the neglected effects, the composite surface model presented here and the curves of Figure 6 are in striking agreement with measurements of σ^o from certain classes of surfaces. Among the types of natural surfaces appearing to fit this model are the sea surface, certain sections of terrain (including desert and mountainous areas), and the lunar surface. A few samples of measured curves will be presented later.

4. Vegetation Cover: Average Radar Cross Section per Unit Area

Vegetation cannot be modelled well as a rough surface whose height varies about a mean plane, as in the preceding sections. Hence, there have been very few meaningful analytical treatments of the problem because of the general complexity. Several things occur in vegetation to complicate the problem. Nearly vertically oriented leaves, stems, and trunks result in multiple scattering between neighboring parts, especially where the foliage is dense. Furthermore, since the foliage represents no neatly defined interface, the incident wave can penetrate and even propagate through the foliage later for a certain distance.

The only meaningful analysis of a vegetation-resembling model (to this author's knowledge) was done by Peake.[11,12] He considers a model consisting of a layer of randomly-placed vertical-preferring dielectric cylinders. While he neglects multiple scattering between cylinders, he does take into account the fact that the wave can propagate into the layer and be attenuated by the cylinders. The final results he obtains for the average radar cross section per unit area are a function of four parameters related to the foliage: (1) the density of the cylinder spacing, (2) the cross-sectional area of the stems, or cylinders, (3) the water content of the stems, or cylinders, and (4) wavelength. The results are too complicated to be presented here, but two "typical" sets of curves are shown in Figure 7 as a function of angle of incidence.[9] Water content is taken to be 40 percent, and an X-band frequency is assumed. The quantity σ^o for both the vertical and the horizontal polarization states is shown. The parameters which are varied are A, the average cross sectional area of a typical stem, or cylinder, in cm^2, and N, the average number of stems, or cylinders, per cm^2. Peake notes that for a grass field, typical values of A are 1.3×10^{-2} cm^2 and for N are 1 to 4 blades/cm^2.

One notes that there is no strong return near normal incidence and that the return may actually increase near grazing incidence, most significantly for vertical polarization but also for horizontal. This is of course due to the stems, or cylinders, which are oriented near the vertical direction. This is a characteristic of much of the measured radar return from foliage also.

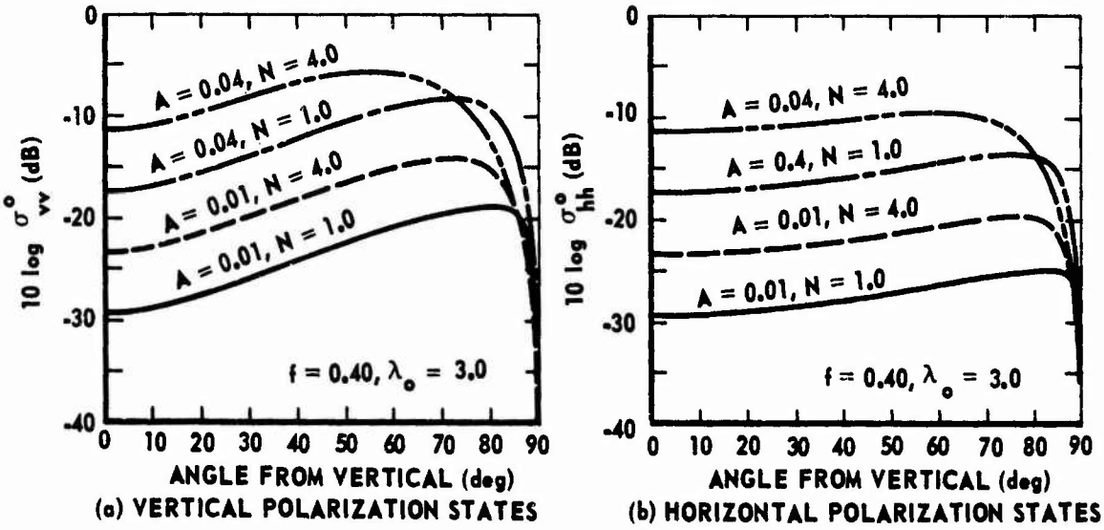

FIGURE 7. AVERAGE RADAR CROSS SECTION PER UNIT AREA σ^o FOR PEAKE'S VEGETATION-COVERED SURFACE MODEL VERSUS INCIDENCE ANGLE FOR VERTICAL AND HORIZONTAL POLARIZATION STATES

5. Slightly Rough Surface: Variance of Radar Cross Section per Unit Area

As mentioned in the section on volume clutter, it is often desirable to know the variance of the radar cross section in order to have an estimate of how far the received clutter power will deviate from its mean value. The variance of the radar cross section per unit area σ is defined as the average of the square of this quantity minus the square of the average, i.e.,

$$\text{Var}\,\sigma = \langle\sigma^2\rangle - \langle\sigma\rangle^2 = \langle\sigma^2\rangle - \sigma^{o2} \quad . \tag{22}$$

Since σ^o has been derived in a former section for a slightly rough surface, only $\langle\sigma^2\rangle$, or the second moment of the radar cross section per unit area, is needed.

An expression for $\langle\sigma^2\rangle$ has been obtained by this author using the same perturbation techniques as discussed previously (paragraph 1). Because of the complexity of the details, only the results will be presented here.

$$\langle\sigma^2\rangle = \frac{2}{3}\left(4\pi k_o^4 \cos^4\theta_i\ |\alpha|^2\right)^2 \left[W_2\left(-2k_o \sin\theta_i,\ 0\right)\right]^2 \quad , \tag{23}$$

where in this case $W_2(p,q)$ is defined in terms of the correlation function between $\zeta^3(x,y)$ and $\zeta(x + \Delta x,\ y + \Delta y)$, i.e., let $\langle\zeta^4\rangle R_2(\Delta x, \Delta y)\rangle$ $= \langle\zeta^3(x,y)\,\zeta(x + \Delta x,\ y + \Delta y)\rangle$. Then

$$W_2(p,q) = \frac{\sqrt{\langle\zeta^4\rangle}}{\pi^2}\int_{-\infty}^{\infty}\int_{-\infty}^{\infty} R_2(\Delta x,\Delta y)\, e^{-i\Delta x p\ -\ \Delta x q}\, d(\Delta x)\ d(\Delta y) \quad . \qquad (24)$$

As an example, when the surface height ζ is Gaussian distributed, $R_2(\Delta x,\Delta y) = R_1(\Delta x,\Delta y)$, and $\langle\zeta^4\rangle = 3\langle\zeta^2\rangle = 3(h^2)^2$. Then

$$\langle\sigma^2\rangle = 2\sigma^{02} \quad \text{and Var}\,[\sigma] = \sigma^{02} \quad . \qquad (25)$$

These equations show an important result: When the surface height is a Gaussian variable, the variance of the radar cross section per unit area is equal to the square of the average radar cross section per unit area. This relationship was shown to hold also for volume-distributed clutter. In fact it can be shown by finding the higher moments than the second that the probability density of the radar cross section is exponential when the surface is Gaussian. Hence the conclusion: The clutter power return from a slightly rough Gaussian surface has an exponential probability density distribution typical of separate distributed clutter sources.

When the surface height is not a Gaussian variable, the above statement is not strictly true. The error involved in this assumption is not expected to be appreciable, however.

6. Very Rough Surface: Variance of Radar Cross Section per Unit Area

The variance of the radar cross section per unit area is defined here in the same manner as in the preceding subsection, i.e., Eq. (22). As there the variance provides an estimate of the amount of deviation of received clutter power from a very rough surface from its average value. An expression for $\langle\sigma^2\rangle$, the average of the square of the radar cross section per unit area, or second moment, has been derived by this author and only the result is given here. The method used is based on the physical optics principle; most of the symbols and terminology used here are defined in paragraph 2 above on the average radar cross section per unit area of a very rough surface.

$$\langle\sigma^2\rangle = 2\left(\pi \sec^4\theta_i\ |R(0)|^2\right) P\left(\tan\theta_i,\ 0;\ \tan\theta_i,\ 0\right) \quad . \qquad (26)$$

The quantity $P\left(\zeta_x, \zeta_y; \zeta_x', \zeta_y'\right)$ in this equation is the joint probability density function for the surface slopes ζ_x, ζ_y in the x- and y-directions at the surface point (x, y) along with the surface slopes ζ_x', ζ_y' at the point (x', y'), where the points (x, y) and (x', y') are widely separated. In effect, if these two points are far enough apart, the surface slopes at one of them are independent of the surface slopes at the other. This demands that the surface region one is illuminating at a given time be considerably larger in its dimensions than the surface height correlation length ℓ; when this requirement is satisfied, then the random variables ζ_x, ζ_y are statistically independent of the random variables ζ_x', ζ_y'. Then the above probability density function can be written

$$P\left(\zeta_x, \zeta_y; \zeta_x', \zeta_y'\right) = P\left(\zeta_x, \zeta_y\right) P\left(\zeta_x', \zeta_y'\right) , \qquad (27)$$

where $P\left(\zeta_x, \zeta_y\right)$ is the simple joint density function of ζ_x, ζ_y at a given point (x, y) as defined in a previous section. Then Eq. (26) can be simplified and written in terms of σ^0, and the variance reduces to the expected result:

$$\langle \sigma^2 \rangle = 2\sigma^{02} \quad \text{and Var}\,[\sigma] = \sigma^{02} . \qquad (28)$$

Higher moments of σ may be derived by the same technique, and when the surface area illuminated is large compared to the surface height correlation length ℓ, the results simplify in the same manner as the above equation. The probability distribution of the radar cross section per unit area σ becomes exponential also. Again the conclusion can be stated: The clutter power return from a very rough surface, whose illuminated area is large compared to surface correlation length, has an exponential probability density distribution typical of separate distributed clutter sources.

When the surface area inside the resolution cell is not large compared to the very rough scale correlation length, the above results for the variance and conclusions are not true. In a short pulse radar, the area inside the resolution cell may not be large enough to meet this requirement. Such is the case, for example, when a radar pulse illuminates only a portion of a mountain simultaneously. In such a case, the variance of the received power from a very rough surface can be shown to approach infinity as the surface area inside the resolution cell approaches zero. The mathematics for this case are complicated and have not been solved, to this author's knowledge.

7. Measured Radar Cross Section per Unit Area for Sea Surface

Many measurements of σ^o have been made for the sea surface since World War II at a variety of frequencies, sea states, and incidence angles. Unfortunately, they are too numerous and at the same time, many of the measurements are incomplete or sketchy. Only a brief attempt is made to summarize them here.

Two sets of curves at different sea states as a function of incidence angle from vertical θ_i are presented here. These are made at X-band for both the vertical and horizontal polarization states.[9] In Figure 8(a), the wind is 3 knots, the waves are about 5 in. high (above the mean surface), and the ripples are about 0.8 in. or less. In Figure 8(b), the wind is 30 knots, the average wave height is 4 to 5 ft (above the mean surface), and the ripples are about 3.5 in. high. In this figure the surface contains very rough scales as well as slightly rough, and hence is a composite. The presence of the strong specular component near normal incidence is especially evident in (a), where the surface is not as disturbed. The larger return near grazing for the vertical polarization states is also evident, in agreement with mathematical results of previous sections.

A recent excellent collection or radar cross section measurements of the sea at various sea states and frequencies has been made by Nathanson.[5] Some of his results are presented here in Table II. These measurements are generally accurate to about 3 dB. The data presented here give a clear enough estimate of the magnitude of sea clutter power and should serve as a tool in radar system design.

One important fact is predicted by the tables: The sea clutter power return increases substantially, especially near grazing angles, as frequency increases. This behavior is expected and is in agreement with the mathematical results of previous sections.

8. Measured Radar Cross Section per Unit Area for Terrain

Measurements of σ^o for various types of terrain have also been produced in abundance. One of the most extensive sets of measurements was made by The Ohio State University.[13] These measurements were made at X-band through K_a-band frequencies. Dependence of σ^o upon angle of incidence for typical terrain types are shown here.[9] Figure 9 shows σ^o for a plowed field at X- and K_a-bands. Figure 10 shows σ^o for a 2 in. grass surface at these

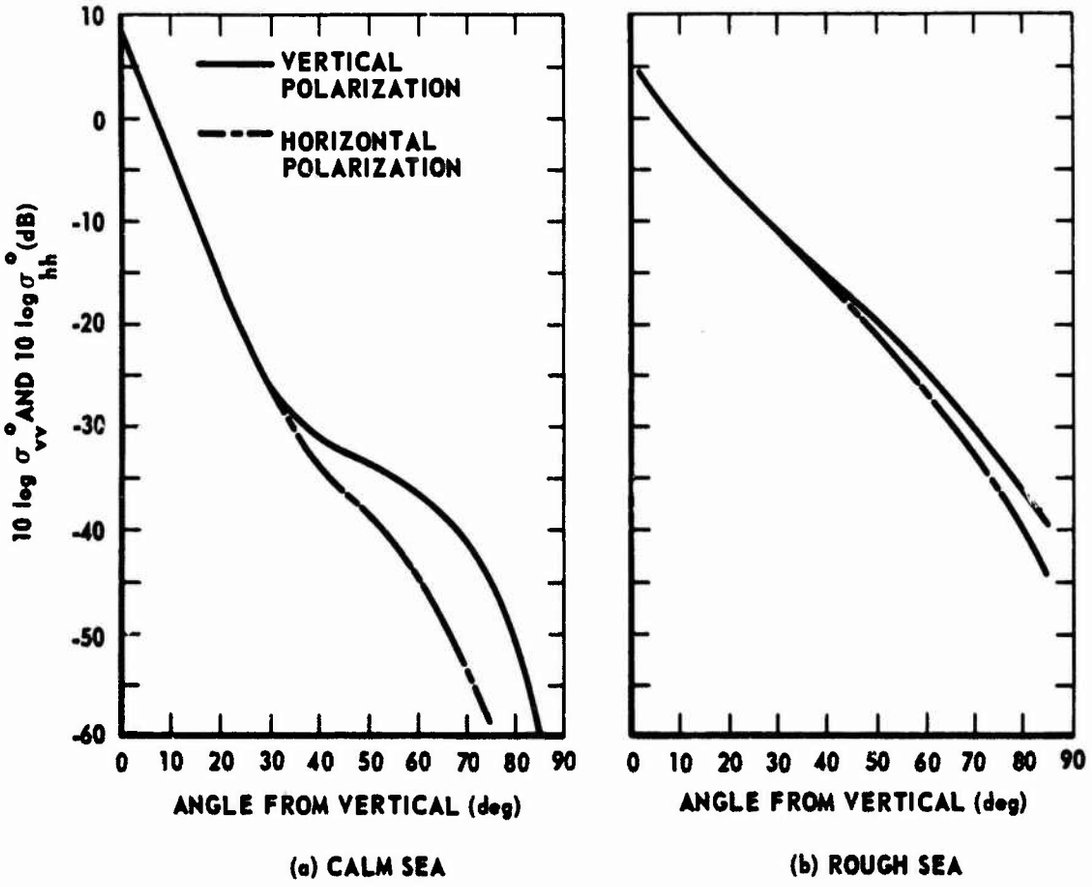

FIGURE 8. MEASURED AVERAGE RADAR CROSS SECTION PER UNIT AREA σ^{o} VERSUS INCIDENCE ANGLE FOR CALM AND ROUGH SEA SURFACE AT X-BAND

frequencies, while Figure 11 shows σ^{o} for a field of soybeans 3 ft deep. Figure 12 shows the return at X-band for a desert area, and Figure 13 shows σ^{o} for a built-up area (city) containing buildings.

To get a better idea of how σ^{o} varies over a wider frequency range, Table III was prepared from results collected by Nathanson.[5] Several important facts are evident from this table. (1) Land clutter power return near grazing is considerably greater than for sea clutter. (2) At lower frequencies, land clutter power return does not decrease significantly as it does for the sea clutter. These conclusions are undoubtedly caused by terrain features causing

TABLE II(a). MEASURED AVERAGE RADAR CROSS SECTION PER UNIT AREA σ^o FOR SEA SURFACE UNDER SEA STATE 1 (5 KNOT WIND)

Frequency	Polarization States	σ^o in dB for Various Grazing (or Depression) Angles					
		0.3 deg	1.0 deg	3.0 deg	10 deg	30 deg	60 deg
UHF	VV		-70	-60		-38	-23
0.5 GHz	HH		-84	-70			-22
S-band	VV	-62	-56	-52		-40	-24
3.0 GHz	HH	-74	-65	-59			-25
X-band	VV	-58	-50	-45	-42	-39	-28
9.36 GHz	HH	-66	-51	-48	-51		-26
K_a-band	VV			-41	-38	-37	-26
35 GHz	HH		-40	-43			

TABLE II(b). MEASURED AVERAGE RADAR CROSS SECTION PER UNIT AREA σ^o FOR SEA SURFACE UNDER SEA STATE 3 (15 KNOT WIND)

UHF	VV		-58	-43	-34	-28	-18
0.5 GHz	HH		-76	-61	-50	-40	-21
S-band	VV	-55	-48	-43	-34	-29	-19
3.0 GHz	HH	-58	-48	-46	-46	-38	
X-band	VV	-45	-39	-38	-32	-28	-17
9.36 GHz	HH	-46	-49	-39	-37	-34	-21
K_a-band	VV		-34	-34	-31	-23	-14
35 GHz	HH		-36	-37	-31		

TABLE II(c). MEASURED AVERAGE RADAR CROSS SECTION PER UNIT AREA σ^o FOR SEA SURFACE UNDER SEA STATE 5 (22 KNOT WIND) (Concluded)

Frequency	Polarization States	σ^o in dB for Various Grazing (or Depression) Angles					
		0.3 deg	1.0 deg	3.0 deg	10 deg	30 deg	60 deg
UHF	VV	-75			-25		
0.5 GHz	HH		-65	-53	-46		
S-band	VV	-50	-38	-35	-28		
3.0 GHz	HH	-44	-42	-37	-38		
X-band	VV	-39	-33	-31	-26	-20	-10
9.36 GHz	HH	-39	-33	-32	-31	-24	-12
K_a-band	VV		-31	-30	-26	-20	- 4
35 GHz	HH				-27	-20	

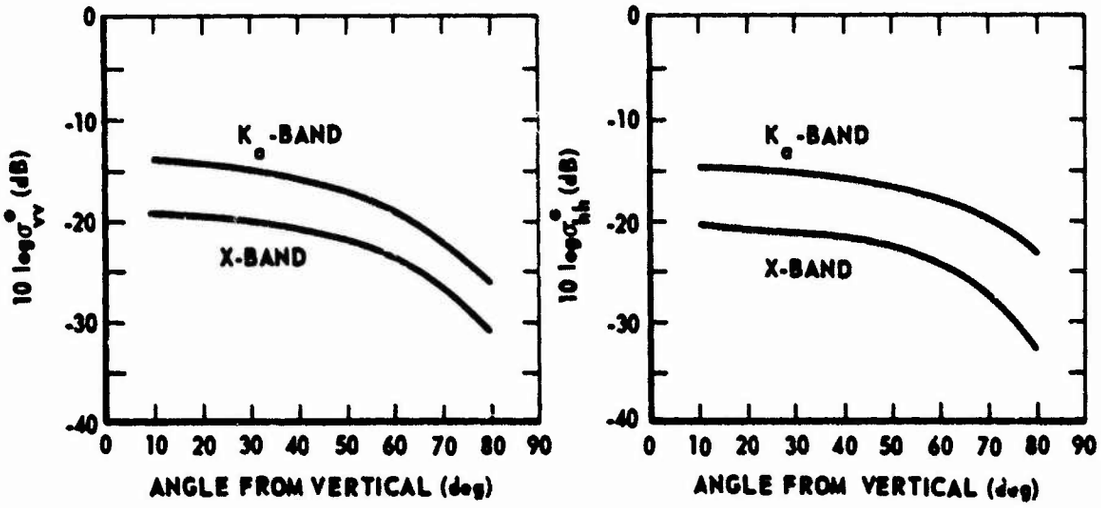

(b) HORIZONTAL POLARIZATION STATES (a) VERTICAL POLARIZATION STATES

FIGURE 9. MEASURED AVERAGE RADAR CROSS SECTION PER UNIT AREA σ^o VERSUS INCIDENCE ANGLE FOR PLOWED FIELD AT X- AND K_a-BAND

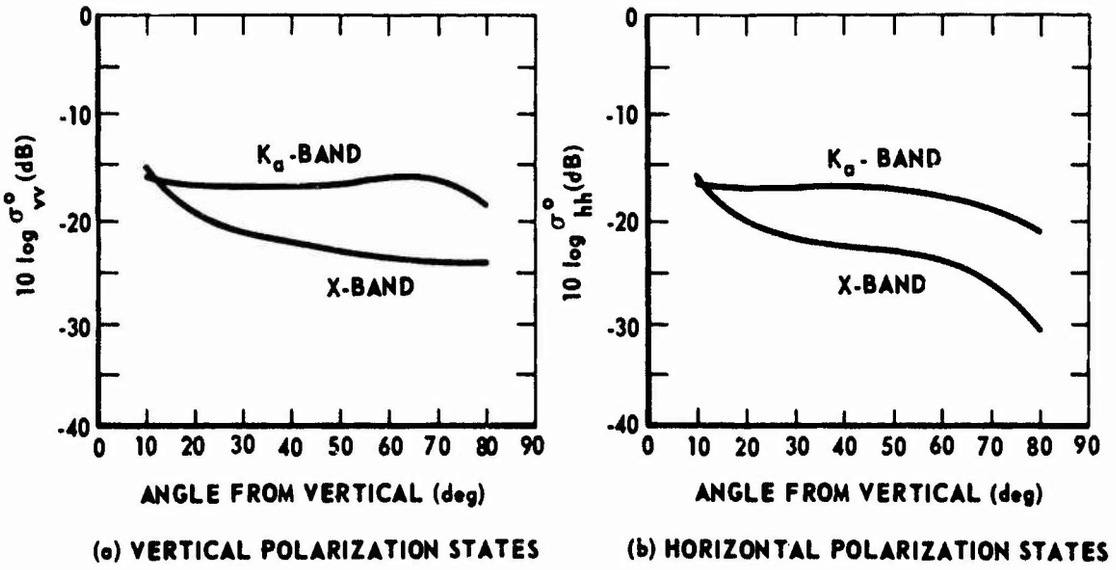

FIGURE 10. MEASURED AVERAGE RADAR CROSS SECTION PER UNIT AREA σ^{o} VERSUS INCIDENCE ANGLE FOR 2 INCH HIGH GRASS FIELD AT X- AND K_a-BAND

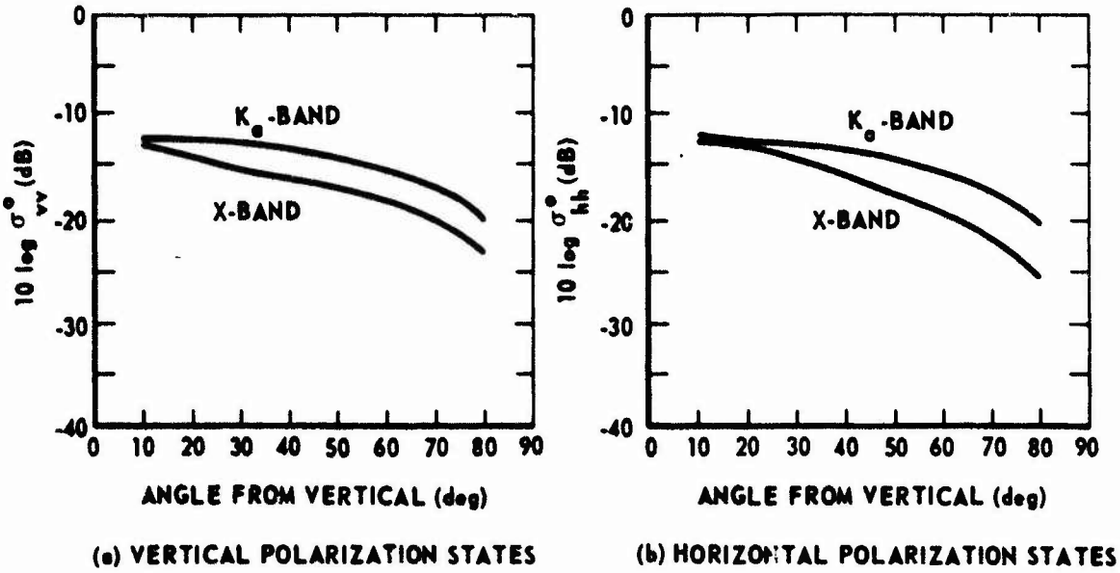

FIGURE 11. MEASURED AVERAGE RADAR CROSS SECTION PER UNIT AREA σ^{o} VERSUS INCIDENCE ANGLE FOR 3 FOOT DEEP SOYBEAN FIELD AT X- AND K_a-BAND

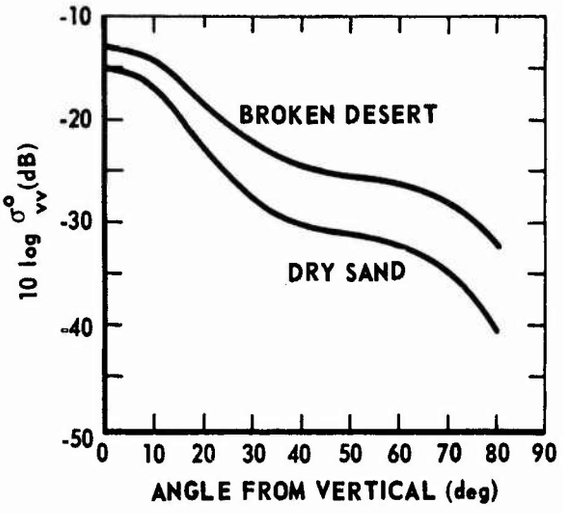

FIGURE 12. MEASURED AVERAGE RADAR CROSS SECTION PER UNIT AREA σ^{o} VERSUS INCIDENCE ANGLE AT X-BAND FOR GENTLY SLOPING DRY DESERT SAND AND FOR DESERT BROKEN BY PATCHES OF VEGETATION AND ROCKS

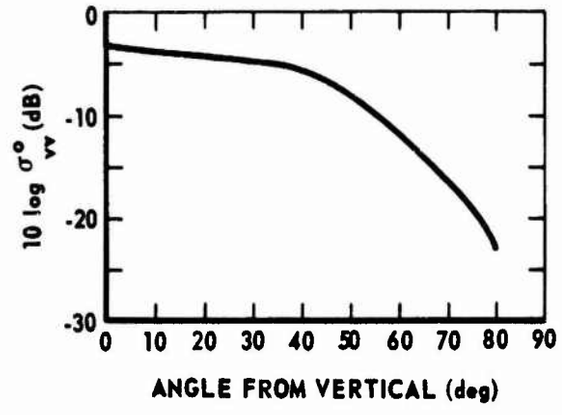

FIGURE 13. MEASURED AVERAGE RADAR CROSS SECTION PER UNIT AREA σ^{o} VERSUS INCIDENCE ANGLE AT X-BAND FOR BUILT-UP URBAN AREAS

scatter (viz., trees, buildings, hills, etc.) are large in terms of wavelength even down to the UHF band whereas sea waves are only large in terms of wavelength down to about S-band.

TABLE III. MEASURED AVERAGE RADAR CROSS SECTION PER UNIT AREA σ^o FOR LAND AND TERRAIN SURFACES. AVERAGE OF VERTICAL AND HORIZONTAL POLARIZATION STATES IS GIVEN

Frequency	σ^o in dB for Various Terrain Types and Grazing Angles											
	Desert		Cultivated Land		Open Woods		Wooded Hills		Small Houses		Cities	
	0-1 deg	10 deg	0-1 deg	10 deg	0-1 deg	10 deg	0-1 deg	10 deg	0-1 deg	10 deg	0-1 deg	10 deg
UHF			-38				-34				-30	
		-40	to	-36		-23	to	-22		-23	to	- 9
0.5 GHz			-30				-24				-22	
S-band							-47					
		-25		-21	-33	-23	to		-35	-23		-15
3.0 GHz							-32					
X-band							-36		-36			
	-38	-26	-36	-25	-30	-23	to	-25	to	-23	-24	-12
9.3 GHz							-30		-30			
K_a-band		-22	-20	-20		-19	-17	-19				
35 GHz												

Section VI. SPECTRA OF CLUTTER ECHOES

1. Signal Length and Its Relationship to Signal Spectrum

This section is concerned with the spectrum of echoes received from clutter. For the most part, the subject of interest will be the change in the received signal spectrum, produced by the clutter itself, from that of the transmitted signal. In general, the phenomena associated with clutter can produce widening of the transmitter signal spectrum,* as well as a shift to a new center frequency; narrowing of the spectrum can never be produced by random clutter sources. This subsection, however, is concerned with the spectrum of the signal itself without any change or degradation by the clutter sources. The section is not meant to be a thorough treatment of the subject; Section II provides a more thorough description of radar waveforms and their spectra which are commonly used in clutter rejection schemes. It does provide a necessary base, however, on which to discuss the further changes brought about by the clutter.

In general, the width of the signal spectrum centered at the carrier frequency is equal to the reciprocal of the signal length. For most systems attempting to separate a moving target from clutter by the Doppler shift between the signals, this spectrum width must be relatively small, e.g., of the order or 500 Hz or less. This in turn requires quite long signal trains, of the order of 2 msec or greater. Usually, the only way in a conventional radar of providing a signal this long and maintaining any kind of range resolution capability is to transmit a pulse train. The signal, then, is considered to be made up of the entire train of pulses, even though each individual pulse may be quite narrow. The frequency spectrum of such a pulse train consists of a train of spikes, each of which is narrow, e.g., 500 Hz for a 2 msec duration train, and which are separated in frequency by the pulse repetition rate f_{PR}.

While the width of an individual spike in the frequency spectrum is roughly proportional to the reciprocal of the total signal duration, the exact shape of the spike and its sidelobes, if any, are a function of the broad amplitude weighting of the time signal. Lower sidelobes about the spike can be obtained by amplitude tapering the pulse train. Specifically, the exact shape of one of the spikes is the Fourier transform of the amplitude modulation, or weighting, of the time signal train. In a phased array antenna, for example, one may desire to transmit a train of pulses in a given direction to separate a moving

---

* Broadening of the signal spectrum by clutter degrades the ability to resolve it in frequency and, hence, to reject it by any of the techniques described in Section II which are based on relative motion between target and clutter.

target from the clutter background. In this case, amplitude tapering of the pulse train may be necessary to reduce the sidelobes. The amplitude time weighting to provide minimum frequency sidelobes is directly analogous to the antenna aperture amplitude distribution problem for minimum antenna pattern sidelobes; the considerable amount of technology already available concerning the latter problem can be applied to the former with little difficulty.

In older, mechanically scanned systems, such as ground-based search radars where the antenna is rotated in azimuth, an amplitude tapering of the pulse train is provided by the antenna pattern itself. As the antenna rotates, its main lobe sweeps across a point target so that the individual pulses striking the target appear to start near zero, rise to a maximum as the antenna boresight points directly at the target, and fall off to zero as the antenna rotates off-target. Assume that $g_{AZ}(\varphi)$ is the one-way voltage pattern of the antenna in azimuth (normalized to unity at $\varphi = 0$). If the antenna is rotating, then $\varphi = \Omega t$, where Ω is the rotation rate in rad/sec. The received voltage amplitude of a pulse train from a point target is then proportional to $|g_{AZ}(\Omega t)|^2$ if the same antenna is used for transmitting and receiving. Then the shape of a spike of the frequency spectrum F(f) is proportional to the Fourier transform of this quantity, i.e.,

$$F(f) \sim \int_{-\infty}^{\infty} |g_{AZ}(\Omega t)|^2 e^{-i2\pi ft}\, dt \ . \tag{29}$$

For instance, if the antenna pattern is Gaussian, i.e., $|g_{AZ}(\varphi)|^2 = \exp(-2\varphi^2/\Delta^2)$, where Δ is the 3 dB azimuth beamwidth of the antenna, then the spectrum is $F(f) \sim \exp(\pi^2\Delta^2 f^2/2\Omega^2)$. In this case, the total 3 dB width of the frequency spectrum is $f_s = \frac{2\Omega}{\pi\Delta}$. As an example, the spectrum width for an antenna with a 2 deg azimuth beamwidth and rotation rate of 3 rps is $f_s \simeq 170$ Hz.

2. Spectrum Width due to Clutter Source Velocity Differences

In certain distributed clutter situations, signals reflected from the clutter are spread in frequency due to slight velocity differences between the clutter sources. This is the case, for instance, with falling raindrops which in practice have slightly differing velocities depending on drop size. It is also the case for trees and foliage waving in the wind. It is true for the sea surface, but the sea surface will be dealt with specifically later.

Figure 14 shows an infinitesimal packet of clutter particles moving in a vertical direction, while the radar views it from an aspect α with respect to the vertical. The praticles could represent raindrops, or they could represent

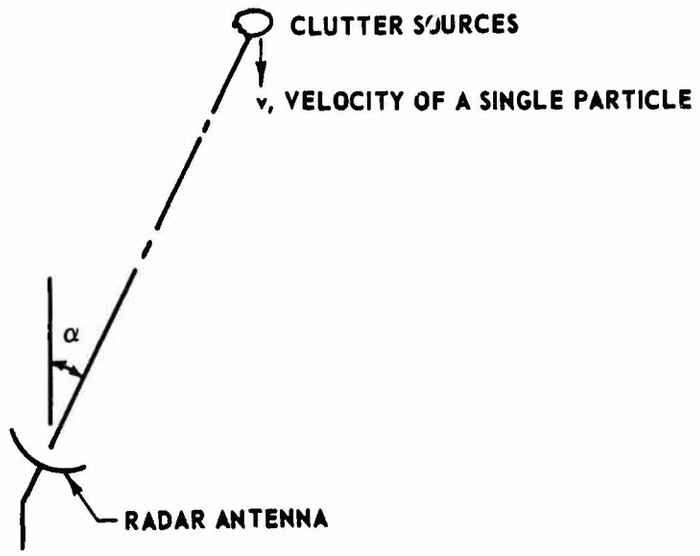

FIGURE 14. GEOMETRY FOR DISTRIBUTED CLUTTER SOURCES MOVING AT VELOCITIES CLOSE TO v WITH RESPECT TO RADAR ANTENNA

leaves of a tree. Assume all the N particles are moving in the same direction, i.e., the vertical direction, but have different velocities, i.e., v_1, v_2, ..., v_N. For simplicity, assume that a monochromatic signal illuminates the particles; the power density spectrum of such a signal is a unit impulse in the frequency domain centered at f_o, the carrier frequency, i.e., $S_i(f) = \delta\left(f - f_o\right)$. Define $p(v)$ as the probability density function for the velocity of a given particle. Then it may be shown in an elementary manner that the signal reflected from the particles has a power density spectrum $S_o(f)$ proportional to this probability density, i.e.,

$$S_o(f) \sim \frac{c}{2f_o \cos\alpha}\, p\left[\frac{f - f_o}{\left(2f_o \cos\alpha\right)/c}\right] . \qquad (30)$$

Simply interpreted, this equation shows that the received signal spectrum has the same shape, or functional form, as the probability density function for the particle velocities.

If the standard deviation, i.e., square root of the variance, of the random variable v is v_{sd}, then the half-power bandwidth Δf of the clutter spectrum is given roughly by the following equation

$$\Delta f = \frac{4v_{sd}}{c} f_o \cos \alpha \quad , \tag{31}$$

which is easily seen from inspection of Eq. (30).

Mean drop velocities in a rainfall vary between 4 to 6 m/sec for light rains to 9 m/sec for heavy rains.[6] The standard deviation of drop velocities about the mean v_{sd} is about 1 m/sec. There are usually a significant number of smaller sized raindrops which fall very slowly, even in a heavy storm, resulting in a slow fall off of p(v) for small v. As an example, at S-band $\left(f_o = 3000 \text{ MHz}\right)$ and at an elevation angle of 10 deg, i.e., $\alpha = 80$ deg, a heavy rainfall will shift the center frequency of the clutter return by 31 Hz and will produce a frequency spread for a monochromatic incident wave of about 7 Hz between half-power points. In general, however, there will be a significant amount of power in a bandwidth of about 40 Hz, since the energy does not fall off rapidly beneath the lower 3 dB point. This spreading also increases as the elevation angle increases; if the radar is looking vertically ($\alpha = 0$), the spread is about 200 Hz at S-band.

The standard deviation of foliage velocity is a function of the wind speed. Nathanson[5] has found from examination of experimental data that this velocity standard deviation for wooded terrain averages about 0.03 m/sec for 0 to 10 knot winds, about 0.1 m/sec for a 15 knot wind, and about 0.3 m/sec for a 20 knot wind. For an S-band search radar looking in the horizontal direction across the foliage, i.e., $\alpha = 0$ in this case because foliage motion is horizontal, this results in a half-power frequency spread of a monochromatic incident wave of about 4 Hz.

3. Spectrum Spreading for Distributed Clutter due to Relative Motion and Finite Beamwidth

The preceding subsection examined the spectral shift and spreading of a monochromatic incident wave due strictly to velocity deviations of the clutter particles. This subsection is concerned with the spectrum spreading effect of distributed clutter sources moving at a velocity v caused by a finite beamwidth.* All of the clutter sources inside the resolution cell are assumed to

* In practice, spectral spreading is a result of several effects acting simultaneously; for example, one usually has both a finite beamwidth as well

be moving in the same direction with respect to the radar antenna and at the same velocity v. The results of this subsection apply to the situation where the antenna beam itself is in motion with respect to the clutter, as in an airborne or missile-mounted radar. It can also apply to the case where the radar is stationary but the clutter particles are in motion, as, for instance, in a rain shower.

The analysis here can apply to volume-distributed clutter, such as rain, inside the resolution (Figure 15). The clutter particles in this case fill a

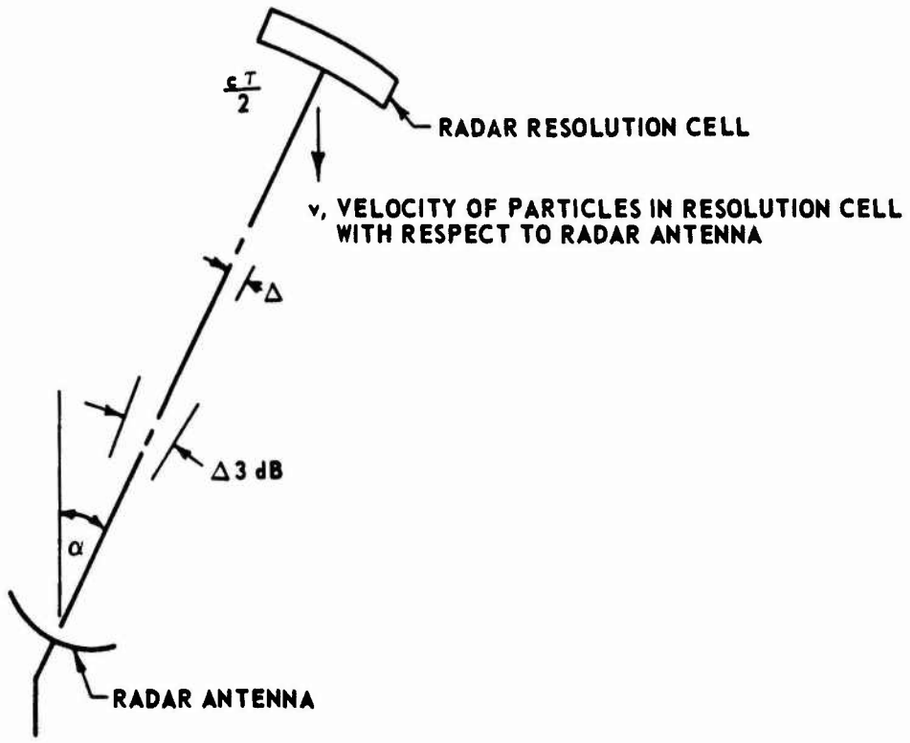

FIGURE 15. GEOMETRY OF VOLUME-DISTRIBUTED CLUTTER SOURCES MOVING AT CONSTANT VELOCITY v WITHIN A RADAR RESOLUTION CELL OF FINITE BEAMWIDTH

---

as clutter particle velocity differences. It is least confusing, however, to analyze these effects separately, and later it will be shown how they can be combined.

truncated section of cone of thickness $\frac{c\tau}{2}$. The angle α is measured between the velocity vector and the antenna boresight. The angle Δ to a portion of the resolution cell from boresight lies in the plane containing these two directions, i.e., the plane of the page, in that case. For a ground-based radar looking up through rain clutter, the raindrop velocity is usually close to the vertical direction and, in this case, the angle $\frac{\pi}{2} \alpha$ is the elevation angle of the beam.

The analysis can also apply to surface-distributed clutter when viewed from a moving airplane or missile platform (Figure 16). The radar platform velocity is v_A and the component of velocity on the surface in this case is v. The angle α, then, is the angle between the velocity vector projection on the ground plane and the plane of incidence. The plane of incidence contains the vertical to the surface and the antenna boresight. The angle Δ is measured in a plane containing the antenna boresight and an arc struck on the surface by the range resolution cell, i.e., in a plane normal to the plane of incidence.

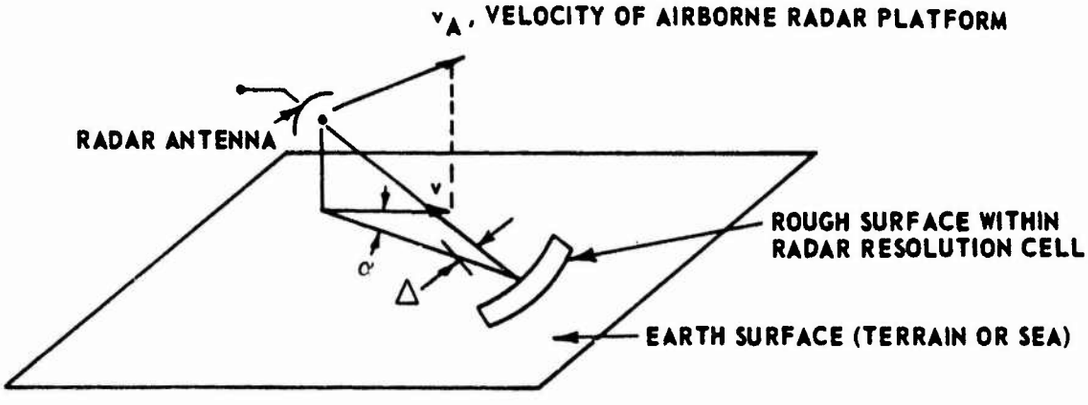

FIGURE 16. GEOMETRY OF SURFACE-DISTRIBUTED CLUTTER VIEWED FROM MOVING RADAR PLATFORM FOR RADAR RESOLUTION CELL OF FINITE DIMENSIONS

The mechanism responsible for spreading of the spectrum in this case is not difficult to understand. Even though the velocity of all the clutter sources across the resolution cell is the same with respect to the antenna, the radial component of their velocities varies slightly with Δ over the finite beamwidth of the resolution cell. It is the radial velocity component of a moving particle

which determines the Doppler shift of the wave reflected from it. Hence, the return signal spectrum from the clutter sources within the entire resolution cell will be spread over a finite bandwidth when the incident signal is monochromatic. This spectral spreading is a function of antenna beamwidth in the Δ direction, being less for narrower beamwidths; it is independent of range.

As before, assume a one-way voltage pattern of the antenna in the Δ-direction as $g(\Delta, \epsilon)$, normalized to unity on boresight, i.e., at $\Delta = \epsilon = 0$. The angle ϵ is measured in the plane perpendicular to that containing Δ. The power spectral density received when the same antenna is used for transmitting and receiving is obtained by integration $|g(\Delta, \epsilon)|^4$ times the reflected power spectrum from a given point at angle Δ from boresight. The latter energy spectrum is an impulse function which varies with Δ.* Only the integration over Δ is of concern here, for it is this process which provides the received signal spectrum. Other constants appearing in the radar range equations, i.e., Eq. (2) and (4), are neglected here also for simplicity. Then the received signal spectrum due to spectral spreading of the incident monochromatic signal is

$$S(f) \sim \frac{1}{\frac{2v}{c} f_o \sin \alpha} \left| g\left(\frac{f - f_o \left(1 - \frac{2v}{c} \cos \alpha\right)}{\frac{2v}{c} f_o \sin \alpha}, \epsilon \right) \right|^4 . \qquad (32)$$

Interpreted simply, the above equation shows that the received signal power spectrum has the same shape, or functional form, as the antenna pattern. The above result is valid so long as $\alpha \neq 0$. The approximate half-power bandwidth Δf of the clutter spectrum may be easily determined from the above equation in terms of the 3 dB beamwidth Δ_{3dB} in the Δ-direction:

$$\Delta f = \frac{2v}{c} f_o \Delta_{3dB} \sin \alpha \quad , \qquad (33)$$

here Δ_{3dB} is expressed in radians.

---

* For volume clutter, one also integrates over ϵ. Since the radial velocity of clutter sources does not vary with ϵ, this integration may be approximated in the usual manner, i.e., $\int_{-\infty}^{\infty} |g(\Delta, \epsilon)|^4 \, d\epsilon = \epsilon_{3dB} |g(\Delta, 0)|^4$, where ϵ_{3dB} is the half-power beamwidth in the ϵ direction. For surface clutter, ϵ is a function of time as the pulse propagates across the ground. One does not integrate over ϵ in this case, but multiples by $\frac{c\tau}{2 \cos \beta}$, the surface width subtended by the resolution cell. (β is grazing angle.)

As an example, consider a ground-based S-band radar with a half-power elevation beamwidth of 6 deg. Let the elevation angle of the beam be 10 deg, i.e., α = 80 deg. Assume a moderate rainstorm where the drops are falling vertically at a mean velocity of 9 m/sec. The Doppler shift in the center of the spectrum is 31 Hz. The half-power bandwidth Δf of the received clutter spectrum, for a monochromatic transmitted signal, is about 18.6 Hz. This spectrum spreading caused by raindrops falling through a finite sized resolution cell is often called "shear."

When $\alpha \simeq 0$, the clutter signal power spectrum has approximately the following form:

$$S_o(f) \sim \frac{1}{\sqrt{\frac{vf_o}{c}\left|f - f_o\left(1 - \frac{2v}{c}\right)\right|}} \left| g\left[\sqrt{\frac{c}{vf_o}\left|f - f_o\left(1 - \frac{2v}{c}\right)\right|}, \epsilon\right]\right|^4 . \quad (34)$$

The half-power bandwidth in this case is

$$\Delta f \simeq \frac{vf_o}{2c} \Delta_{3dB}^2 , \quad (35)$$

where Δ_{3dB} beamwidth is measured in radians. The above results for $\alpha \simeq 0$ have application to a moving radar, such as that on a homing missile looking directly ahead through rain, or the terrain-avoidance radar on an aircraft, which is looking at the ground straight ahead. As an example, assume that a missile looking ahead is flying at 600 knots, i.e., v $\simeq$ 300 m/sec, and its S-band radar half-power beamwidth is 6 deg. Then the rain clutter spectrum spreading due to the finite beamwidth is about 15 Hz, while the Doppler shift of the spectrum center is about 6 kHz from that of the transmitter frequency. One can see that the clutter spectrum spreading is not nearly as great when the radar is looking ahead, i.e., $\alpha \simeq 0$, as it is when the radar is looking off to the side. For comparison, if the same 6 deg beamwidth S-band antenna on an aircraft at 600 knots were looking off to the side, α = 90 deg, the clutter spectral spread would be about 700 Hz.

4. Spectrum Spreading for Distributed Clutter due to Relative Motion and Finite Pulse Length

Another factor causes spectral spreading of a monochromatic wave incident on distributed clutter. This is the finite size of the illuminated area. The effect is illustrated in Figure 17. The component of velocity in a direction containing the plane of incidence is v. The range resolution cell depth is

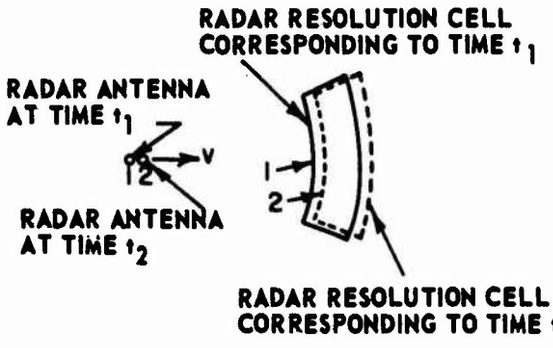

FIGURE 17. GEOMETRY OF DISTRIBUTED CLUTTER AT GIVEN RANGE FROM MOVING RADAR AS VIEWED AT TWO DIFFERENT TIMES

$\frac{c\tau}{2}$ for volume-distributed clutter. It is $\frac{c\tau}{2 \cos \beta}$ for surface clutter, where β is the grazing angle, and the velocity is assumed to be in a plane parallel to the surface. Assume that the return at radar position 1 at elapsed time t_a comes from the solid resolution cell. Then on the next pulse transmission, the radar is located at position 2. The return at elapsed time t_a now comes from the dashed resolution cell. Both of these resolution cells do not contain the same clutter sources, but a portion of the sources are shared by the two. As the velocity increases there is less overlap for a given time.

If one computes the correlation coefficient for the overlapping areas for a given elapsed time T he finds it is

$$R(T) = \begin{cases} 1 - \frac{vT}{L} & \text{for } \frac{vT}{L} < 1 \\ 0 & \text{for } \frac{vT}{L} > 1 \end{cases}, \qquad (36)$$

where L is the length of the resolution cell, i.e., $\frac{c\tau}{2}$ for volume clutter and $\frac{c\tau}{2 \cos \beta}$ for surface clutter.

The Fourier transform of this correlation function is then the received power density spectrum of the returned signal. This is

$$S_o(f) = \frac{\sin^2\left(\frac{\pi L}{v} f\right)}{\pi^2 \frac{L}{v} f^2}. \tag{37}$$

The approximate half-power bandwidth of this spectrum is

$$\Delta f = \frac{v}{L} \tag{38}$$

As an example, consider an aircraft with a narrow pulse (τ = 0.1 μsec) flying at 600 knots and looking straight ahead. The length L of the area is then $\frac{c\tau}{2}$, where the grazing angle β for surface clutter is considered small. Then the half-power bandwidth of the clutter spectrum is 20 Hz.

Notice from Eq. (37) that as velocity v approaches zero or as the resolution cell length L approaches infinity, the spectrum approximates an impulse function. This is expected, since the input power spectrum is an impulse function, and when there is no apparent motion, there should be no effect on the input spectrum. It is also interesting to note that the preceding section showed that decreasing the size of the resolution cell by decreasing beamwidth has the effect of decreasing the spectral spreading. Here, however, the decrease of the cell size L is shown to increase the spectral spreading. This is because the spectral spreading arises from different mechanisms in each case.

5. Spectrum Spreading from Sea Surface due to Surface Movement: Slightly Rough Scale

The sea surface is unique in that the roughness is in motion as a function of time. Hence, one would expect the sea to produce spreading of a monochromatic incident signal spectrum, even for a stationary or ground-based radar. This subsection will be concerned with the slight roughness present on the ocean surface, i.e., capillary waves. In a preceding section it was shown that this slight roughness, roughness whose scale is less than wavelength, can be treated analytically by a perturbation technique. It was also noted that when larger scale roughness is also present, i.e., swell, or gravity waves, the slight roughness is responsible for backscattered power near grazing incidence. It will be the purpose of this section to show the effect of this slight roughness, when it is in motion, on the spectral spreading of a monochromatic incident wave.

The analysis of the case where the roughness is in motion proceeds in much the same manner as where the roughness is stationary. The surface in this case is merely made a function of another variable, time. The perturbation approach is used.[7, 11, 12] Details in the derivation are omitted here for lack of space and only the result is given. Much of the terminology is as defined in Section V accompanying Eq. (13) and (14). The results presented below for the power density spectrum are normalized as radar cross section per unit surface area per hertz bandwidth.

$$S_o(f) = 4\pi^2 k_o^4 \cos^4 \theta_i \, |\alpha|^2 \, W_i\left(-2k_o \sin \theta_i, \, 0, \, 2\pi f\right) , \qquad (39)$$

where all symbols are as defined with Eq. (13), and $W_i(p, q, w)$ is the spectral density of the surface roughness height in two spatial dimensions (corresponding to p and q) and the time variable (corresponding to w). It is defined in terms of the surface height correlation function, $\langle \zeta(x, y, t)\, \zeta(x + \Delta x, y + \Delta y, t + \Delta t) \rangle = h^2 R_1(\Delta x, \Delta y, \Delta t)$, as follows:

$$W_i(p, q, w) = \frac{h^2}{\pi^2} \int_{-\infty}^{\infty} \int_{-\infty}^{\infty} \int_{-\infty}^{\infty} R_1(\Delta x, \Delta y, \Delta t)\, e^{-i\Delta x p \, - \, i\Delta y q \, - \, i\Delta t w} \, d(\Delta x)\, d(\Delta y)\, d(\Delta t) \quad . \qquad (40)$$

Here $\zeta(x, y, t)$ is the random variable representing the slightly rough surface above the x-y plane at time t.

Equation (39) shows that the power spectral density of a monochromatic signal scattered from an undulating slightly rough surface is directly proportional to the height spectral density of the moving surface itself. As an example, consider a Guassian height correlation coefficient, $R_1(\Delta x, \Delta y, \Delta t) = \exp[-(\Delta x^2 + \Delta y^2)/\ell^2 + \Delta t^2/T^2]$, where all three of the variables, Δx, Δy, and Δt, are assumed uncorrelated. Physically T has the interpretation of the correlation time duration of the rough surface and the height roughness spectrum from Eq. (40) becomes

$$W\left(-2k_o \sin \theta_i, \, 0 \, 2\pi f\right) = \frac{h^2 \ell^2 T}{\pi^{3/2}} \exp\left(-k_o^2 \ell^2 \sin^2 \theta_i \, - \pi^2 T^2 f^2\right) . \qquad (41)$$

Then the power spectral density for the slight roughness becomes

$$S_o(f) = \sigma^o \pi^{1/2} T \exp(-\pi^2 T^2 f^2) \quad , \qquad (42)$$

where σ^o is the average radar scattering cross section per unit surface area as defined by Eq. (13) and (17).

For the slight roughness on a water surface, the correlation duration T is likely to be short, i.e., of the order of 0.2 sec. Then the bandwidth of the signal is relatively small, i.e., 2.5 Hz. One point is important, however; the bandwidth of the received signal does not vary with the transmitted frequency. In all the other sections here involving clutter source relative motion, the bandwidth is shown to be directly proportional to transmitted frequency. In all the other sections, however, the individual clutter sources are assumed relatively far apart with respect to each, and hence the phase change introduced by each is independent, being proportional to source velocity and incident frequency. For the slightly rough surface, however, the distance between wavelets is small compared to wavelength, and their motion does not exceed a wavelength. Hence, a different mechanism is responsible for producing spectral spreading here.

6. Spectrum Spreading from Sea Surface due to Surface Movement: Very Rough Scale

This section will be concerned with that portion of the sea surface roughness which may be larger than wavelength in height scale, i.e., the very rough component. The latter usually includes what oceanographers term "swell," which is one of the two types of gravity waves. This large-scale roughness is also in motion, and hence will produce spectral broadening of an incident monochromatic radar wave. The analysis is based upon physical optics, where one allows the surface height $\zeta(x, y, t)$ to be a function of time as well as space. Then the correlation coefficient of the surface height is a function of these three variables also, as described in the preceding paragraphs. Again, the mathematical details are omitted here and only the results are presented.

The received power spectral density for an incident monochromatic signal is again expressed in terms of radar scattering cross section per unit surface area per hertz bandwidth. Much of the symbols and terminology have been defined previously in Section V for Eq. (18).

$$S_o(f) = \frac{c}{4f_o} \sec^5 \theta_i \, |R(0)|^2 \, P\left(\tan \theta_i,\ 0,\ \frac{f}{2\frac{f_o}{c}\cos \theta_i}\right), \qquad (43)$$

where $P\ \zeta_x, \zeta_y, \zeta_t$ is the joint probability density function for the surface slopes ζ_x and ζ_y in the x- and y-directions and for the vertical surface velocity ζ_t, i.e., $\zeta_t = \frac{\partial \zeta}{\partial t}$. For the sea surface under normal conditions, these three variables are usually correlated to some extent, as witnessed by the presence of horizontally moving waves, which appear to last for a certain time duration.

A more thorough analysis would take this surface anisotropy into account. For the brief consideration here, however, the surface will be assumed to be isotropic with ζ_x, ζ_y, and ζ_t uncorrelated.* Such an isotropic roughness may be thought of as an average of the sea surface over all possible look directions.

For example, assume a Gaussian joint density function for $P(\zeta_x, \zeta_y, \zeta_t)$. Then the power spectral density becomes

$$S_o(f) = \sigma^o \frac{1}{(2\pi)^{3/2} 2\frac{v_{sd}}{c} f_o \cos\theta_i} \exp\left[-\frac{1}{2}\left(\frac{f}{2\frac{v_{sd}}{c}\cos\theta_i}\right)^2\right]. \quad (44)$$

Here σ^o is the average radar cross section per unit surface area, as defined by Eq. (20). The quantity v_{sd} is the standard deviation of the vertical surface velocity ζ_t and is given in terms of the mean square surface height h^2 and wave correlation duration T as follows

$$v_{sd}^2 = \frac{2h^2}{T^2} . \quad (45)$$

Equations (43) and (44) illustrate that clutter spectral spreading arising from undulation of a very rough surface produces a bandwidth proportional to the surface velocity and illuminating frequency. This is expected, since scattering from a very rough surface arises from areas whose slopes are oriented so that they specularly reflect. As the surface moves, these specular areas move about and produce phase changes proportional to surface velocity and illuminating frequency. In this respect, the mechanism here is nearly the same as that for isolated, moving particles, such as chaff or raindrops; the similarity is also borne out by the similarity of Eq. (43) with (30) for isolated particles. The mechanism is different from that of the slightly rough surface, as discussed in the preceding section.

---

*An attempt to include surface anisotropy would necessarily include at least two, and possibly three, additional constants in the model. These would define the ocean wave propagation direction with respect to the radar, the wave phase velocity, the correlation lengths in the x- and y-directions, etc. More parameters are accompanied, unfortunately, by greater obscurity.

As an example, assume a surface velocity standard deviation $v_{sd} \approx 1$ m/sec, typical of the sea surface. At S-band $\left(f_o = 3000 \text{ MHz}\right)$ and incidence angle $\theta_i = 80$ deg (grazing angle of 10 deg), the half-power bandwidth induced by the roughness motion is about 8 Hz.

7. Spectrum Spreading from Sea Surface due to Surface Movement: Experimental Results

In practice, the sea surface consists of several scales of roughness, with at least one scale which is smaller in height than wavelength, i.e., slight roughness, and usually with a roughness scale larger in height than wavelength, i.e., very rough component. As discussed in paragraph 4, the scattered power from such a composite surface can be modelled by adding the cross sections of each of these components, and the result is at least more valid than either one alone. The same superposition is also valid for the clutter spectrum, but the results are complicated and depend upon many parameters, e.g., angle of incidence, wavelength, polarization, slight roughness surface statistics, large-scale roughness surface statistics, and the sea surface time statistics. A precise treatment would involve a more thorough study of actual ocean surface space and time statistics for different sea states. Then the results could be added together in a meaningful fashion to obtain a parametric study of the sea-induced clutter spectrum. Without a more detailed knowledge of these sea surface statistics, it is difficult to see at which incidence angles the slight roughness clutter spectrum dominates the very rough scale spectrum, and conversely. The purpose of the preceding two sections was to provide a physical interpretation of the clutter mechanisms giving rise to spectral spreading.

For the purposes of this report, only rough estimates are needed for clutter power bandwidths induced by the sea. Many measurements have been made of this clutter bandwidth.[5] It is understood here that the clutter signal spectrum under discussion is the coherent signal, i.e., at an IF frequency. Another clutter signal spectrum can be defined after amplitude detection; the one-sided bandwidth of the latter is approximately twice that of the former.

The half-power bandwidth may be roughly defined as follows

$$\Delta f = \frac{2\Delta v}{c} , \tag{46}$$

where Δv is the average half-power sea surface velocity spread. This average is over various grazing angles and polarization directions. It is found that Δv varies linearly from about 0.7 m/sec for Sea State 1 (wind speed of 5 knots),

being about 1.8 m/sec for Sea State 3 (wind speed about 13 knots), to about 2.7 m/sec for Sea State 5 (wind speed about 22 knots).[5] The measurements show that Δv is often somewhat larger than these values for horizontal polarization, by 20 to 30 percent, while it is often somewhat lower for vertical polarization, also about 20 to 30 percent. As an example, at S-band $\left(f_o = 3000 \text{ MHz}\right)$, one can expect spectral spreading as much as 54 Hz for Sea State 5 from these data.

8. Combination of Several Spectral Spreading Effects

The past subsections have considered separately several properties of clutter which can cause spectral spreading of an incident monochromatic signal. In practice, several of these effects are usually present simultaneously. Furthermore, the incident signal itself, as mentioned in the first subsection, is not monochromatic, but has a central spectral spike of finite bandwidth. How then does one combine these various effects to obtain the total spectrum of the received clutter signal?

It is not difficult theoretically to show that the resultant signal spectrum $S_{or}(f)$, when several of the preceding processes interact, is the convolution of the separate spectra. Assume three of the preceding processes produce spreading, each with its own spectral response $S_{o1}(f)$, $S_{o2}(f)$, $S_{o3}(f)$, to a monochromatic incident signal. Then

$$S_{or}(f) = \int_{-\infty}^{\infty} \int_{-\infty}^{\infty} S_{o1}(\mu) S_{o2}(\xi - \eta) S_{o3}(f - \eta) d\eta d\xi \ . \tag{47}$$

Although the above convolution technique is exact, it is not very handy when one is able only to make rough estimates of the various power spectra. A simpler rule of thumb is available in this case for the total bandwidth of the clutter spectrum. It is obtained from the above equation when one assumes that the processes responsible for each spectrum are independent of each other. The total 3 dB clutter signal bandwidth Δf_t may be found as follows:

$$\Delta f_t^2 = \Delta f_s^2 + \Delta f_1^2 + \Delta f_2^2 + \ldots \ . \tag{48}$$

where Δf_s is the half-power bandwidth of the transmitted signal, Δf_1 is the half-power bandwidth of the $S_{o1}(f)$, etc.

Section VII. SUMMARY AND CONCLUSIONS

The magnitude of the received signal from distributed clutter sources is shown to depend on the size of the radar resolution cell; it depends on its volume for space-distributed clutter particles and upon a surface area subtended by the cell for surface clutter. Since the resolution cell size increases with radar range, the clutter return increases also at greater ranges; this is especially true of volume clutter, such as rain. The obvious means of reducing the clutter echo is to reduce the size of the resolution cell by decreasing the antenna beam-width and signal pulse length. The problem of surface clutter with a ground-based radar can be obviated considerably by the use of horizontal polarization.

The average radar cross section per unit volume for particle scatterers is shown to depend on the particle density times the scattering cross section of each individual particle. For raindrops at frequencies up through K-band, this cross section varies with the fourth power of frequency, indicating the significant advantage in the use of lower frequencies to minimize weather clutter. Experimental results are presented which clearly show this fourth power dependence of the clutter power on frequency. The average radar cross section of rain is also shown to depend upon the sixth power of the drop radius; this points up the considerable increase in clutter return one can expect from storms with large raindrops. For half-wave chaff dipoles, the radar cross section depends upon the reciprocal of the square of frequency.

The standard deviation (or square root of the variance) of the radar cross section per unit volume for space clutter is equal to the mean itself. (The standard deviation gives an estimate of how much the received power fluctuates about the mean.) Furthermore, the probability density of this radar cross section is exponential, and hence the voltage received from volume-distributed clutter is a narrow-band Gaussian signal.

Radar waves are shown to attenuate exponentially with distance through rain; this is derived theoretically in Appendix A, and is confirmed by measured results presented. The mathematics shows that the attenuation coefficient (in decibels per propagation distance) varies at least linearly with frequency; the exact theoretical relationship is complicated because of the variation of the water drop dielectric constant with frequency also. Experimental evidence indicates a variation with frequency to the 2.8 power over the upper end of the microwave region. Theory shows that this attenuation coefficient also varies linearly with raindrop density and with the third power with drop radius. These results are also in general agreement with measurements.

The average radar cross section per unit area for a rough surface is produced in general by two mechanisms: the presence of both a large-scale roughness, i.e., roughness height is greater than a wavelength, and small-scale roughness, i.e., roughness height is less than a wavelength. The physical processes responsible for scatter in each case are different. Areas of the surface oriented normal to the line of sight are responsible for the backscattered power in the case of the large-scale roughness; hence, this component is dominant for backscattering near the vertical to the surface. The analysis shows that the backscattered power for large-scale roughness is independent of frequency, and is dependent only on the probability that the surface slope in a given region is oriented normal to the line of sight. The power scattered from the small-scale roughness, however, is proportional to the spectral density of the surface height components which make up the rough surface. In addition, this power varies with the fourth power of frequency. Curves are shown for radar cross section computed from these models as a function of the surface parameters.

Results derived for the report show that when the rough surface height is a Gaussian random variable, the standard deviation of the power scattered from the slightly rough surface is equal to the mean power. Higher moments can be derived, and the results show that the received voltage from such a Gaussian surface is itself a narrow band Gaussian signal. This fact has not been mentioned before, and it indicates that clutter signals from this type of surface have the same statistical nature as clutter from volume-distributed scatterers.

On the other hand, the standard deviation of the power scattered from the large-scale roughness becomes equal to the mean power when the surface area illuminated is large compared to the surface roughness dimensions; when this is true, the received voltage from the very rough surface is also a narrow band Gaussian signal. Hence the Gaussian nature of the received signal is established even when the large-scale roughness height itself is not Gaussian.

In general, most natural surfaces (such as the sea surface) at microwave frequencies are made up of both large-scale and small-scale roughnesses. It is shown that the small-scale roughness is responsible for power backscattered near grazing incidence; it is near grazing that most of the terrain and sea surface clutter problems of practical interest in a radar system arise. Experimental results for the average radar cross section of the sea surface are presented. The measured data near grazing show that this quantity increases with frequency, verifying the fact that the small-scale roughness is indeed the mechanism producing the scattering.

Land surfaces covered with foliage or vegetation are more difficult to analyze theoretically. One model for a vegetation layer has been treated, and curves for the average radar cross section per unit area computed from this model are given. Analysis of the model shows that scattered power remains strong even near grazing incidence. Return is greater for vertical polarization than for horizontal. Both of these facts can be attributed to the presence of stems and stalks which are oriented near the vertical direction. Experimental results are also presented for grassy fields, crops, and wooded areas; these tend to follow the predictions of the model. The measured results are not as sensitive to frequency as the scattered power from the sea. Analytical modelling of urban areas and cities is much more difficult, and no successful mathematical treatment has yet been completed. Experimental results for clutter return from such urban areas are presented, and, as with vegetation, they show that received power is relatively independent of frequency.

Several properties of radar and clutter are shown to produce both spreading and a shift in the spectrum of the transmitted signal. One mechanism which produces spectral distortion is the relative velocity difference between particles of volume-distributed clutter such as rain. If the incident signal is monochromatic, the spectral density of the signal scattered from the collection of random moving particles is proportional to the probability density of their velocities along the line of sight.

Another mechanism which produces a spectral shift and spreading is the motion of the radar platform with respect to the clutter and the finite antenna beamwidth. It is shown that the spectral response to a monochromatic incident signal in this case is proportional to the antenna radiation pattern; a narrow main beam will result in less spectral spread than a wide one.

A third mechanism producing spectral spreading in the case of the moving radar platform is the finite length of the illuminated area along the velocity direction. The greatest spectral spreading occurs when the platform velocity is high and the illuminated area is small.

The motion of the sea surface also produces spectral spreading of an incident monochromatic signal. An analysis of both the small-scale and large-scale sea surface roughnesses shows that each component has its own separate effect on the received signal spectrum. The small-scale roughness has a spectral response which is directly proportional to the motion spectrum of the surface itself; the signal bandwidth in this case is relatively independent of frequency. The large-scale roughness imparts a signal spectral density proportional to the probability density of the sea surface vertical velocity. The signal bandwidth due to this roughness component varies directly with frequency and sea surface velocity. This result for very rough surfaces is nearly identical

with that for volume-distributed particles having different velocities, even though the analysis is entirely different. One should expect the slight roughness mechanism to dominate near grazing incidence. Experimental results for sea clutter spectra are also given, but they are so sketchy as to make concrete comparison with the theory inconclusive.

Usually several mechanisms interact simultaneously to produce spectral spreading. When this is the case, the final received clutter spectrum is obtained as a convolution of the incident wave spectrum with all of the separate spectral responses of the interacting mechanisms. A more useful result states that the total received clutter signal bandwidth is the square root of the sum of the bandwidths of the various processes producing spreading. Examples calculated for each of the spectral spreading mechanisms show that some of these half-power bandwidths for a practical ground-based S-band radar system can be as great as 30 Hz, while the clutter spread in a missile-based homing radar can be several hundred hertz. If the central spike of the incident signal spectrum is considerably wider than this amount, this clutter spectral spreading has little additional effect on the received signal spectrum and can be neglected. However, this bandwidth of the spectral spreading produced by the clutter represents the lower limit on the coherence of the received signal. At higher microwave frequencies, this limit often dictates the optimum performance of clutter rejection systems.

LITERATURE CITED

1. M. I. Skolnik, INTRODUCTION TO RADAR SYSTEMS, New York, McGraw-Hill Book Co., 1962.

2. D. K. Barton, RADAR SYSTEM ANALYSIS, New Jersey, Prentice-Hall, Inc., 1965.

3. MODERN RADAR, ANALYSIS, EVALUATION, AND SYSTEM DESIGN, R. S. Berkowitz, ed., New York, John Wiley & Sons, Inc., 1965.

4. C. E. Cook and M. Bernfield, RADAR SIGNALS. AN INTRODUCTION TO THEORY AND APPLICATION, New York, Academic Press, 1967.

5. F. C. Watters and F. J. Nathanson, RADAR AND CLUTTER, Short Course Notes, University of Alabama in Huntsville (also, RADAR SIGNAL PROCESSING, by F. E. Nathanson, McGraw-Hill Book Co., to be published).

6. R. G. Medhurst, RAINFALL ATTENUATION OF CENTIMETER WAVES: COMPARISON OF THEORY AND MEASUREMENT, IEEE Transactions on Antennas and Propagation, AP-13, No. 4, 1965, pp. 550-564.

7. Battelle Memorial Institute, Columbus Laboratories, SCATTERING FROM SURFACES WITH DIFFERENT ROUGHNESS SCALES: ANALYSIS AND INTERPRETATION by D. E. Barrick and W. H. Peake, November 1967, Contract No. DA-49-083-OSA-3176.

8. G. Valenzuela, DEPOLARIZATION OF EM WAVES BY SLIGHTLY ROUGH SURFACES, IEEE Transactions on Antennas and Propagation, AP-15, No. 4, 1967, p. 552.

9. G. T. Ruck, D. E. Barrick, and W. E. Stuart, RADAR CROSS SECTION HANDBOOK, Plenum Press, 1968, Chapter 9.

10. R. Kodis, A NOTE ON THE THEORY OF SCATTERING FROM AN IRREGULAR SURFACE, IEEE Transactions on Antennas and Propagation, AP-14, No. 1, 1967, p. 77.

11. W. H. Peake, THE INTERACTION OF ELECTROMAGNETIC WAVES WITH SOME NATURAL SURFACES, Ph. D. Dissertation, The Ohio State University, Physics Department, 1959.

LITERATURE CITED (Concluded)

12. W. H. Peake, THEORY OF RADAR RETURN FROM TERRAIN, IRE Convention Record, 7, 1959, p. 27.

13. R. L. Cosgriff, W. H. Peake, and R. Taylor, TERRAIN SCATTERING PROPERTIES FOR SENSOR SYSTEM DESIGN, (TERRAIN HANDBOOK II), The Ohio State University Engineering Experiment Station Bulletin, No. 181, 1960.

Appendix A

THEORY OF RADAR WAVE SCATTERING FROM AND PROPAGATION THROUGH VOLUME-DISTRIBUTED PARTICLES

1. Introduction

This article treats the interaction of a radar wave with many separate objects distributed in space. These objects may have a fixed orientation with respect to each other, such as the molecules in a crystalline lattice. But more often than not, the objects of interest at radar frequencies are randomly arranged as raindrops or particles of chaff. Only the random configuration will be discussed in this section.

The general solution to this problem is considerably more complex than the solution for scattering from a single object. The field which excites any given object, say the n^{th} object, consists not only of the incident wave, but also the fields scattered from all the other objects toward this n^{th} object. In turn, the fields scattered from all these other objects depend to some degree on the fields scattered from the n^{th} object. This mutual interaction makes it extremely difficult to determine a closed form solution for the total scattered field without several approximations.

The first two sections are concerned with the incoherent radar cross section of the group of particles. The final section deals with propagation of a coherent wave through the collection of scatterers; a rigorous analysis is briefly retraced, and then a simpler derivation of the same result is presented. All sections employ the scattering characteristics of each scattering object considered alone, and hence presuppose that this information is already available or is to be obtained by other means.

2. Incoherent Cross Section Obtained from Superposition

(a) General Theory

To a crude approximation, one can simply add the scattered fields from the individual scatterers, assuming that the scattered field from, say, the n^{th} particle, is the same as if all the other particles were removed. In this approximation, then, the following assumptions are implicit:

1) All multiple scattering interactions between the various particles are ignored.

2) Each particle is assumed to be excited by only the incident plane wave, which is not attenuated as it moves through the region containing the scatterers.*

These assumptions will be valid when the multiple scattering problems meet both of the following requirements:

1) The average distance between scatterers is much greater than both wavelength and the size of each scatterer.

2) The number of scatterers is sufficiently small so that the total energy removed by them is small compared with the total energy in that portion of the incident wave striking the scattering medium. This means that for scatterers large compared to wavelength, the area masked by the scatterers looking in the direction of the incident wave should be very small compared to the total area normal to the incident wave direction (Figure A-1) .

Under these assumptions, the total scattered field at an angle θ from the backscattering direction can be written

$$\underset{\sim}{E}^{s}_{T} = \sum_{n=1}^{N} \frac{|E^{s}_{n}|}{R_{n}} e^{i\phi_{n}} \underset{\sim}{\hat{\tau}}_{n\alpha} \qquad \text{(A-1)}$$

where $|E^{s}_{n}|$ is the magnitude of the scattered far field from the n^{th} particle in the direction shown, ϕ_{n} is the phase angle introduced in the scattering process by the n^{th} particle, and $\underset{\sim}{\hat{\tau}}_{n\alpha}$ is a unit vector perpendicular to the scattering direction, representing the polarization direction of the scattered E-field when the incident E-field is polarized in a direction α. R_{n} is the distance from the n^{th}

---

* Physically, each time the incident wave strikes a particle, a portion of energy is removed from it and scattered in various directions. Thus, the incident wave moving through the particle medium is attenuated. This effect is ignored here, and energy is not conserved as a result.

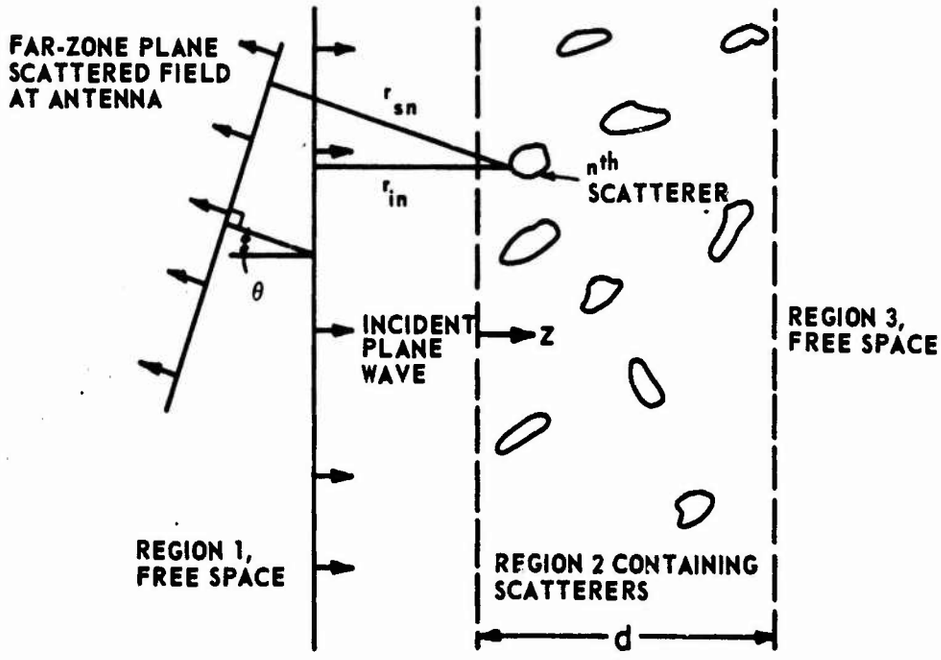

FIGURE A-1. GEOMETRY AND COORDINATES
FOR A MULTIPLE PARTICLE REGION

particle to the observation point. The total number of particles is N. In general the particles may be all different; then $|E_n^s|$, $\hat{\tau}_{n\alpha}$, and ϕ_n will be different for each particle.

The phase angle ϕ_n of the scattered field from the n^{th} particle can be broken into two components;

$$\phi_n = \psi_n + k_o\left(r_{in} + r_{sn}\right) . \qquad (A\text{-}2)$$

Here, $r_{in} + r_{sn}$ is the total distance from any fixed plane perpendicular to the incident field, to the center of the n^{th} scatterer, and out to a fixed plane locally perpendicular to the scattered field. The wave number of free space k_o is defined as $k_o = 2\pi/\lambda_o$. ψ_n is then the phase shift introduced by the scatterer itself and is a function of the scatterer size, shape, orientation, material, and the incident wavelength.

If the scattering cross section of the n^{th} particle is desired for the received polarization state β, then

$$\sigma^{n}_{\beta\alpha} = \frac{4\pi R_n^2 \left|E^{s}_{n}\right|^2 \left|\hat{\tau}_{n\alpha} \cdot \hat{\beta}\right|^2}{\left|E^{i}_{\alpha}\right|^2}, \tag{A-3}$$

where $\hat{\beta}$ is a unit vector representing the received polarization state and $\left|E^{i}_{\alpha}\right|$ represents the electric field strength incident upon the particles.

In terms of this definition, the total scattering cross section of the collection of particles can be written,

$$\sigma^{T}_{\beta\alpha} = \frac{4\pi R_T^2 \left|E^{s}_{T} \cdot \hat{\beta}\right|^2}{\left|E^{i}_{\alpha}\right|^2}, \tag{A-4}$$

or using Eq. (A-1), $\sigma^{T}_{\beta\alpha}$ becomes

$$\sigma^{T}_{\beta\alpha} = \left| \sum_{n=1}^{N} \sqrt{\sigma^{n}_{\beta\alpha}}\, e^{i\phi_n} \right|^2 = \sum_{n=1}^{N} \sum_{m=1}^{N} \sqrt{\sigma^{n}_{\beta\alpha}} \sqrt{\sigma^{m}_{\beta\alpha}}\, e^{i\left(\phi_n - \phi_m\right)}. \tag{A-5}$$

The approximation has been made here that $R_n \approx R_T$, i.e., at large distances from the particles the distance to an individual particle may be replaced by a distance R_T to the approximate center of the collection except in computing the phase factor ϕ_n.

Equation (A-5) can be and is used to compute the total cross section from a fixed array of scatterers when r_{in} and r_{sn} are known. But in most situations the particles are randomly arranged and $r_{in} + r_{sn}$ is a random variable. In particular when the n^{th} particle is equally likely to be anywhere in the slab region of dimension d containing the scatterers (Figure A-1), and when d is large compared to wavelength λ_o, then the second term of ϕ_n, i.e., $k_o\left(r_{in} + r_{sn}\right)$, is said to be uniformly distributed between 0 and 2π. This means that any value is equally likely for this number within the range

$0 \le k_o\left(r_{in} + r_{sn}\right) \le 2\pi$. Moreover, this random variable $k_o\left(r_{in} + r_{sn}\right)$ is independent of the scattering properties of the n^{th} particle and may be averaged separately. But when $k_o\left(r_{in} + r_{sn}\right)$ is uniformly distributed as described, the average of $e^{i\left[k_o\left(r_{in} + r_{sn}\right) - k_o\left(r_{im} + r_{sm}\right)\right]}$ is zero except when $n = m$. Hence the average scattering cross section from a randomly arranged collection of particles may be obtained from Eq. (A-5) by setting $m = n$, or

$$\left\langle \sigma^T_{\beta\alpha} \right\rangle = \sum_{n=1}^{N} \left\langle \sigma^n_{\beta\alpha} \right\rangle , \qquad \text{(A-6)}$$

where the brackets <> indicate an average. In general, $\sigma^n_{\beta\alpha}$ varies with the orientation of the particle, and if any orientation is equally likely, then $\left\langle \sigma^n_{\beta\alpha} \right\rangle$ indicates the scattering cross section averaged over all orientations or aspects of the n^{th} particle.

If all the particles are identical so that $\left\langle \sigma^n_{\beta\alpha} \right\rangle = \left\langle \sigma^m_{\beta\alpha} \right\rangle = \left\langle \sigma_{\beta\alpha} \right\rangle$ then Eq. (A-6) simplifies to become

$$\left\langle \sigma^T_{\beta\alpha} \right\rangle = N\left\langle \sigma_{\beta\alpha} \right\rangle . \qquad \text{(A-7)}$$

Examples of the backscattering cross sections for particular collections of particles are given and discussed below.

(b) Small Dielectric Spheres (Radar Echoes from Rain)

Consider a collection of equally sized dielectric spheres of radii a and refractive index $m = \sqrt{\epsilon_r}$, where ϵ_r is the relative dielectric constant of the sphere material. The radius a is considered small in terms of wavelength. The backscattering cross section of such a sphere in the low frequency region is a well known result and can be found, for example, in Eq. (A-7).[1]

$$\sigma = 4\pi a^2 \left(\frac{m^2 - 1}{m^2 + 2}\right)^2 \left(k_o a\right)^4 . \qquad \text{(A-8)}$$

The backscattering cross section of this particle does not depend upon particle orientation or aspect due to its rotational symmetry. The polarization state of the backscattered field is the same as that of the incident field. If the receiver polarization is the same as the transmitter polarization, then the cross section of such a collection of particles is

$$\left\langle \sigma^{T}_{\alpha\alpha} \right\rangle = N \cdot 4\pi a^2 \left(\frac{m^2 - 1}{m^2 + 2} \right)^2 \left(k_o a \right)^4 . \qquad \text{(A-9)}$$

This model is often employed to discuss the clutter effect on microwave radar by scattering from rain. The particles are represented by spheres. In this case it is inconvenient to determine N, the total number of raindrops in the radar beam. A more meaningful parameter might be $N = \rho V$, where ρ is the average number of drops per unit volume. In this case the volume would be that within a radar resolution cell at a distance R_T.

Knowing m, the refractive index for fresh water as a function of frequency, Eq. (A-9) has been used to estimate the raindrop density ρ and the average drop size a of an approaching rainstorm.

Typical values of raindrop diameter are $2a \approx 1$-3 mm. The value of ρ for rain is a function of the drop size. A graph of the number of drops per cubic meter as a function of drop diameter 2a is shown in Figure A-2 for a typical rain shower.[2] For an introduction to radar meteorology, see Battan[2]; an additional advanced treatment has been given by Bean and Dutton.[3]

(c) Half-Wave Thin Dipoles or Chaff

Consider a random collection of thin perfectly conducting rods of length $\ell = \lambda_o/2$. The backscattering cross section of a single such dipole lying in a plane normal to the direction of incidence and oriented with its axis along the incident polarization direction α has been given as approximately

$$\sigma \approx 0.75\lambda_o^2 \qquad \text{(A-10)}$$

when the wire is copper and its radius is of the order of 0.001ℓ. In this case, however, the backscattering cross section changes with the orientation of the dipole; for example, when the dipole has its axis normal to the polarization direction of the incident wave, the backscattering cross section of the particle is effectively zero. Hence the backscattering cross section must be averaged

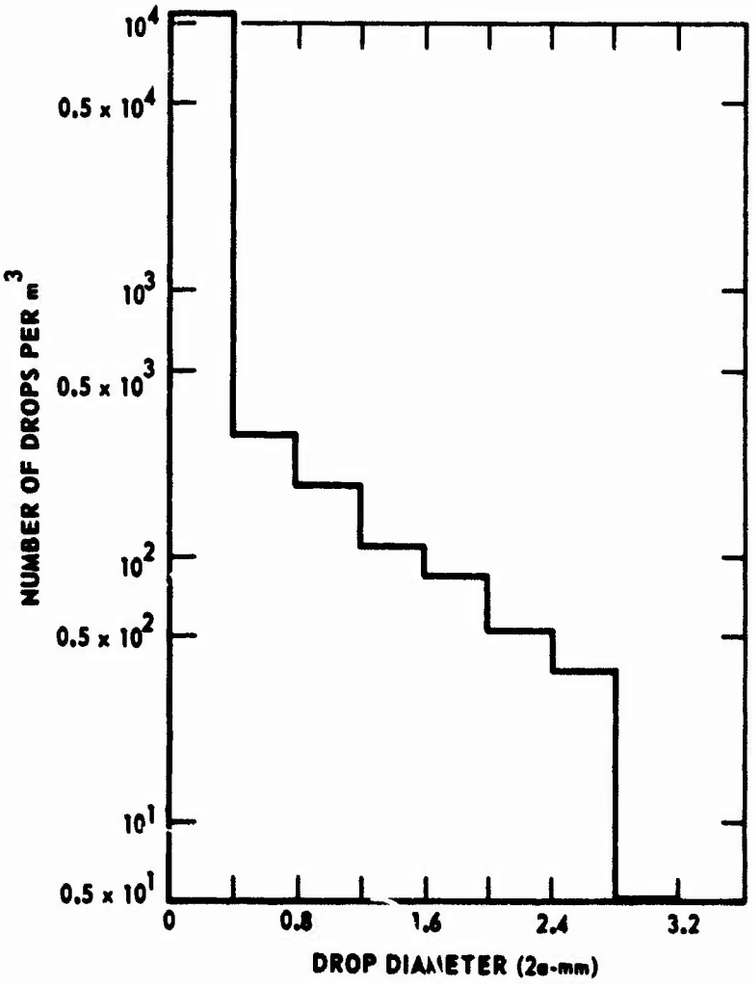

FIGURE A-2. RAINDROP DENSITY VERSUS DROP SIZE FOR A TYPICAL RAIN SHOWER

over all possible orientations, since it is assumed that in a random collection all orientations are equally likely. This has been done in the literature,[4,5] and the result is

$$\left\langle \sigma_{\alpha\alpha} \right\rangle \approx 0.17\lambda_o^2 \quad . \tag{A-11}$$

Hence the backscattering cross section of N such particles is

$$\left\langle \sigma_{\alpha\alpha}^{T} \right\rangle \approx 0.17\lambda_o^2 N \quad . \tag{A-12}$$

If the receiving antenna is linearly polarized perpendicular to the transmitting antenna, the cross section will be*

$$\left\langle \sigma^{T}_{\alpha + \pi 2\alpha} \right\rangle = \frac{1}{3} \left\langle \sigma^{T}_{\alpha\alpha} \right\rangle \approx 0.057\lambda_o^2 N \quad . \tag{A-13}$$

Such a cloud of dipoles, often called chaff, is employed as a radar reflector for various purposes. Thin strips or needles weigh much less than spheres of comparable dimensions; consequently, one can employ many more of them and obtain a much larger total cross section per given weight than with spheres.

A cloud of these chaff particles has long been considered an effective means of concealing a military target or of confusing enemy radars. This short wire scatterer presents the maximum cross section when its length is one-half the wavelength or any integral multiple of $\lambda_o/2$ (the dipole is resonant at these lengths). The one-half power bandwidth about the first resonant frequency of such a scatterer (averaged over all orientations) is approximately 12 percent of this frequency.[5] In order to make such a cloud of chaff effective over a wider band of frequencies, several dipole lengths are generally used in steps of about 12 percent starting from the longest length (the longest length corresponding to $\lambda_o/2$ for the lowest desired frequency). These different lengths then fill the frequency gap between the half-wave resonant frequency of the longest dipole and twice that frequency at which the longest dipole is again resonant. At frequencies any higher, the dipoles resonate at harmonics, maintaining the cross section at a high level. Then the total number N of particles contributing at a given frequency appearing in Eq. (A-12) actually represents the number of particles of a given length corresponding to $\lambda_o/2$ for that frequency. This analysis of chaff is intended to be only of a very elementary level. For a more detailed discussion and review of scattering from chaff, see Van Vleck and Block.[5]** A more detailed discussion of scattering from long, thin particles is given by Ruck, Barrick, and Stuart.[1]

*This "cross-polarized" backscattered component for the previous example employing spheres is zero, since spheres scatter back waves polarized only in the direction of the incident field.

**For several comprehensive articles on the use and characteristics of dipole scatterers, see Proc. IEEE, 52, 1964, p. 449. The papers in this issue are devoted entirely to Project West Ford.

A promising use of such chaff particles involves scatter communications. This potential was demonstrated by Project West Ford,* where thin copper dipoles were placed in orbit and dispersed to form a belt circling the earth. The belt was then used as a passive reflector at microwave frequencies, and beyond-the-horizon communication experiments were conducted. The dipole lengths were all 1.78 cm and diameters were 0.00178 cm. With a weight per dipole of only 40 μg, the measured scattering cross section per dipole averaged over all possible orientations was about 2 cm^2 at the first resonant frequency. These half-wave dipoles were designed to be resonant at about 8000 MHz, i.e., X-band. This frequency was considered optimum. Below that frequency, atmospheric and ionospheric noise increases, while above that frequency attenuation due to the atmosphere and precipitation becomes significant.

3. Probability Distribution of Incoherent Cross Section

If one observes the radar power (or scattering cross section) returned from a collection of scatterers which are individually moving in a random fashion, this power will vary as a function of time. If this power or radar cross section is plotted on a linear scale as a function of time, one would expect to see the cross section oscillate randomly about an average value, remaining always positive, of course, as the scattering particles move about.** It is often useful to know the statistics of this signal. A statistical model for the signal will be presented here. Before squaring, Eq. (A-5) can be written as

$$\sqrt{\sigma_{\beta\alpha}^{T}}\, e^{i\phi_T} = \sum_{n=1}^{N} \sqrt{\sigma_{\beta\alpha}^{n}}\, e^{i\phi_n} , \qquad \text{(A-14)}$$

---

* Ibid.

** The same restrictions are assumed here as were discussed in Section (a) above. In addition, the particles are assumed to move very slowly with respect to the speed of light, and their velocities are small enough so that the Doppler shift introduced by any moving particle is small compared to the monochromatic incident frequency. Hence, the fluctuation in voltage at the receiving antenna will be a narrow-band signal.

and writing this equation in terms of its real and imaginary parts,

$$\sqrt{\sigma^{T}_{\beta\alpha}}\cos\phi_T + i\sqrt{\sigma^{T}_{\beta\alpha}}\sin\phi_T = \sum_{n=1}^{N}\sqrt{\sigma^{n}_{\beta\alpha}}\cos\phi_n$$

$$+ i\sum_{n=1}^{N}\sqrt{\sigma^{n}_{\beta\alpha}}\sin\phi_n \ . \qquad \text{(A-15)}$$

Now ϕ_n varies randomly as a function of time due to the motion of the particles and the changing distances $r_{in} + r_{sn}$ in Eq. (A-2). Thus, ϕ_n is a uniformly distributed random variable between 0 and 2π. Consequently, $\cos\phi_n$ and $\sin\phi_n$ are random variables having zero means, making each term in the series a random variable.* Even though each random series term is not necessarily Gaussian, the fundamental central limit theorem of statistics states that the sum of N random variables becomes a Gaussian random variable as N becomes very large. Thus the first and second terms on the left side of the equation, representing the first and second sums on the right side, become Gaussian random variables. Since the mean value of each series term is zero, the mean values of the Gaussian random variables on the left side are zero. The mean square value of each term on the right side of the equation is

$$\left\langle\left(\sqrt{\sigma^{n}_{\beta\alpha}}\cos\phi_n\right)^2\right\rangle = \left\langle\left(\sqrt{\sigma^{n}_{\beta\alpha}}\sin\phi_n\right)^2\right\rangle = \frac{1}{2}\left\langle\left(\sqrt{\sigma^{n}_{\beta\alpha}}\right)^2\right\rangle$$

$$= \frac{1}{2}\left\langle\sigma^{n}_{\beta\alpha}\right\rangle \equiv \frac{1}{2}\left\langle\sigma_{\beta\alpha}\right\rangle \qquad \text{(A-16)}$$

since $\left\langle\cos^2\phi_n\right\rangle = \left\langle\sin^2\phi_n\right\rangle = \frac{1}{2}$.

According to the central limit theorem, $\sqrt{\sigma^{T}_{\beta\alpha}}\cos\phi_T$ and $\sqrt{\sigma^{T}_{\beta\alpha}}\sin\phi_T$ are both Gaussian random variables with zero means and variances $\frac{1}{2}N\left\langle\sigma_{\beta\alpha}\right\rangle$. Employing this fact, it is not difficult to show that $\sqrt{\sigma^{T}_{\beta\alpha}}$ is a

---

* Note that $\sqrt{\sigma^{n}_{\beta\alpha}}$ may itself be a random variable, as in the case of a dipole changing its orientation, or it may be a constant, as in the case of a sphere. There is no difference in the results which follow.

random variable with a Rayleigh probability distribution, and $\sigma^T_{\beta\alpha}$ itself has an exponential distribution with probability density functions as follows:

$$P\left(\sqrt{\sigma^T_{\beta\alpha}}\right) = \frac{2\sqrt{\sigma^T_{\beta\alpha}}}{N\langle\sigma_{\beta\alpha}\rangle} e^{-\frac{\sigma^T_{\beta\alpha}}{N\langle\sigma_{\beta\alpha}\rangle}} \text{ for } 0 \leq \sqrt{\sigma^T_{\beta\alpha}} \leq \infty \,, \tag{A-17}$$

and

$$P\left(\sigma^T_{\beta\alpha}\right) = \frac{1}{N\langle\sigma_{\beta\alpha}\rangle} e^{-\frac{\sigma^T_{\beta\alpha}}{N\langle\sigma_{\beta\alpha}\rangle}} \text{ for } 0 \leq \sigma^T_{\beta\alpha} \leq \infty \,. \tag{A-18}$$

Physically, $\sqrt{\sigma^T_{\beta\alpha}}$ is proportional to the received rectified field strength, whereas $\sigma^T_{\beta\alpha}$, the cross section, is proportional to the received power.

From Eq. (A-18), one can calculate the mean and variance of the radar cross section for a random collection of identical scatterers, or

$$\left\langle\sigma^T_{\beta\alpha}\right\rangle = N\langle\sigma_{\beta\alpha}\rangle \,, \text{ (this is identical to A-7)}, \tag{A-19}$$

and

$$\left\langle\left(\sigma^T_{\beta\alpha}\right)^2\right\rangle - \left(\left\langle\sigma^T_{\beta\alpha}\right\rangle\right)^2 = \left(N\langle\sigma_{\beta\alpha}\rangle\right)^2 \,. \tag{A-20}$$

The normalized variance is given by

$$\frac{\left\langle\left(\sigma^T_{\beta\alpha}\right)^2\right\rangle - \left(\left\langle\sigma^T_{\beta\alpha}\right\rangle\right)^2}{\left\langle\left(\sigma^T_{\beta\alpha}\right)^2\right\rangle} = \frac{1}{2} \tag{A-21}$$

Thus, one can see that the mean and variance of the total cross section increase with the number of scatterers as one would naturally expect. The percent or

normalized variance, however, remains a constant independent of the number of scatterers. Hence, the instantaneous radar echo does not become more steady or constant as the number of scatterers increases.*

4. Multiply Scattered Coherent Fields

(a) Theory

Consider a plane wave normally incident upon a "slab" (Figure A-1) or region of thickness d containing many random scatterers. Assume that the slab is infinitely high and wide and that only its thickness is finite. As the incident wave enters this region, part of its energy is removed upon striking each scatterer in the following ways:

1) Part of the electromagnetic energy striking a scatterer may be absorbed and converted to heat. If the scatterer is a perfect conductor or perfect dielectric, no absorption takes place.

2) Part of the incident energy is scattered unequally (in general) in all directions.

A wave will emerge to the right of the slab which should begin to look like a plane wave far from the slab. The intensity of this wave is less than that of the incident wave. Another wave should be reflected to the left of the slab in the direction from which the incident field came; this wave should also appear almost planar far to the left of the slab. These fields will be called the coherent fields. They will vary in magnitude and phase for each configuration of scatterers. In this section expressions will be given for the average coherent fields. (Besides the "coherent" field, there is the incoherent field which is scattered in all directions. This incoherent field does not emerge as a plane wave, and its average value is zero in most cases. A crude estimate of the intensity of the incoherent field, or average cross section, has been already treated in Section 2.) Since the coherent fields are planar, one cannot in general define a scattering cross section because these fields do not decrease with increasing distance from the slab.

---

*Often, however, one does not observe the true target cross section fluctuation on a radar indicator. If the radar system bandwidth from the receiving antenna to the radar indicator is less than the bandwidth of the scattered field, the rapid oscillatory behavior of the total radar cross section (due to the randomly moving scatterers) will be damped out by the system and only an average will be observed.

Alternately, one can relate the average coherent plane wave emerging to the right of region 2 to the plane wave transmitted through a slab of thickness d of homogeneous partially absorbing material. The average coherent field emerging to the left of region 2 is similarly related to a reflected plane wave from such a slab. According to this analogy, there should be two plane coherent waves within the slab, one moving to the right and the other to the left. Hence the actual scatterer region (region 2) can be replaced by a slab of material of the same thickness having permittivity ϵ_r and permeability μ_r (both complex) for the purpose of analyzing the average coherent fields. The equivalent permittivity ϵ_r and permeability μ_r of the scatterer region will be given in this section. Such a model then permits one to visualize and analyze the complicated multiple scattering problem in the same manner as reflection and transmission of a plane wave through a slab of homogeneous material.

Interest in the multiple scattering of waves dates back as far as Lord Rayleigh.[6,7] Since that time there have been many treatises on various aspects of the problem. Some of the most thorough treatments of multiple scattering in the recent literature are due to Twersky; consequently, his work will be used here.[8] Since the theory is lengthy and complex, the results given here will in no way constitute a complete analysis of the problem. Rather, the intuitive model discussed in the preceding paragraph will be used to explain Twersky's results. The following restrictions and assumptions are necessary to obtain the results.

1) The simplified geometry of Figure A-1 is assumed. All scatterers are confined to the slab region shown, and a plane wave is normally incident upon the slab.

2) The scatterers are randomly distributed in this slab in a uniform manner. Thus, the probability that one given scatterer center lies within a given volume element, dV is $\frac{\rho}{N}dV$, where ρ is the scatterer density, or the average number of scatterers per unit volume.

3) The percentage volume occupied by the scatterers is assumed small in comparison with the volume of unoccupied space within the slab, i.e., the scatterer concentration is rare rather than dense. The concentration should be rare enough that $k_o R_{t-s} \gg 1$, where R_{t-s} is the average distance between two neighboring scatterers, s and t, and $\frac{L}{R_{t-s}} \ll 1$, where L is the largest dimension of either scatterer.

4) All of the scatterers are assumed to be identical. If the scattering pattern of a scatterer varies with its orientation, it is assumed that an average pattern over all equally likely orientations is employed.

Let the x-axis be chosen along the polarization direction of the incident plane wave, while the z-axis be chosen in the direction of propagation of the incident wave and normal to the slab. As a consequence of 3) above, the E-field component polarized in the x-direction scattered by the j^{th} scatterer when the x-polarized plane wave is incident upon it can be given by its far-zone expression:

$$\underset{\sim}{E}^s = E^s_x \hat{\underset{\sim}{x}} = E^i_x \frac{e^{ik_o R_{js}}}{R_{js}} f_{xj}\left(\hat{\underset{\sim}{k}}_s, \hat{\underset{\sim}{k}}_i\right) \hat{\underset{\sim}{x}} \qquad \text{(A-22)}$$

where $f_{xj}\left(\hat{\underset{\sim}{k}}_s, \hat{\underset{\sim}{k}}_i\right)$ is called the complex scattering amplitude of the j^{th} object in the scattering direction $\hat{\underset{\sim}{k}}_s$ produced by an incident wave in the direction $\hat{\underset{\sim}{k}}_i = \hat{\underset{\sim}{z}}$. Written in this form, the scattering amplitude, $f_{xj}\left(\hat{\underset{\sim}{k}}_s, \hat{\underset{\sim}{k}}_i\right)$, is dimensionless and does not depend upon the distance from the object, but only upon the angular direction from the scatterer; thus it can be thought of as giving a scattering pattern for the object. E^i_x is the incident field amplitude and R_{js} is the distance from an arbitrary center in the j^{th} object to an observation point. E^s_x (any Cartesian component of the fields) and $f_{xj}\left(\hat{\underset{\sim}{k}}_s, \hat{\underset{\sim}{k}}_i\right)$ satisfy the scalar Helmholtz equation.

The method of solution of the multiple scattering problem assumes that the solution for scattering from each of the objects taken alone is already known or determinable by other means; thus $f_{xj}\left(\hat{\underset{\sim}{k}}_s, \hat{\underset{\sim}{k}}_i\right)$ is known. From this single-body solution, the multiple-body solution can be constructed basically as follows.[8]

1) The coherent components of the total field are assumed to be planar and polarized in the x-direction. They propagate in the plus and minus z-directions in regions 1 and 2 (corresponding to the incident and reflected fields and the internal fields in terms of the analogous homogeneous slab problem) and in the plus z-direction in region 3 (the field transmitted through the slab). These components, after averaging, are assumed to be independent of the x- and y-directions (just as with the homogeneous slab) due to restriction (d) and due to the averaging process in these directions.

2) The total average coherent fields in all three regions are then shown to be expressible as integrals within region 2 over z, i.e., $0 < z < d$. These integrals arise from averaging the total coherent fields over all possible particle positions in the z-direction. The integrands contain the total average fields scattered from one of the identical particles at $z = \zeta$ propagating in the plus or minus z-directions.

3) The average excitation on a particle located at $z = \zeta$ within region 2 is assumed to come from the two average internal coherent plane waves travelling in the plus or minus z-directions. Thus the total average scattered fields needed in the integrands of 2) above are postulated to come from these two internal coherent plane waves incident upon the typcial particle located at $z = \zeta$ and multiplied by $f_{xj}\left(\hat{k}_{\sim s}, \hat{k}_{\sim i}\right)$, where $\hat{k}_{\sim i} = \pm\hat{z}_{\sim}$ for these two average internal incident waves.

4) Hence the average coherent multiple scattered plane waves are shown to satisfy integral equations. These integral equations are easily reduced to differential equations which have the same form as the scalar second order differential equation for a scalar wave in one dimension. However, the new wave number for the scatterer is now given by

$$k_s^2 = \left\{ k_o + \frac{2\pi\rho}{k_o^2} \left[f_x(\hat{z}, \hat{z}) + f_x(-\hat{z}, \hat{z}) \right] \right\} \left\{ k_o + \frac{2\pi\rho}{k_o^2} \left[f_x(\hat{z}, \hat{z}) - f_x(-\hat{z}, \hat{z}) \right] \right\}. \tag{A-23}$$

Further, the scatterer region can be assigned a relative permittivity ϵ_{rs} and permeability μ_{rs} as follows:

$$k_s^2 = k_o \epsilon_{rs} \mu_{rs} ,$$

where

$$\epsilon_{rs} = 1 + \frac{2\pi\rho}{k_o^3} \left[f_x(\hat{z}, \hat{z}) + f_x(-\hat{z}, \hat{z}) \right] , \tag{A-24}$$

$$\mu_{rs} = 1 + \frac{2\pi\rho}{k_o^3} \left[f_x(\hat{z}, \hat{z}) - f_x(-\hat{z}, \hat{z}) \right] . \tag{A-25}$$

Since it is assumed that all particles are identical, the j subscript from the scattering amplitudes has been dropped. As before, ρ represents the average particle density (number of scatterers per unit volume).* Particular examples of multiple scatterers will be given subsequently, and the resulting scatterer region permittivity and permeability will be derived. Before passing it should be noted that the scattering amplitudes appearing in the above equations are complex, in general. Thus the wave number k_s has an imaginary part which gives rise to attenuation of the waves inside the medium. This attenuation of the coherent plane waves is due to heat losses within the particles and scattering of a portion of the incident energy into bistatic directions.

5) The resulting linear second-order differential equation for the coherent fields with wave number k_s in region 2 and k_o in regions 1 and 3 is easily solved. As mentioned previously, the coherent fields are plane waves independent of x and y, and vary only along the z-direction. Boundary conditions are obtained at the two faces bounding the scatterers, and these correspond to the boundary conditions for a slab of homogeneous material having wave number k_s. Thus the solutions for the average coherent fields in the three regions for an incident plane wave $E_x^i e^{ik_o z}$ are:

$$\underset{\sim}{E}^i = E_x^i e^{ik_o z} \hat{\underset{\sim}{x}}, \text{ for } z \leq 0 \qquad \text{(Incident Field)},$$

$$\left\langle E_x^R \right\rangle = -E_x^i Q\left(1 - e^{i2k_s d}\right) e^{-ik_o z}, \text{ for } z \leq 0 \qquad \text{(Reflected Field)}, \qquad \text{(A-26)}$$

---

* Physically, $f_x(\hat{\underset{\sim}{z}}, \hat{\underset{\sim}{z}})$ is the forward scattering amplitude (it represents the field scattered from an isolated object into the forward direction) whereas $f_x(-\hat{\underset{\sim}{z}}, \hat{\underset{\sim}{z}})$ is the backscattering amplitude. These quantities are simply related to the forward and backscattering cross sections (x-polarization) as follows:

$$\sigma_{xx}(\pi) = \frac{4}{k_o^2}\left|f_x(\hat{\underset{\sim}{z}}, \hat{\underset{\sim}{z}})\right|^2 \text{ and } \sigma_{xx}(0) = \frac{4}{k_o^2}\left|f_x(-\hat{\underset{\sim}{z}}, \hat{\underset{\sim}{z}})\right|^2 .$$

$$\left\langle E_x^{INT} \right\rangle = E_x^i \left[(1 - Q) e^{ik_s z} + Q e^{-ik_s (z - d) + ik_s d} \right],$$

for $0 \leq z \leq d$ (Internal Fields), (A-27)

$$\left\langle E_x^T \right\rangle = E_x^i e^{ik_s d + ik_o (z - d)}, \text{ for } z \geq d \text{ (Transmitted Field)} \quad \text{(A-28)}$$

where

$$Q = \frac{\frac{2\pi\rho}{k_o^3} f_x(-\hat{z}, \hat{z})}{1 + \frac{k_s}{k_o} + \frac{2\pi\rho}{k_o^3} f_x(\hat{z}, \hat{z})} . \quad \text{(A-29)}$$

It can be seen that the average coherent electric fields tangent to the slab interfaces satisfy the usual boundary conditions at an interface, i.e.,

$$\left[E_x^i + \left\langle E_x^R \right\rangle \right]_{z = 0} = \left[E_x^{INT} \right]_{z = 0}, \text{ and } \left[E_x^{INT} \right]_{z = d} = \left[E_x^T \right]_{z = d} .$$

It should be noted that because of restriction (c), the parameter Q above will be small in absolute value compared to unity, i.e., the particle density is sparse.* This means that $\frac{2\pi\rho}{k_o^3} f_x(\hat{z}, \hat{z})$ and $\frac{2\pi\rho}{k_o^3} f_x(-\hat{z}, \hat{z})$ are small in magnitude compared to unity, and consequently the parameter Q may be simplified under these restrictions to

---

* The restriction to sparse particle concentrations is violated very rarely in practical applications. For example, the quantities $\frac{2\pi\rho}{k_o^3} f_x(\hat{z}, \hat{z})$ and $\frac{2\pi\rho}{k_o^3} f_x(-\hat{z}, \hat{z})$ are small even for the densest rainstorm at both microwave and optical frequencies. Models of gases, where the scattering particles are the gas molecules, also have extremely sparse concentrations. When the particles are large compared to wavelength, these variables become even smaller in general.

$$Q \approx \frac{\rho}{k_o^3} f_x(-\hat{z}, \hat{z}) \quad . \tag{A-30}$$

(b) Simplification of Results and Relationship to Extinction or Total Cross Section

The fact that the scatterer concentration was assumed to be sparse permits considerable simplification for the effective wave number within the medium. One can then neglect higher powers in $\frac{2\pi\rho}{k_o^3} f_x(\hat{z}, \hat{z})$ and $\frac{2\pi\rho}{k_o^3} f_x(-\hat{z}, \hat{z})$. Using this simplification

$$k_s \approx k_o \sqrt{1 + \frac{4\pi\rho}{k_o^3} f_x(\hat{z}, \hat{z})} \approx k_o + \frac{2\pi\rho}{k_o^2} f_x(\hat{z}, \hat{z}) \quad . \tag{A-31}$$

Of the results derived in the previous section, the quantity of most practical interest is the main coherent wave propagating forward through the scatterer medium. This wave is attenuated as it passes through the scatterer medium, and it is often desirable to know this attenuation in solving radio communication or radar problems (e.g., radar wave propagation through a rainstorm or chaff). This forward wave is the first term of Eq. (A-27), and when the value for k_s of Eq. (A-31) is employed, it becomes

$$\left\langle E_x^F \right\rangle = E_x^i e^{ik_s z}$$

$$= E_x^i \exp\left[ik_o\left(1 + \frac{2\pi\rho}{k_o^3} \mathrm{Re}\left[f_x(\hat{z}, \hat{z})\right]\right) z - \frac{2\pi\rho}{k_o^2} \mathrm{Im}\left[f_x(\hat{z}, \hat{z})\right] z\right] . \tag{A-32}$$

Hence the imaginary part of the forward scattering amplitude represents the attenuation factor of this wave as it moves through the medium. Obviously, the imaginary part of $f_x(\hat{z}, \hat{z})$ must always be positive in a passive medium; otherwise, the wave would increase in magnitude rather than attenuate, which violates conservation of energy.

The imaginary part of the forward scattering amplitude is related to the power removed from the incident wave by the forward scattering theorem. The total scattering cross section for an isolated particle is defined as

$$\sigma_T = \frac{1}{4\pi}\int \sigma(\theta', \phi')\, d\Omega = \frac{1}{k_o^3}\int \left| f\left(\hat{k}_{\sim s}, \hat{k}_{\sim i}\right)\right|^2 d\Omega \quad . \tag{A-33}$$

This quantity physically gives the total power scattered by a particle into all directions divided by the power density in the incident wave striking it ($d\Omega$ is an element of solid angle in the scattering direction $\hat{k}_{\sim s}$). In a similar manner, one can define an absorption cross section σ_A as the power absorbed by the particle and converted into heat divided by the incident power density. Then the total power removed from the incident wave upon striking the particle is equal to the sum of the total scattered power and the absorbed power, and the related cross section,

$$\sigma_E = \sigma_T + \sigma_A \quad , \tag{A-34}$$

is called the extinction cross section. It gives the total power removed from the incident field divided by the incident power density striking the given particle. The cross section theorem[9] states that

$$\sigma_E = \frac{4\pi}{k_o^2} \mathrm{Im}\left[f(\hat{z}, \hat{z}) \right] \quad . \tag{A-35}$$

(c) Alternative Derivation of Attenuation Coefficient of Forward-Propagating Wave

An often-used alternative analysis can be used to find the attenuation of a plane wave propagating through a region containing many scatterers on the basis of the extinguished power or extinction cross section σ_E. This method has the advantage that it is easily developed and understood. It gives the same result as that formerly derived from Eq. (A-32), as will be shown below, and thus offers reassurance of the correctness of the previous results, especially since the theoretical basis for the development below is different.

Consider a slab of volume $\Delta V = X Y \Delta Z$ containing identical scatterers (Figure A-3). Let a total power P_{in} strike the slab normally from the left, and a total power P_{out} leave the slab toward the right. Then the total power removed by the scatterers within the slab is given by

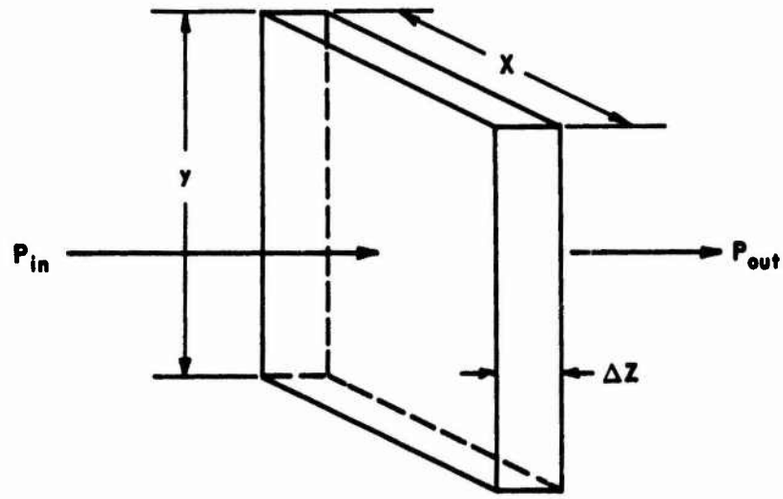

FIGURE A-3. GEOMETRY USED IN ESTIMATING PLANE WAVE ATTENUATION IN PASSAGE THROUGH A MEDIUM CONTAINING MANY IDENTICAL SCATTERERS

$$-\Delta P = P_{out} - P_{in} = \Delta N \sigma_E S \ , \qquad \text{(A-36)}$$

where S is the incident power density. This result is evident, since $\sigma_E S$ is the total power removed from the incident beam (due to scattering and absorption) by a single scatterer according to the definition of σ_E. Now $\frac{\Delta P}{XY}$ is the increment in power density ΔS, thus

$$-\Delta S = -\frac{\Delta P}{XY} = \frac{\Delta N}{XY}\sigma_E S = \frac{\Delta N}{XY\Delta Z}\sigma_E S\Delta Z = \frac{\Delta N}{\Delta V}\sigma_E S\Delta Z \ . \qquad \text{(A-37)}$$

But $\frac{\Delta N}{\Delta V}$ is the number of particles per unit volume of the slab and is equal to ρ as defined previously. Taking limits and integrating both sides, one obtains

$$\int \frac{dS}{S} = -\rho\sigma_E \int dz + c \ ,$$

so

$$\ell n \frac{S}{S_o} = -\rho\sigma_E z \ ,$$

and

$$S = S_o e^{-\rho\sigma_E z} .$$

Employing the cross section theorem then

$$S = S_o \exp\left(\frac{-4\pi\rho}{k_o^2} \operatorname{Im}\left[f_x(\hat{z}, \hat{z})\right] z\right) . \tag{A-38}$$

These last two equations give the power density in a wave propagating through a scatterer region where the initial power density at $z = 0$ is S_o.

In comparison, the power density in the coherent wave of Eq. (A-32) is given by

$$\frac{1}{\eta_o}\left|\left\langle E_x^F \right\rangle\right|^2 = \frac{1}{\eta_o}\left|E_x^i\right|^2 \exp\left(\frac{-4\pi\rho}{k_o^2} \operatorname{Im}\left[f_x(\hat{z}, \hat{z})\right] z\right) , \tag{A-39}$$

where η_o is the free space impedance. The results are identical, confirming the former theory. The former theory is more useful because it gives the proper phase relationships and effective wave number k_s in the scatterer medium. The development given above is more elementary and intuitive, and was first set forth by Lord Rayleigh.[6, 7]

The results derived in this section, especially those for the attenuation of a wave propagating through a multiple scatterer region, are often used in practice even though the scatterer region may not be a slab. Propagation through rainstorms, clouds of water droplets or chaff, and even light wave propagation through an atmosphere of dust or molecular scatterers is analyzed on this basis. Several examples are given in the following paragraphs.

(d) Small Dielectric Spherical Scatterers

The forward scattering amplitude for a sphere of radius "a" small compared with wavelength λ_o with refractive index m is given by[1]

$$f_x(\hat{z}, \hat{z}) = \frac{m^2 - 1}{m^2 + 2}\left(k_o a\right)^3 . \tag{A-40}$$

so long as the conditions $k_o a < 1$ and $k_o a |m| < 1$ are met. From Eq. (A-31), (A-35), and (A-40), the wave number and power attenuation constant are

$$k_s = k_o \left[1 + 2\pi\rho a^3 \frac{m^2 - 1}{m^2 + 2} \right] \tag{A-41}$$

and

$$\frac{4\pi\rho}{k_o^2} \operatorname{Im}\left[f_x(\hat{z}, \hat{z}) \right] = 4\pi\rho a^3 k_o \operatorname{Im}\left[\frac{m^2 - 1}{m^2 + 1} \right]. \tag{A-42}$$

It can be seen from Eq. (A-42) that the attenuation constant is zero unless the refractive index m is complex. If the refractive index is real, there is no attenuation of the incident wave according to the theory, even though some bistatic scattering by the drops takes place. Thus in the low frequency limit, these results show that the only mechanism responsible for attenuation is absorption of the incident energy by the drops.

For raindrops at microwave frequencies, a typical value for m is $m = 7.14 + i\,2.89$ at 0°C and $\lambda = 3.21$ cm.[3] Using this value and assuming an average drop radius a = 1 mm, and ρ = 100 drops/m^3, then*

$$\frac{4\pi\rho}{k_o^2} \operatorname{Im}\left[f_x(\hat{z}, \hat{z}) \right] = 8.1 \times 10^{-3} \text{ nepers/km} = 0.0652 \text{ dB/n.mi.} \tag{A-43}$$

Thus a radar wave at this frequency will lose one-half of its initial power after traveling through the rain a distance of 46 n.mi. If the frequency is less, i.e., at radio frequencies, this attenuation constant is even smaller due to k_o on the right side of (A-41) becoming smaller and $\operatorname{Im}\left[\frac{m_i^2 - 1}{m_i^2 + 2}\right]$ becoming smaller. Hence one can say that a plane wave at C-band frequencies and lower is attenuated little by rain or by clouds. At $\lambda = 1$ cm (i.e., K_a-band), $k_o a \approx \frac{1}{2}$ for drop radius a = 1 mm. The particle is no longer strictly in the low frequency region by virtue of its size, and Eq. (A-40) is no longer strictly valid. There

---

* At this wavelength, drop size, and refractive index, $k_o a\, m \approx 1\frac{1}{2}$, and hence the approximation (A-40) is not strictly valid. The results here are not in error by much, however: the error is approximately 18 percent.

is an imaginary part of f_x which does not depend upon the refractive index having at imaginary part. This means that the particle is sufficiently large that part of the energy is being removed from the incident wave and scattered in other directions. This is in addition to that portion being absorbed by the particle and converted to heat; this latter portion is due to the complex refractive index. In fact, as the particle becomes bigger (i.e., $k_o a > 5$), the energy removed by scattering is far greater than that absorbed and converted to heat, as will be shown in the next section. Hence, raindrops can be considered small only up to K_a-band frequencies, permitting use of Eq. (A-40).

(e) Large Spherical Scatterers

For large spherical scatterers where $k_o a >> 1$ (a is the sphere radius), the forward scattering amplitude is independent of the sphere material.[1] The quantity $f_x(\hat{z}, \hat{z})$ is given there as $-f(\pi)$.

$$f_x(\hat{z}, \hat{z}) = i\frac{(k_o a)^2}{2} . \tag{A-44}$$

Then the wave number and power attenuation constant become

$$k_e = k_o\left[1 + i\frac{\pi\rho a}{k_o}\right] , \tag{A-45}$$

and

$$\frac{4\pi\rho}{k_o^2}\,\mathrm{Im}\left[f_x(\hat{z}, \hat{z})\right] = 2\pi\rho a^2 . \tag{A-46}$$

This example presents the other extreme to the preceding section. Here the significant attenuation mechanism is scattering by the particles rather than absorption. Even though absorption can and does take place in large lossy spheres, its contribution to the power removed from the incident wave is so small compared to that removed by scattering as to be insignificant. Hence, the entire forward scattering amplitude is pure imaginary and contributes toward attenuation.

In the preceding section, raindrops appeared small at microwave frequencies ($\lambda_o > 3$ cm). At optical and infrared frequencies, however, these same drops appear large so that the results of this section may be used to predict attenuation. At an average drop radius of a = 1 mm and ρ = 100 drops/m^3, the attenuation constant becomes

$$\frac{4\pi\rho}{k_o^2} \operatorname{Im}\left[f_x(\hat{z}, \hat{z})\right] = 0.628 \text{ nepers/km} \approx 5.06 \text{ dB/n. mi.} \qquad \text{(A-47)}$$

In contrast to the preceding section, an optical or infrared wave (any frequency such that $k_o a > 100$) will attenuate to 10 percent of its original power (10 dB) after travelling only 2 n. mi. through rain. This is easily confirmed visually.

The primary or coherent wave from an object can be rapidly attenuated at optical frequencies in a medium such as the rain in the above example. Thus one cannot see the sun on a rainy day. Nonetheless, the light level striking the ground may still be fairly high; this light level is due entirely to the incoherent multiple scattering. This example shows that there are cases where the incoherent scattered power from multiple scatterers may be much larger than the coherent field such as that containing the sun's image.

(f) Half-Wave Dipole Scatterers or Chaff

As one final example, consider the chaff or half-wave dipole scatterers of Section 1, (c). A single such dipole (perfectly conducting thin cylinder of length-to-radius ratio of 0.001) optimally oriented gives the same back and forward scattering cross sections. The scattering amplitudes become

$$f_x(\hat{z}, \hat{z}) = f_x(-\hat{z}, \hat{z}) \approx 1.54 \ . \qquad \text{(A-48)}$$

This example, however, represents a case where the scattering amplitude depends upon the particle orientation. If the particles are arranged completely randomly, then $f_x(\hat{z}, \hat{z})$ must be averaged over all possible dipole orientations to obtain $\left\langle f_x(\hat{z}, \hat{z})\right\rangle$ for a typical dipole. When this is done

$$\left\langle f_x(\hat{z}, \hat{z})\right\rangle = \left\langle f_x(-\hat{z}, \hat{z})\right\rangle \approx 0.73 \ . \qquad \text{(A-49)}$$

From this the average wave number and attenuation constant are

$$\left\langle k_s \right\rangle = k_o \left[1 + \frac{2\pi\rho}{k_o^3} \times 0.73 \right] , \tag{A-50}$$

$$\frac{4\pi\rho}{k_o^2} \mathrm{Im} \left[\left\langle f(z, z) \right\rangle \right] = 0 . \tag{A-51}$$

This example shows that for an ideal half-wave dipole, the attenuation of the coherent wave is negligible. However, in practice the dipoles are not ideal and there is some loss produced by the induced currents; this loss plus a small reactive term due to finite dipole radius when properly taken into account will introduce an imaginary term to $f(\hat{\underset{\sim}{z}}, \hat{\underset{\sim}{z}})$ and some small attenuation will take place.

LITERATURE CITED (Appendix A)

1. G. Ruck, D. Barrick, and W. Stuart, RADAR CROSS SECTION HANDBOOK, Plenum Press, 1968.

2. L. J. Battan, RADAR METEOROLOGY, University of Chicago Press, 1959.

3. B. R. Bean and E. J. Dutton, RADIO METEOROLOGY, National Bureau of Standards Monograph No. 92, 1966.

4. C. L. Mack, Jr. and B. Reiffen, RF CHARACTERISTICS OF THIN DIPOLES, Proc. IEEE, 52, 533, 1964.

5. J. H. Van Vleck, F. Block, and M. Hamermesh, THEORY OF RADAR REFLECTION FROM WIRES OR THIN METALLIC STRIPS, J. Appl. Phys., 18, 274, 1947.

6. Lord Rayleigh, ON THE TRANSMISSION OF LIGHT THROUGH AN ATMOSPHERE CONTAINING SMALL PARTICLES IN SUSPENSION, AND ON THE ORIGIN OF THE BLUE OF THE SKY, Philosophical Magazine, XLVII, 375, 1899.

7. Lord Rayleigh, SCIENTIFIC PAPERS, IV, Dover, 1964.

8. V. Twersky, ON SCATTERING OF WAVES BY RANDOM DISTRIBUTION. I. FREESPACE SCATTER FORMALISM, J. Math. Phys., 3, 700, 1962.

9. A. T. de Hoop, ON THE PLANE-WAVE EXTINCTION CROSS SECTION OF AN OBSTACLE, Appl. Sci. Res., 7, 463, 1959.

Appendix B
ROUGH SURFACE SCATTERING BASED ON SPECULAR POINT THEORY

1. Introduction

Two approaches have been employed for the solution of scattering from very rough surfaces* in the past. The first begins with a form of the physical optics integral, alternately referred to as the Kirchhoff approximation. In order to evaluate this integral, it is necessary to approximate a complicated factor in the integrand which involves local surface slopes, angle of incidence, and Fresnel reflection coefficients. Several recent analyses, such as that of Hagfors,[1] who treats backscattering, and those of Semenov[2] and Stogryn,[3] who deal with bistatic scattering, justify the removal of this factor from the integrand as a constant by virtue of the stationary phase principle. In other words, one assumes at the outset that all scattering comes from local areas which are oriented in such a manner as to specularly reflect into the desired scattering direction. The factor is then evaluated at the slopes of these specular or stationary phase points. The remaining integral in these analyses, whose integrand now consists entirely of an exponential factor, is not solved by this stationary phase approach. The integral for the scattered power is evaluated after the averaging process, and hence the stationary phase principle, used to approximate the first factor, is not employed after all to solve the integral. Nonetheless, the process of averaging under the integral sign can be justified mathematically. Hence, while this autocorrelation approach, as referred to by Hagfors, is correct, it does not provide the needed physical interpretation of the scattering process.

Recently, Muhleman[4] analyzed rough surface scattering by what he termed a ray optics approach. This model approximates the random surface by a patchwork of planar facets. The model is based solely upon energy or power reflection, and ignores the role of the phase angle of the scattered field. The model postulates that all scattering takes place from those facets which are in a direction to specularly reflect. While the results compare with those of the autocorrelation approach and the technique provides needed physical insight into the scattering process, it leaves much to be desired as far as rigor. The stationary phase approach shows that the intensity of the scattered field is proportional to the principal radii of curvature at the specular point and the number of such points; none of these quantities is [illegible] the ray optics approach nor is polarization information for bistatic scattering.

*Very rough is the term often used to denote surfaces whose rms roughness height is considerably greater than wavelength.

The physical optics and geometrical or ray optics approach must yield identical results in the high frequency limit. It should be possible to derive a geometrical optics formulation from the physical optics integral which places in evidence the important physical quantities of the rough surface which produce the scattering. Kodis[5] has done exactly this. However, instead of averaging the integral, he evaluates it entirely by the stationary phase method. As one intuitively expects, he rigorously demonstrates that the scattering cross section from any very rough, but locally continuous curving surface, is proportional to the average number of specular points and the average of the principal radii of curvature at the specular points.

The purpose of this paper is to begin with Kodis' results for one- and two-dimensionally rough surfaces and derive general expressions for the average number of specular points, and the average curvature at the specular points. These quantities of themselves provide insight into the surface properties which affect the scattered field. When these factors are used in the expressions for the scattering cross sections, we obtain the same result here as the autocorrelation and the ray optics techniques. This therefore justifies the partial use of the stationary phase principle, as discussed before. The results of Kodis will be generalized here to apply to bistatic as well as backscattering, and to homogeneous surface materials $(\text{with relative constitutive constants } \epsilon_r, \mu_r)$ as well as perfectly conducting.

Longuet-Higgins[6] has derived expressions for the average number of specular points when the surface height is a Gaussian variable and when one examines an infinitely long surface from source and observation points at a finite distance from the mean surface. The results derived here apply to surfaces of finite extent and where the source and observation points much further from the surface than the mean roughness correlation length. Moreover, our results are not only simpler in form, but are more general in that they apply to non-Gaussian surfaces as well.

(a) One-Dimensionally Rough Surface $\zeta(x)$

Consider a surface which is square with side length L, which is rough in the x-direction only, and whose mean plane coincides with the $z = 0$ plane (Figure B-1). The plane of incidence is taken to be the x-z plane, and we consider scattering only in this plane $(\text{i.e., } \varphi_s = 0)$. Then the average bistatic cross section per unit surface area is:

$$\sigma^{o}_{\xi\xi} = k_o L \cos\left(\frac{\theta_i + \theta_s}{2}\right) n_L \langle|\mathcal{C}|\rangle \; |R_\xi(\iota)|^2 \;, \qquad \text{(B-1)}$$

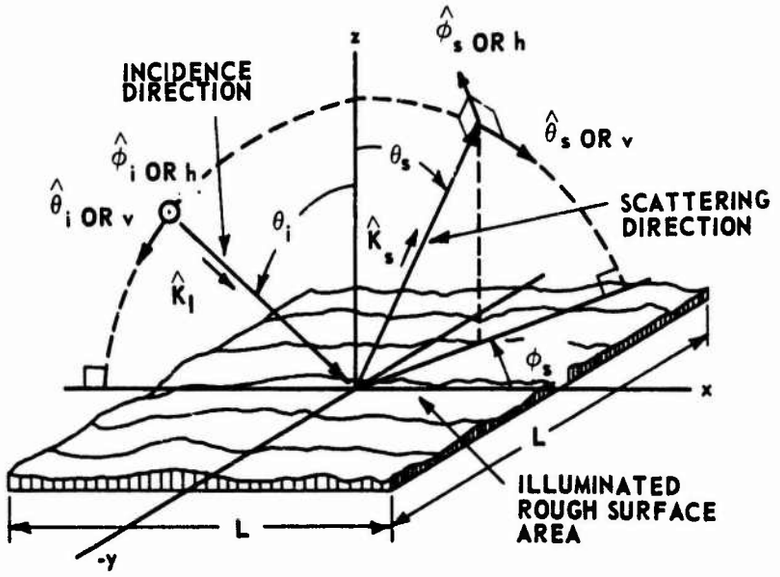

FIGURE B-1. ROUGH SURFACE AND SCATTERING GEOMETRICS

where

L = side length of illuminated area.

n_L = average number of specular ridges on the corrugated surface per unit length.

$\langle |\mathcal{R}| \rangle$ = averaged absolute value of radius of curvature at the specular ridge.

$R_{\xi\xi}(\iota)$ = reflection coefficient from an infinite plane tangent to the surface at a specular ridge for incident and scattered polarization states. $\xi\xi$ corresponds here to the vertical and horizontal states, vv and hh. These reflection coefficients are derived in the Appendix for a homogeneous surface and given in Eq. (B-29) and (B-30). Note that R_{vh} and R_{hv} are zero because scattering is in the incidence plane, i.e., $\varphi_s = 0$.

ι = local angle of incidence, derived in the Appendix and given in Eq. (B-3).

The angle of incidence is taken positive if scattering is forward and negative if it is backward.

(b) Two-Dimensionally Rough Surface $\zeta(x, y)$

The scattering geometry is shown in Figure B-1, but for this surface whose height varies in the y-direction also, we consider scattering at arbitrary polar angles θ_s, φ_s. The average bistatic cross section per unit surface area is:

$$\sigma^o_{\xi\eta} = \pi n_A < |\tau_1 \tau_2| > \left| R_{\xi\eta}(\iota) \right|^2 , \qquad \text{(B-2)}$$

where

n_A = average number of specular points per unit area.

$< |\tau_1 \tau_2| >$ = average absolute value of product of principal radii of curvature (or reciprocal of Gaussian curvature) at specular point.

$R_{\xi\eta}(\iota)$ = reflection coefficient from infinite plane tangent to the surface at the specular points for incident (right subscript) and scattered (left subscript) polarization states. ξ and η refer to the horizontal and vertical states h and/or v. They are derived in the Appendix for a homogeneous surface. They are given in Eq. (B-29) and (B-30) for bistatic scattering and Eq. (B-31) for backscattering.

ι = local angle of incidence at specular point as derived in the Appendix and given below in terms of its cosine:

$$\cos \iota = \frac{1}{2} \sqrt{1 - \sin \theta_i \sin \theta_s \cos \varphi_s + \cos \theta_i \cos \theta_s} .$$

The above equations for the scattering cross sections are consistent with what one expects from a surface made up of many specular points having smooth curvatures. Equation (B-2), without the average sign on $|\tau_1 \tau_2|$ and without n_A, is the well known expression for the bistatic scattering cross section of any simple curved surface having principal radii of curvature τ_1, τ_2 at the specular point. Hence, without ever having gone through the stationary phase analysis, one should be able to appreciate and understand the use of Eq. (B-1) and (B-2) as the basis for rough surface scattering.

The restrictions under which the above equations are valid are the following:

1) $k_o \rho > 1$, i.e., the radius of curvature everywhere on the surface is much greater than wavelength. Hence, the tangent plane approximation can be applied.

2) Shadowing and multiple scattering between various parts of the surface are neglected.

3) $k_o^2 h^2 >> 1$, i.e., the mean square surface height h^2, is much greater than wavelength. This permits us to sum the power from each specular point incoherently.

4) $\langle(\partial\zeta/\partial x)^2\rangle = \langle(\partial\zeta/\partial y)^2\rangle$, i.e., the surface roughness is isotropic in nature. This restriction is not necessary to obtain the solution but is employed here for simplicity.

2. One-Dimensionally Rough Surface $\zeta(x)$

(a) Average Number of Specular Ridges

The slope of the surface ζ_x (or $\partial\zeta/\partial x$) at the specular ridge is $\tan\gamma$; denote it ζ_{xsp}. The problem here is then similar to the better known zero-crossing problem of communication theory, i.e., to find the average number of points per length of surface where the random variables $\zeta_x - \zeta_{xsp}$ passes through zero. The most general solution to this problem is attributed to Kac and is found in Rice.[7] We shall briefly retrace Rice's technique, because it will aid in understanding the more complicated two-dimensional surface case.

Let $p(\zeta_x, \zeta_{xx}; x)$ be the joint probability density function of the slope and second derivative random variables, ζ_x and ζ_{xx}, at surface point x. Assume for the moment that the quantity $\zeta_x - \zeta_{xsp}$ passes through zero with positive rate of change, i.e., $\zeta_{xx} > 0$, in the interval between x_1 and $x_1 + dx$. For dx sufficiently small, the curve in this interval can be considered linear with x intercept equal to $x_1 - \dfrac{\zeta_x - \zeta_{xsp}}{\zeta_{xx}}$. Then, since by hypothesis this intercept falls within the defined interval, the following inequality holds

$$x_1 < x_1 - \frac{\zeta_x - \zeta_{xsp}}{\zeta_{xx}} < x_1 + dx_1 \ ,$$

from which it follows that the range of interest of the random variable ζ_x is given by

$$-\zeta_{xx}dx + \zeta_{xsp} < \zeta_x < \zeta_{xsp} ,$$

while that of ζ_{xx} is

$$0 < \zeta_{xx} < \infty .$$

The probability that the curve passes through zero is then found by integrating $p(\zeta_x, \zeta_{xx}; x_1)$ over this range; i.e.,

$$P^+ = \int_0^\infty d\zeta_{xx} \int_{-\zeta_{xx}dx + \zeta_{xsp}}^{\zeta_{xsp}} d\zeta_x \, p(\zeta_x, \zeta_{xx}; x_1)$$

$$\approx dx \int_0^\infty \zeta_{xx} p(\zeta_{xsp}, \zeta_{xx}; x_1) d\zeta_{xx} .$$

Likewise the probability P^- of the quantity $\zeta_x - \zeta_{xsp}$ passing through zero with a negative rate of change $(\text{i.e., } \zeta_{xx} > 0)$ is easily established, and assuming $p(\zeta_x, \zeta_{xx}; x)$ is symmetric in ζ_{xx}, the total probability of a zero crossing in dx is

$$P = P^+ + P^- = dx \int_0^\infty |\zeta_{xx}| \, p(\zeta_{xsp}, \zeta_{xx}; x_1) d\zeta_{xx} . \qquad \text{(B-4)}$$

Hence, we see that the probability of having a zero of $\zeta_x - \zeta_{xsp}$ varies directly with the length of the surface dx for short intervals. This is a characteristic of Poisson distributed everts, and it is readily established from the theory of Poisson processes that the average number of zeros per unit length of the surface n_L is defined as

$$P = n_L dx . \qquad \text{(B-5)}$$

Comparison of Eq. (B-4) and (B-5) gives the desired relationship for the average number of specular points per unit surface length. The integral can be written in a more meaningful form and one more useful later by expressing the joint probability as the product of the single density in ζ_x and the conditional density of ζ_{xx} given ζ_{xsp}.

$$n_L = p(\zeta_{xsp}) \int_{-\infty}^{\infty} |\zeta_{xx}| \, p(\zeta_{xx}/\zeta_{xsp};x_1) d\zeta_{xx} \quad . \tag{B-6}$$

This form places in evidence an important fact: The average number of specular points on a rough surface is directly proportional to the probability density of the surface slope ζ_{xsp} at the specular point, as one intuitively would expect.

As a specific and commonly used example, consider the Gaussian surface height joint probability density function

$$p(\zeta,\zeta') = \frac{1}{2\pi h^2 [1 - \rho^2(r)]^{1/2}} \exp\left\{ - \frac{\zeta^2 - 2\rho(r)\zeta\zeta' + \zeta'^2}{2h^2[1 - \rho^2(r)]} \right\}, \tag{B-7}$$

where $h^2 = \langle \zeta^2 \rangle$ is the mean square surface height, and $\rho(r)$ is the correlation coefficient for the surface height variables $\zeta(x)$ and $\zeta(x')$ separated by horizontal distance r. For the one dimensional surface, $r = |x - x'|$. The definition of $\rho(r)$ is

$$\rho(r) = \frac{1}{h^2} \langle \zeta(x) \zeta(x + r) \rangle \quad .$$

Near $r = 0$, $\rho(r)$ must be parabolic, since the presence of a linear term in r results in an infinite mean square slope, which means that the probability density functions in ζ_x and ζ_{xx} do not exist so that we cannot determine n_L. For the sake of example, let us assume that the second and third terms in the expansion of $\rho(r)$ follow a Gaussian model, i.e.,

$$\rho(r) = \exp\{-r^2/\ell^2\} \approx 1 - \frac{r^2}{\ell^2} + \frac{r^4}{2\ell^4} .$$

Here ℓ is termed the correlation length. Then the following averages for the slopes may be established:

$$\left\langle \zeta_x(x)\,\zeta_x(x')\right\rangle = \left\langle \lim_{\Delta_1\to 0}\left[\frac{\zeta(x+\Delta_1)-\zeta(x)}{\Delta_1}\right]\lim_{\Delta_2\to 0}\left[\frac{\zeta(x'+\Delta_2)-\zeta(x')}{\Delta_2}\right]\right\rangle$$

$$= \lim_{\Delta_1,\Delta_2\to 0}\frac{1}{\Delta_1\Delta_2}\left\langle \zeta(x+\Delta_1)\,\zeta(x'+\Delta_2)\right.$$

$$\left. -\,\zeta(x+\Delta_1)\,\zeta(x') - \zeta(x'+\Delta_2)\,\zeta(x) + \zeta(x)\,\zeta(x')\right\rangle$$

$$= \lim_{\Delta_1\Delta_2\to 0}\frac{h^2}{\Delta_1\Delta_2}\left[\rho(x-x'+\Delta_1-\Delta_2)\right.$$

$$-\,\rho(x-x'-\Delta_1) - \rho(x-x'+\Delta_2)$$

$$\left. +\,\rho(x-x')\right] .$$

Expanding the individual terms into series in powers of Δ_1 and Δ_2 and taking the limit shown, we obtain

$$\left\langle \zeta_x(x)\,\zeta_x(x')\right\rangle = \frac{2h^2}{\ell^2}\left[1 - 2\,\frac{(x-x')^2}{\ell^2}\,\rho(r)\right] .$$

From this it follows that the mean square slope s_x^2 in the x-direction is

$$s_x^2 \left\langle \zeta_x^2(x)\right\rangle = \frac{2h^2}{\ell^2} . \qquad \text{(B-8a)}$$

Likewise, the following averages may be established:

$$\eta_{xx}^2 = \left\langle \zeta_{xx}^2(x)\right\rangle = \frac{12h^2}{\ell^4}, \text{ and } \left\langle \zeta_x(x)\,\zeta_{xx}(x)\right\rangle = 0 . \qquad \text{(B-8b,c)}$$

Notice that the first and second surface derivatives, ζ_x and ζ_{xx}, at a given point x are uncorrelated.

Now, the fact that ζ and ζ' are Gaussian provides us with the well known result that all its derivatives are Gaussian, since any linear operation, such as differentiation, on a Gaussian variable yields another Gaussian random variable. Further, since the correlation coefficient between ζ_x and ζ_{xx}, at the same surface point x is zero, these Gaussian variables are statistically independent. The conditional density can thus be written

$$p\left(\zeta_{xx} | \zeta_x; x\right) = p\left(\zeta_{xx}\right) .$$

The integral in Eq. (B-6) for the Gaussian model when evaluated is $\eta_{xx}\sqrt{\frac{2}{\pi}}$, and n_L becomes

$$n_L = \frac{\eta_{xx}}{\pi s_x} \exp\left\{\frac{-\zeta_{xsp}^2}{2s_x}\right\} = \frac{\sqrt{6}}{\pi \ell} \exp\left\{\frac{-\tan^2\gamma}{2s_x^2}\right\} . \qquad \text{(B-9)}$$

(b) Average Curvature at Specular Ridges

A result of the stationary phase analysis was the determination that the slope at a specular point is $\zeta_{xsp} = \tan\gamma$, where γ is defined in terms of the incidence and scattering angles in Eq. (B-27). Hence, using this prior knowledge of the slope at these specular ridges, we wish to determine their average radius of curvature. Any treatment of curves, such as Taylor[8] or Struik,[9] will show that the radius of curvature of a curve $\zeta(x)$ which lies within a plane (the $y = 0$ plane in this case) is

$$|\tau| = \frac{\left(1 + \zeta_x^2\right)^{3/2}}{|\zeta_{xx}|} .$$

To find the average value of $|\tau|$ at a specular point, we substitute $\zeta_{xsp} = \tan\gamma$ for ζ_x and average over the random variable ζ_{xx}. To perform a strict averaging of $\frac{1}{\zeta_{xx}}$, we must multiply by $p\left(\zeta_{xx} \middle| \zeta_{xsp}\right)$ and integrate over the range $-\infty < \zeta_{xx} < \infty$. To conditional probability density function must be used because we have prior knowledge of ζ_x at the specular points. Unfortunately, however, the resulting integral does not converge, due to the singularity of $\frac{1}{|\zeta_{xx}|}$ at the origin. Therefore, we employ the following approximation to obtain an estimate of the average curvature:

$$\left\langle \frac{1}{|\zeta_{xx}|} \right\rangle \approx \frac{1}{\langle |\zeta_{xx}| \rangle} .$$

Then an estimate of the average radius of curvature at the specular point becomes

$$\langle|\gamma|\rangle \frac{\left[1 + \zeta_{xsp}^2\right]^{3/2}}{\left\langle\left|\zeta_{xx}\right|\right\rangle} ,$$

or

$$\langle|\gamma|\rangle = \frac{\sec^3\gamma}{\int_{-\infty}^{\infty} \left|\zeta_{xx}\right| p\left(\zeta_{xx}\left|\zeta_{xsp}\right.\right) \, d\zeta_{xx}} . \qquad \text{(B-10)}$$

Obviously, the above procedure is not exact, and we have no ready quantitative measure of error. The approximation becomes better as we exclude the region around $\zeta_{xx} = 0$, the neighborhood of the singular point. Actually this neighborhood around the origin has already been excluded implicitly in the application of the stationary phase principle. The basis of the stationary phase technique is the expansion of the argument of the exponential $iK\zeta$ into a series about the specular point x_{sp} at which the second or linear term vanishes; i.e.,

$$K\zeta(x) = K\zeta\left(x_{sp}\right) \pm \frac{1}{2!} K \zeta_{xx}\left(x_{sp}\right)^2 \pm \frac{1}{3!} K \zeta_{xxx}\left(x_{sp}\right)\left(x - x_{sp}\right)^3 + \ldots , \qquad \text{(B-11)}$$

K, being proportional to $\frac{1}{\lambda}$.

The stationary phase technique is applicable when K is large and when $\zeta_{xx}\left(x_{sp}\right)$ is not too small, for then the cubic and all higher order terms can be neglected. If, on the other hand, $\zeta_{xx}\left(x_{sp}\right)$ is very small, the cubic term is dominant, and one does not obtain the result of Eq. (B-1) for the scattering width written in terms of the radius of curvature. Hence, the region at and around the singular point $\zeta_{xx} = 0$ has already been excluded in obtaining Eq. (B-1).

Averaging ζ_{xx} instead of its reciprocal is equivalent to assigning a non-zero average value to the coefficient of the quadratic term of Eq. (B-11) before integrating. This insures that the quadratic term will always determine the value of the integral for sufficiently large K. Although we have no exact error bounds, we should not expect any error incurred to be excessive. This expectation is borne out by the identity of the resulting scattering cross section with those derived using two other techniques.

For the Gaussian surface model, Eq. (B-10) can be written immediately because the integral in the denominator has been evaluated in the preceding section.

$$\langle |\zeta| \rangle = \sqrt{\frac{\pi}{2}} \frac{\sec^3 \gamma}{\eta_{xx}} . \qquad \text{(B-12)}$$

(c) Average Scattering Cross Sections per Unit Area

Now that we have determined general expressions for a number of specular ridges per unit length, given in Eq. (B-6), and the average curvature at the specular point, from Eq. (B-10), these expressions can be substituted into Eq. (B-1) to give the average scattering cross section per unit surface area. The integrals in the first two equations cancel exactly in the substitution process.

$$\sigma^o_{\xi\xi} = k_o L \cos\left(\frac{\theta_i + \theta_s}{2}\right) \sec^3 \gamma \, p(\tan \gamma) \left| R_{\xi\xi}\left(\frac{\theta_i + \theta_s}{2}\right)\right|^2 , \qquad \text{(B-13)}$$

where $p(\zeta_x)$ is the probability density function for one-dimensional surface slope ζ_x. In particular, for the Gaussian model, the bistatic (bistatic here means within the y = 0 plane) and backscattering cross sections respectively become

$$\sigma^o_{\xi\xi} = \frac{k_o L}{\sqrt{2\pi}\, s_x} \cos\left(\frac{\theta_i + \theta_s}{2}\right) \sec^3 \gamma \, e^{-\frac{\tan^2 \gamma}{2 s_x^2}} \left| R_{\xi\xi}\left(\frac{\theta_i + \theta_s}{2}\right)\right|^2 , \qquad \text{(B-14a)}$$

and

$$\sigma^o_{vv} = \sigma^o_{hh} = \frac{k_o L}{\sqrt{2\pi}\, s_x} \sec^3 \theta_i \, e^{-\frac{\tan^2 \theta_i}{2 s_x^2}} |R(0)|^2 , \qquad \text{(B-14b)}$$

where R(0) is merely the Fresnel reflection coefficient at normal incidence.

3. Two-Dimensionally Rough Surface $\zeta(x,y)$

(a) Average Number of Specular Points

In order to simplify the analysis, let us choose the x and y axes for this section such that the plane defined by the normal to the surface at specular point and the x axis coincides with the x-z plane (Figure B-2). This may be

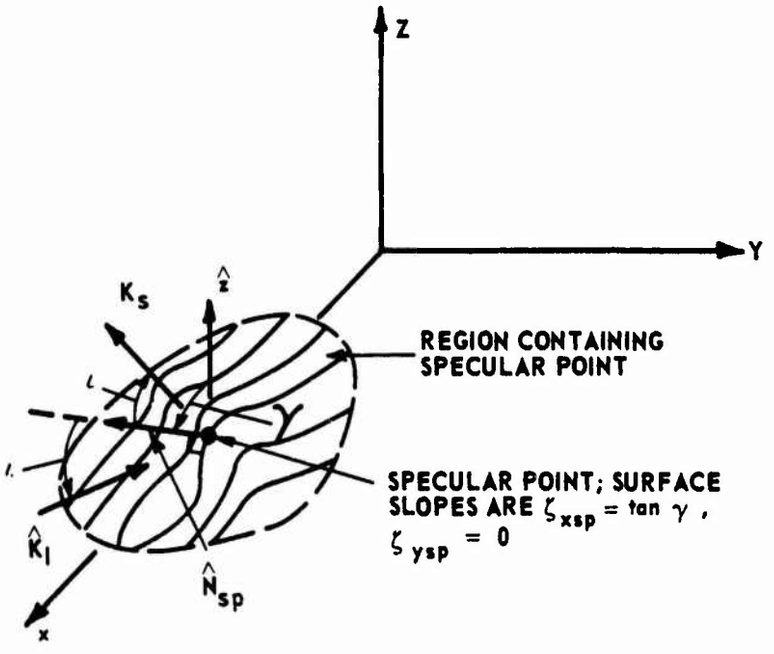

FIGURE B-2. COORDINATE SYSTEM ROTATED ABOUT z-AXIS SO THAT BISECTOR OF INCIDENCE AND SCATTERING DIRECTIONS (i.e., SURFACE NORMAL AT SPECULAR POINT) LIES IN x-z PLANE

done with no loss of generality because the surface roughness is isotropic and the surface statistics are invariant under a rotation of the x-y axes. Then the slopes of the surface at the specular point in the x- and y-directions become $\zeta_x = \tan\gamma$ and $\zeta_y = 0$. Denote these particular values by ζ_{xsp} and ζ_{ysp}. The analysis here proceeds in the same manner as for the one-dimensionally rough surface.

Define $p(\zeta_x, \zeta_y, \zeta_{xx}, \zeta_{xy}, \zeta_{yy}; x, y)$ as the joint probability of the surface first and second derivatives in the x- and y-directions. In order for the

surface to have a specular point with the proper slopes ζ_{xsp} and ζ_{ysp}, there must exist a point somewhere in the region x_1, $x_1 + dx$ and y_1, $y_1 + dy$, where $\zeta_x - \zeta_{xsp}$ and $\zeta_y - \zeta_{ysp}$ both pass through zero. If the increments dx, dy are sufficiently small, the slope surface $\zeta_x(x,y)$ in this increment can be considered nearly planar and can be written in terms of its first series terms:

$$\zeta_x\left(x_1 + \Delta_x,\ y_1 + \Delta_y\right) = \zeta_x(x_1, y_1) + \zeta_{xx}(x_1, y_1)\Delta_x + \zeta_{xy}(x_1, y_1)\Delta_y \ . \tag{B-15a}$$

Likewise for ζ_y,

$$\zeta_y\left(x_1 + \Delta_x, y_1 + \Delta_y\right) = \zeta_y(x_1, y_1) + \zeta_{xy}(x_1, y_1)\Delta_x + \zeta_{yy}(x_1, y_1)\Delta_y \ , \tag{B-15b}$$

where $\Delta_x < dx$ and $\Delta_y < dy$. Now the intersection of the $\zeta_x(x,y)$ plane with the $\zeta_{xsp} = \tan\gamma$ plane within dx, dy is a straight line. Another similar line is formed by $\zeta_y(x,y)$ in the $\zeta_{ysp} = 0$ plane. These lines are determined by setting the left sides of Eq. (B-15) equal to ζ_{xsp} and ζ_{ysp}. The point at which the projections of these lines cross in the x-y plane is the specular point. It is found by solving Eq. (B-15) for Δ_x and Δ_y, and the result is:

$$\Delta_{xsp} = \frac{1}{J}\left[\zeta_{xy}\left(\zeta_y - \zeta_{ysp}\right) - \zeta_{yy}\left(\zeta_x - \zeta_{xsp}\right)\right]\Big|_{x_1, y_1} \ , \tag{B-16a}$$

$$\Delta_{ysp} = \frac{1}{J}\left[\zeta_{xy}\left(\zeta_x - \zeta_{xsp}\right) - \zeta_{xx}\left(\zeta_y - \zeta_{ysp}\right)\right]\Big|_{x_1, y_1} \ , \tag{B-16b}$$

where $J = \zeta_{xx}\zeta_{yy} - \zeta_{xy}^2$. Then for a specular point to occur within the desired interval, the following two inequalities must hold:

$$x_1 < x_1 + \Delta_{xsp} < x_1 + dx, \tag{B-17a}$$

and

$$y_1 < y_1 + \Delta_{ysp} < y_1 + dy \ . \tag{B-17b}$$

Substituting Eq. (B-16) into (B-17), the following inequality pair results when $J > 0$.

$$0 < u < Jdx \ , \tag{B-18a}$$

and

$$0 < v < Jdy \ , \tag{B-18b}$$

where u, v are new variables to replace $\zeta_x - \zeta_{ysp}$ and $\zeta_y - \zeta_{ysp}$, defined as follows:

$$u = \zeta_{xy}\left(\zeta_y - \zeta_{ysp}\right) - \zeta_{yy}\left(\zeta_x - \zeta_{xsp}\right) \ ,$$

and

$$v = \zeta_{xy}\left(\zeta_x - \zeta_{xsp}\right) - \zeta_{xx}\left(\zeta_y - \zeta_{ysp}\right) \ .$$

Thus for given values of ζ_{xx}, ζ_{xy}, and ζ_{yy} (which themselves may range between $\pm\infty$), the ranges of these new random variables are given by Eq. (B-18).

The probability, then, of a specular point within x_1, $x_1 + dx$ and y_1, $y_1 + dy$ for positive J is found by integrating $p\left(\zeta_x, \zeta_y, \zeta_{xx}, \zeta_{xy}, \zeta_{yy}; x_1 y_1\right)$ between these limits. For dx and dy sufficiently small, the value ζ_x and ζ_y in the above probability density take on the values at the specular point ζ_{xsp} and ζ_{ysp}. This probability is

$$P^+ = \iiint\limits_{J>0} d\zeta_{xx} d\zeta_{yy} d\zeta_{xy} \left\{ \iint d\zeta_x d\zeta_y p\left(\zeta_{xsp}, \zeta_{ysp}, \zeta_{xx}, \zeta_{xy}, \zeta_{yy}; x_1 y_1\right) \right\}.$$

Making the change of variables to u, v we obtain

$$P^+ = \iiint\limits_{J>0} d\zeta_{xx} d\zeta_{yy} d\zeta_{xy} \left\{ \int_0^{Jdx} \int_0^{Jdy} \frac{1}{J} p\left(\zeta_{xsp}, \zeta_{ysp}, \zeta_{xx}, \zeta_{xy}, \zeta_{yy}; x_1, y_1\right) du dv \right\} .$$

Since dx and dy are small, the integral in braces can be simplified

$$P^{+} = dx\,dy \iiint\limits_{J>0} \left(\zeta_{xx}\zeta_{yy} - \zeta_{xy}^2\right) p\Big(\zeta_{xsp}, \zeta_{ysp}, \zeta_{xx}, \zeta_{xy}, \zeta_{yy};$$

$$x_1, y_1\Big) d\zeta_{xx} d\zeta_{yy} d\zeta_{xy} \ .$$

Likewise the probability P^{-} for $J < 0$ can be computed. Then the total probability of a specular point in dx dy is

$$P = dx\,dy \int_{-\infty}^{\infty}\int_{-\infty}^{\infty}\int_{-\infty}^{\infty} \left|\zeta_{xx}\zeta_{yy} - \zeta_{xy}^2\right| p\Big(\zeta_{xsp}, \zeta_{ysp}, \zeta_{xx}, \zeta_{xy}, \zeta_{yy};$$

$$x_1, y_1\Big) d\zeta_{xx} d\zeta_{yy} d\zeta_{xy} \ .$$

The average number of specular points per unit area n_A is the integral in the above equation, as one readily sees by analogy with the one-dimensional surface. Writing the joint probability density in the integral as the product of the joint density in the slopes ζ_x and ζ_y, and the conditional density in the remaining second derivative variables, we obtain the following result for n_A:

$$n_A = p\Big(\zeta_{xsp}, \zeta_{ysp}\Big) \int_{-\infty}^{\infty}\int_{-\infty}^{\infty}\int_{-\infty}^{\infty} \left|\zeta_{xx}\zeta_{yy} - \zeta_{xy}^2\right| p\Big(\zeta_{xx}, \zeta_{xy}, \zeta_{yy}\Big|$$

$$\zeta_{xsp}, \zeta_{ysp}\Big) d\zeta_{xx} d\zeta_{xy} d\zeta_{yy} \ . \qquad \text{(B-19)}$$

For the same Gaussian joint probability density and correlation coefficient model, the horizontal separation r between the two surface points $\zeta(x, y)$ and $\zeta(x', y')$ is now defined as follows:

$$r = \sqrt{(x - x')^2 + (y - y')^2} \ .$$

Equations (B-8) are correct here as they stand. In addition, the following covariances may be derived in the same manner as Eq. (B-8).

$$\left\langle \zeta_y^2(x, y) \right\rangle = \frac{2h^2}{\ell^2} \equiv s_y^2 = s_x^2 \ ,$$

$$\left\langle \zeta_{yy}^2(x,y) \right\rangle = \frac{12h^2}{\ell^4} = \eta_{xx}^2 \equiv \eta^2 \quad , \tag{B-20}$$

$$\left\langle \zeta_{xx}(x,y)\,\zeta_{yy}(x,y) \right\rangle = \left\langle \zeta_{xy}^2(x,y) \right\rangle = \frac{4h^2}{\ell^4} = \frac{1}{3}\eta^2 \quad .$$

All the remaining covariances between the five random variables $\left(\text{i.e., } \zeta_x, \zeta_y, \zeta_{xx}, \zeta_{xy}, \zeta_{yy}\right)$ at a given surface point (x,y) which are not shown explicitly in Eq. (B-8) or (B-20) are identically zero. Note that only two of these five random variables are correlated, viz., ζ_{xx} and ζ_{yy}, whose correlation coefficient is $\frac{1}{3}$.

It is now a relatively straightforward problem to reduce the integral in Eq. (B-19) for the Gaussian surface. Using the above covariances, we define new variables $w = \zeta_{xx}\zeta_{yy}$ and $v = \zeta_{xy}^2$. Then this integral, expressed in terms of the probability functions of w and v, become

$$I \equiv \int_{-\infty}^{-\infty} dw \int_{-\infty}^{-\infty} dv\,|w - v|\,p(w)\,p(v)$$

$$= \int_{-\infty}^{0} dw\,p(w) \int_{0}^{-\infty} (v - w)\,p(u)\,du$$

$$+ \int_{0}^{\infty} dw\,p(w) \left[\int_{0}^{w} (w - v)\,p(v)\,dv + \int_{w}^{\infty} (v - w)\,p(v)\,dv \right] .$$

This equation can be reduced to the following:

$$I = \frac{\sqrt{2\eta^2}}{3\pi} \int_0^\infty \left[(2x - 1)\,\varphi(\sqrt{x}) + \frac{2}{\sqrt{\pi}} x^{1/2} e^{-x} \right] e^{x/4} K_o\left(\frac{3}{4}x\right) dx \quad ,$$

where $\varphi(y)$ is the standard error function and $K_o(y)$ is the modified zero-order cylindrical Bessel function of the second type. The integral above is a number which is evaluated easiest numerically. The answer is 5.13011. Then using $I = \frac{\sqrt{2}}{3\pi} 5.13\,\eta^2$ in Eq. (B-19), we obtain the following result for the average number of specular points per unit area.

$$n_A = \frac{7.255}{\pi^2 \ell^2} \exp\left\{-\frac{\tan^2\gamma}{s^2}\right\}, \qquad \text{(B-21)}$$

where s^2 is the mean square value of the total slope at a point on a two-dimensionally rough surface, defined as

$$s^2 \equiv \left\langle \zeta_x^2 + \zeta_y^2 \right\rangle = s_x^2 + s_y^2 = 2s_x^2 = \frac{4h^2}{\ell^2} \quad .$$

(b) Average Curvature at Specular Points

When the scattering surface is a function of two variables, the stationary phase principle shows that the scattered power varies inversely with the Gaussian curvature at the specular point. The Gaussian curvature is interpreted simply as the reciprocal of product of the principal radii of curvature at the specular point. The principal radii are the maximum and minimum radii. This is in contrast to scattering from the one-dimensional surface, where the power varied inversely with the simple curvature of the surface at the specular point.

From any treatment of differential geometry[9] it can be shown that the reciprocal of the Gaussian curvature is expressed in terms of the derivatives of $\zeta(x,y)$ as follows:

$$|r_1 r_2| = \frac{\left(1 + \zeta_x^2 + \zeta_y^2\right)^2}{\left|\zeta_{xx}\zeta_{yy} - \zeta_{xy}^2\right|} \quad .$$

The evaluation of the average value of this quantity at the specular point follows the same technique as we used for the one-dimensional surface, and much of the detail will not be retraced again. We know that the values of the slope at the specular point are $\zeta_{xsp} = \tan\gamma$ and $\zeta_{ysp} = 0$ (Figure B-2). The denominator of the above equation then contains the random variables which must be averaged. As before, we average the quantity in the denominator separately rather than its reciprocal; the singularity when the denominator goes to zero is avoided for the same reason here as previously. In averaging the denominator, we use the conditional probability density function in $\zeta_{xx}, \zeta_{xy}, \zeta_{yy}$, given in ζ_x, ζ_y because of our prior knowledge of these surface slopes at the specular point. The average then becomes

$$<|\eta_1\eta_2|> = \frac{\left(1 + \zeta_{xsp}^2 + \zeta_{ysp}^2\right)^2}{\left|\zeta_{xx}\zeta_{yy} - \zeta_{xy}^2\right|} ,$$

or

$$<|\eta_1\eta_2|> = \frac{\sec^4\gamma}{\int\int\int_{-\infty}^{\infty} \left|\zeta_{xx}\zeta_{yy} - \zeta_{xy}^2\right| p\left(\zeta_{xx}, \zeta_{xy}\zeta_{yy} \middle| \zeta_{xsp}, \zeta_{ysp}\right) d\zeta_{xx} d\zeta_{yy} d\zeta_{xy}} . \quad \text{(B-22)}$$

In particular, the denominator will be evaluated for the Gaussian surface model employed previously. The above denominator is the same as the integral of Eq. (B-19). The solution obtained there represented as I, was $\frac{2}{3\pi} 5.13\eta^2$. Hence the average curvature for the Gaussian model becomes

$$<|\eta_1\eta_2|> = 0.327 \frac{\pi}{2} \frac{\sec^4\gamma}{\eta^2} . \quad \text{(B-23)}$$

(c) Average Scattering Cross Sections per Unit Area

In the same manner, let us substitute Eq. (B-19), giving the average number of specular points per unit area, and Eq. (B-22), for the average Gaussian curvature at a specular point, into Eq. (B-2) to give the general expression for the average scattering cross section per unit surface area. Again the integrals cancel, simplifying the result.

$$\sigma^0_{\xi\eta} = \pi \sec^4\gamma \, p(\tan\gamma, 0) \left|R_{\xi\eta}(\iota)\right|^2 , \quad \text{(B-24)}$$

where $p\left(\zeta_x, \zeta_y\right)$ is the joint probability density function for the surface slopes, ζ_x and ζ_y. The total slope of the surface at the specular point, $\tan\gamma$, is given in Eq. (B-27), and the remaining terminology is defined in the introduction.

For the model having Gaussian surface statistics, the bistatic and back-scattering cross sections respectively become:

$$\sigma^{o}_{\xi\eta} = \frac{\sec^4\gamma}{s^2}\, e^{-\frac{\tan^2\gamma}{s^2}} \left|R_{\xi\eta}(\iota)\right|^2 , \qquad \text{(B-25a)}$$

$$\sigma^{o}_{vv} = \sigma^{o}_{hh} = \frac{\sec^4\theta_i}{s^2} e^{-\frac{\tan^2\theta_i}{s^2}} \left|R(0)\right|^2 , \qquad \text{(B-25b)}$$

where again R(0) is the Fresnel reflection coefficient for normal incidence. The latter equation is identical to that obtained by Hagfors[1] by the autocorrelation approach, and Muhleman[4] by the ray optics technique, as corrected by Hagfors.[1] Equation (B-25a) is identical to the result derived by Semenov[2] and later by Stogryn.[3]

4. Conclusions

We have obtained explicit expressions for the average number of specular points per unit surface area and the average curvature at a specular point. The role of these quantities in the scattering process is readily understood from basic geometrical optics (or stationary phase) considerations. For a two-dimensionally rough surface, for example, the scattering cross section for one specular point is π times the product of the principal radii of curvature. For a very rough surface where the power from neighboring specular points adds incoherently, one must multiply by the average number of such specular points. Furthermore, one must multiply by the surface reflection coefficients in order to account properly for polarization. These reflection coefficients are derived here for the vertical and horizontal states.

From examination of the Gaussian model (which several investigators[10] have found typifies the sea surface fairly well) we see that the dominant factor in the scattering cross section for relatively small rms surface slopes is the number of specular points. This quantity varies directly with the surface slope probability density function, which decreases quite rapidly at scattering angles where the slope of the specular points must be considerably different from zero. On the other hand, the average radii of curvature increase with increasing slope at the specular point, but not nearly enough to offset the decrease in the number of specular points.

The two pieces of surface statistical information obtained here, and their simple relationship to a third quantity, the scattering cross section, suggest possible uses in determination of surface properties of an unknown or

inaccessible surface, i.e., in the inverse scattering problem. For instance, the number of specular points on a surface might be counted from optical photographs or by scanning with a collimated laser or radar beam. The intensity of the return from each of these specular points permits one to estimate the product of the principal radii of curvature. If one combines or integrates these separate specular point brightnesses, he obtains the scattering cross section of the entire surface. Measurement of any two of these quantities permits determination of the third. Also, one can obtain the surface slope probability density function. If the functional form of the distribution is not too different from Gaussian so that one can use the model examined in this paper, one can obtain estimates of the rms roughness height and correlation length from a knowledge of two of the three quantities. Normally, these two parameters of a rough surface cannot be determined from the scattering cross section alone, since the only surface parameter appearing explicitly in the model is the surface slope, as seen from Eq. (B-25).

5. Appendix

First, we shall determine the pertinent angles and slopes associated with the specular points. The slopes are determined by applying the stationary phase principle to the exponential $e^{ik_o \bar{q} \cdot \bar{r}}$, of the physical optics integrand. Here $\bar{q} = \hat{k}_i - \hat{k}_s$ (Figure B-1), and $\bar{r} = x\hat{x} + y\hat{y} + \zeta(x,y)\hat{z}$ is the distance from the origin to a point on the surface. The stationary phase point is defined as the point at which the gradient vector in the x, y-directions of the argument of the above exponential vanishes. Equating the two components of this vector to zero, we obtain the surface slopes at the specular point as

$$\zeta_{xsp} = -\frac{q_x}{q_z}, \quad \zeta_{ysp} = -\frac{q_y}{q_z}.$$

Then the normal to the surface at the specular point is given by

$$\hat{n}_{sp} = \frac{-\zeta_{xsp}\hat{x} - \zeta_{ysp}\hat{y} + \hat{z}}{\sqrt{\zeta_{xsp}^2 + \zeta_{ysp}^2 + 1}}$$

$$= \frac{\left(\sin\theta_s \cos\varphi_s - \sin\theta_i\right)\hat{x} + \sin\theta_s \sin\varphi_s \hat{y} + \left(\cos\theta_i + \cos\theta_s\right)\hat{z}}{\sqrt{2}\sqrt{1 - \sin\theta_o \sin\theta_s \cos\varphi_s + \cos\theta_o \cos\theta_s}} \quad \text{(B-26)}$$

The cosine of the angle of incidence ι at the specular point is $-\hat{k}_i \cdot \hat{n}_{sp} = \hat{k}_s \cdot \hat{n}_{sp}$; after simplification, it is given in Eq. (B-3). The angle between the above normal and the vertical γ is determined from $\cos\gamma = \hat{z} \cdot \hat{n}_{sp}$. Its tangent is also the total slope of the surface at specular point, and is readily determined from Eq. (B-26).

$$\tan\gamma = \frac{\sin^2\theta_i - 2\sin\theta_i \sin\theta_s \cos\varphi_s + \sin^2\theta_s}{\cos\theta_i + \cos\theta_s} \quad . \quad \text{(B-27)}$$

Now that we know the angles associated with the specular points, we can determine the manner in which these points reflect the incident polarized wave. Vertical and horizontal polarization states here refer to the incident and scattered E-field vectors along the θ_i, θ_s directions and φ_i, φ_s directions respectively (Figure B-1). The reflection coefficients between the scattered and incident v and h states are the same as those for an infinite plane tangent to the surface at the specular point and having slopes ζ_{xsp} and ζ_{ysp}. This problem has been solved by Mitzner.[11] Briefly, one resolves the incident E-field into components along two vectors, one normal to the local plane of incidence, i.e.,

$$\hat{\upsilon} = \frac{1}{\sin\iota}\hat{k}_i \times \hat{n}_{sp} \quad ,$$

and one in the plane of incidence but perpendicular to $\hat{k}_i$, i.e.,

$$\hat{\alpha} = \hat{k}_i \times \hat{\upsilon} \quad .$$

Likewise, we employ a unit vector perpendicular to $\hat{k}_s$, i.e.,

$$\hat{\beta} = \hat{k}_s \times \hat{\upsilon} \quad .$$

The components of the scattered E-fields resolved along $\hat{\upsilon}$ and $\hat{\beta}$ are then related to the components of the incident $\vec{E}$-fields resolved along $\hat{\upsilon}$ and $\hat{\alpha}$ by the well known Fresnel reflection coefficients:

$$R_{||}(\iota) = \frac{\epsilon_r \cos \iota - \sqrt{\epsilon_r \mu_r - \sin^2 \iota}}{\epsilon_r \cos \iota + \sqrt{\epsilon_r \mu_r - \sin^2 \iota}},$$

and

$$R_{\perp}(\iota) = \frac{\mu_r \cos \iota - \sqrt{\epsilon_r \mu_r - \sin^2 \iota}}{\mu_r \cos \iota + \sqrt{\epsilon_r \mu_r - \sin^2 \iota}}. \qquad \text{(B-28)}$$

If the incident E-field is horizontally polarized, then the reflection coefficients we seek are defined as follows:

$$R_{hh} = \frac{\hat{\theta}_s \cdot \bar{E}^r}{E_h^i}$$

and

$$R_{vh} = \frac{\hat{\varphi}_s \cdot \bar{E}^r}{E_h^i},$$

where $\bar{E}^r$ is the total E-field reflected from the specular points as determined by the technique in the preceding paragraph. An analogous definition gives R_{vv} and R_{hv} when the incident E-field is vertically polarized. After performing the required algebra, we obtain

$$R_{hh} = -\frac{\sin \theta_i \sin \theta_s \sin^2 \varphi_s R_{||}(\iota) + a_2 a_3 R_{\perp}(\iota)}{4 \sin^2 \iota \cos^2 \iota},$$

$$R_{vh} = \sin \varphi_s \frac{a_2 \sin \theta_s R_{||}(\iota) - a_3 \sin \theta_i R_{\perp}(\iota)}{4 \sin^2 \iota \cos^2 \iota}, \qquad \text{(B-29a)}$$

$$R_{hv} = \sin \varphi_s \frac{a_2 \sin \theta_s R_{\perp}(\iota) - a_3 \sin \theta_i R_{||}(\iota)}{4 \sin^2 \iota \cos^2 \iota} ,$$

$$R_{vv} = \frac{\sin \theta_i \sin \theta_s \sin^2 \varphi_s R_{\perp}(\iota) + a_2 a_3 R_{||}(\iota)}{4 \sin^2 \iota \cos^2 \iota} , \qquad \text{(B-29b)}$$

where

$$a_2 = \cos \theta_i \sin \theta_s + \sin \theta_i \cos \theta_s \cos \varphi_s$$

and

$$a_3 = \sin \theta_i \cos \theta_s + \cos \theta_i \sin \theta_s \cos \varphi_s . \qquad \text{(B-30)}$$

For backscattering, $\theta_i = \theta_s$ and $\varphi_s = 0$. These reflection coefficients are simplified by taking the limit of numerator and denominator. The results are:

$$R_{hh} = R_{vv} \rightarrow R_{||}(0), \; -R_{\perp}(0); \; R_{vh} = R_{hv} \rightarrow 0. \qquad \text{(B-31)}$$

LITERATURE CITED (Appendix B)

1. T. Hagfors, RELATIONSHIP OF GEOMETRICAL OPTICS AND AUTO-CORRELATION APPROACHES TO THE ANALYSIS OF LUNAR AND PLANETARY RADAR, Jour. Geoph. Res., 71, 1965, pp. 379-383.

2. V. Semenov, SCATTERING OF ELECTROMAGNETIC WAVES BY BOUNDED REGIONS OF ROUGH SURFACES HAVING FINITE CONDUCTIVITY, Radiotekhnika i Elektronika, 10, 1965, pp. 1952-1960.

3. A. Stogryn, ELECTROMAGNETIC SCATTERING FROM ROUGH, FINITELY CONDUCTING SURFACES, Radio Science, 2, 1967, pp. 415-428.

4. D. Muhleman, RADAR SCATTERING FROM VENUS AND THE MOON, The Astronomical Journal, 69, 1964, pp. 34-41.

5. R. Kodis, A NOTE ON THE THEORY OF SCATTERING FROM AN IRREGULAR SURFACE, IEEE Trans. Ant. Prop., AP-14, 1966, pp. 77-82.

6. M. Longuet-Higgins, REFLECTION AND REFRACTION AT A RANDOM MOVING SURFACE. II. NUMBER OF SPECULAR POINTS ON A GAUSSIAN SURFACE, Opt. Soc. Am. Jour. 50, 1960, pp. 845-850.

7. S. Rice, MATHEMATICAL ANALYSIS OF RANDOM NOISE, Bell System Tech. Jour., Parts I and II, 23, 1944, pp. 282-332; Parts III and IV, 24, 1945, pp. 46-156.

8. A. Taylor, ADVANCED CALCULUS, New York, Ginn and Company, 1955, pp. 359-385.

9. D. Struik, DIFFERENTIAL GEOMETRY, Second Edition, Reading, Massachusetts, Addison-Wesley Publishing Company, Inc., 1961, pp. 1-18, 55-86.

10. C. Cox and W. Munk, MEASUREMENT OF THE ROUGHNESS OF THE SEA SURFACE FROM PHOTOGRAPHS OF THE SUN'S GLITTER, Jour. Opt. Soc. Am., 44, 1954, pp. 838-850.

11. K. Mitzner, CHANGE IN POLARIZATION ON REFLECTION FROM A TILTED PLANE, Radio Science, I, 1966. pp. 27-29.

UNCLASSIFIED
Security Classification

DOCUMENT CONTROL DATA - R & D

(Security classification of title, body of abstract and indexing annotation must be entered when the overall report is classified)

1. ORIGINATING ACTIVITY (Corporate author)	2a. REPORT SECURITY CLASSIFICATION
Battelle Memorial Institute 505 King Avenue Columbus, Ohio 43201	Unclassified 2b. GROUP N/A

3. REPORT TITLE

RADAR CLUTTER IN AN AIR DEFENSE SYSTEM
PART I. CLUTTER PHYSICS

4. DESCRIPTIVE NOTES (Type of report and inclusive dates)

None

5. AUTHOR(S) (First name, middle initial, last name)

Donald E. Barrick

6. REPORT DATE	7a. TOTAL NO. OF PAGES	7b. NO. OF REFS
26 January 1968	124	33

8a. CONTRACT OR GRANT NO.	9a. ORIGINATOR'S REPORT NUMBER(S)
DAAH01-67-C-1921 b. PROJECT NO.	RSIC-798
c.	9b. OTHER REPORT NO(S) (Any other numbers that may be assigned this report) AD
d.	

10. DISTRIBUTION STATEMENT

Each transmittal of this document outside the agencies of the U. S. Government must have prior approval of this Command, ATTN: AMSMI-RB.

11. SUPPLEMENTARY NOTES	12. SPONSORING MILITARY ACTIVITY
None	Redstone Scientific Information Center Research and Development Directorate U. S. Army Missile Command Redstone Arsenal, Alabama 35809

13. ABSTRACT

This report provides an analysis and physical interpretation of the various mechanisms giving rise to radar clutter. Both volume-distributed clutter (rain, chaff, etc.) and surface-distributed clutter (terrain, sea, etc.) are considered. The statistics of the clutter radar cross sections are related to the statistics and properties of the particles or surfaces producing the echoes. The spectral densities of clutter signals are derived in terms of the physical parameters of the clutter sources. Measured results are provided and examples are calculated which indicate the magnitude of the clutter problem for a mid-frequency (S-band) radar system.

DD FORM 1 NOV 68 1473 REPLACES DD FORM 1473, 1 JAN 64, WHICH IS OBSOLETE FOR ARMY USE.

UNCLASSIFIED
Security Classification

14. KEY WORDS	LINK A		LINK B		LINK C	
	ROLE	WT	ROLE	WT	ROLE	WT
Clutter						
Chaff						
Scattering						
Unwanted targets						
Noise						
Echoes						